DEPARTMENT OF PHYSICS, UNIVERSITY OF JYVÄSKYLÄ
RESEARCH REPORT No. 1/1992

STUDIES OF VERY NEUTRON-RICH ODD-MASS NUCLEI WITH $109 \leq A \leq 119$

BY
HEIKKI PENTTILÄ

Academic Dissertation
for the Degree of
Doctor of Philosophy

Jyväskylä, Finland
June 1992

URN:ISBN:978-951-39-9588-1
ISBN 978-951-39-9588-1 (PDF)
ISSN 0075-465X

Jyväskylän yliopisto, 2023

IBSN 951-680-780-1
ISSN 0075-465X

DEPARTMENT OF PHYSICS, UNIVERSITY OF JYVÄSKYLÄ
RESEARCH REPORT No. 1/1992

STUDIES OF VERY NEUTRON–RICH ODD–MASS NUCLEI WITH $109 \leq A \leq 119$

BY
HEIKKI PENTTILÄ

Academic Dissertation
for the Degree of
Doctor of Philosophy

To be presented, by permission of the
Faculty of Mathematics and Natural Sciences
of the University of Jyväskylä,
for public examination in Auditorium S-212 of the
University of Jyväskylä on June 25, 1992,
at 12 o'clock noon

Jyväskylä, Finland
June 1992

Preface

This work has been carried out during the years 1987 – 1992 at the Department of Physics in the University of Jyväskylä. When I joined to the IGISOL group in 1987, the ion guide technique was successfully developed and the work for the application for the fission studies was started. Working in this very enthusiastic atmosphere has been an exceptional privilege.

I wish like to express my warmest thanks to leader of the group and my supervisor Dr. Juha Äystö. His confidence that I know what I am doing has been encouraging. I also would like to greatly thank the "permanent" group members, Dr. J. Honkanen, Mr. P. Taskinen, M.Sc., Mr. P. Jauho, M.Sc., Ms. V. Koponen, Lic.Phil., Mr. A. Jokinen, M.Sc., Mr. J.-M. Parmonen, M.Sc, and all others who worked for shorter periods. Especially I am indebted to Mr. P. Taskinen; only after he left the group I recognized how much he worked for the experiments.

My best thanks go to the visitors who have been of great importance to this work. Particularly I wish to mention Dr. K. Rykaczewski, who introduced me the "WSBETA" code, Prof. J. Zylic, who sometimes encouraged himself to suggest something maybe not so important, and Prof. C. Davids, Prof. R. Beraud, Prof. M. Huyse, and Dr. Z. Preibisz, who have also been most gentle hosts during my visits to other laboratories.

I wish also greatly acknowledge the Academy of Finland, which, besides financing the research projects I have been participating, has offered me opportunity to concentrate on this work as Research Assistant in years 1989 – 1991. I also wish to express my gratitude to the E. J. Sariola Foundation and the Foundation of Vilho, Yrjö and Kalle Väisälä, who have supported my work with research grants.

Most of all I wish to thank my wife, Anu, and our son, Jaakko. Without them I never would have finished this work.

Jyväskylä, June 1992

Heikki Penttilä

Studies of very neutron-rich odd-mass nuclei with $109 \leq A \leq 119$

Abstract

The structure of the odd-A nuclei ^{109}Ru, ^{111,113}Rh, ^{111,113,115,117}Pd, and ^{117,119}Ag were investigated via the beta decay of their parent nuclei. The β-decays of ^{109}Mo, ^{111}Tc, ^{113}Ru, ^{113,115,117}Rh and ^{119}Pd and isomeric decays of ^{113m}Pd and ^{117m}Pd were discovered. The X-, γ-, β- and conversion electron coincidence spectrocopies were performed on mass separated sources produced with the ion guide technique. The experimental systematics of both the normal and the intruder states were extended towards higher neutron excess.

Results are compared with the predictions of deformed macroscopic-microscopic model. The coexistence of oblate and prolate shapes is suggested to explain the exceptional large hindrance in the decay of isomeric states in odd-A Pd nuclei. New β-decay half-lives are compared with the predictions of gross theory and QRPA calculations.

Contents

1. Introduction

This study focusses on the nuclear structure of neutron rich odd mass nuclei with A = 109 – 119. The studied nuclei are shown in figure 1.1. Ten β-decay half-lives have been measured for the first time or remarkably improved from the previous values. The low-energy level systematics of very neutron rich Ru, Rh, Pd and Ag nuclei has been studied mainly via the β-decays of their odd mass Tc, Ru, Rh and Pd parent nuclei.

The IGISOL technique developed in Jyväskylä in early 80's (Ärj81a), (Ärj81b), (Äys84), (Ärj85), (Äys87), (Ärj87), (Tas89), provides a unique method to produce mass separated, short-lived radioactive sources of any element. In this work the ion guide technique has been used to study neutron rich fission products of proton induced fission of ^{238}U. A remarkable feature of this fission process is a strong symmetric component that results in relatively high production of neutron rich nuclei in the A ≈ 110 – 120 region. In addition, these neutron-rich Zr, Mo, Tc, Ru, Rh and also Pd isotopes are very difficult to mass separate because of their chemical properties and because of their short half-lives. Prior to the measurements performed with the IGISOL, there was a noticeable gap in the data of fission products in this region.

The studied nuclei are located in the transitional region below the nearly spherical nuclei close to Z = 50 shell closure. The presence of states of different origin results in high density of states at low excitation energy and also isomerism. In odd-A Ag nuclei, having three holes in the $g_{9/2}$ proton orbital, almost spherical shell-model states and their core-coupled configurations are known to coexist with deformed states arising from the $d_{5/2}$, $g_{7/2}$ orbitals intruding across the Z = 50 shell closure (Hey83), (Fog88), (Kaf88), (Rog90c). This situation results in shape isomerism, leading to retardation of transitions between states of different shapes of the nucleus. The situation is similar also for odd-A Rh nuclei, having five holes in the $g_{9/2}$ proton orbital (Rog88), (Rog90a). In addition, odd-A Rh nuclei are also predicted to have states with broken axial symmetry (Fra87), (Rog90a). This is consistent with the recent results on neutron rich even-even Ru nuclei, in which evidence on triaxial deformation is found (Äys90). Isomerism is also known in the odd neutron Pd nuclei. Here, in the middle of the $\mathcal{N}$ = 4 neutron shell, the isomeric state is due to the unique parity $h_{11/2}$ orbital. The exceptionally high hindrance of the decay of these isomeric states is an interesting feature, which is not observed in transitional odd-A Xe isotones. The large hindrance may reflect the importance of large neutron excess in odd-A Pd nuclei in this region. It most probably results from shape isomerism, possibly due to large oblate deformation connected with the $h_{11/2}$ orbital.

Beta decay in the studied region is mainly mediated by the $\nu g_{7/2} \rightarrow \pi g_{9/2}$ transformation. Deformation results in splitting of these orbitals, but the β-decay still occur mainly between the "Nilsson states" originating from the $\nu g_{7/2}$, $\pi g_{9/2}$ spherical shell model orbitals. This relatively simple spin-flip structure of β-decay in this region allows study of the Gamow-Teller strength as a function of deformation. This, however, necessarily involves some experimental knowledge on the location of the single particle orbitals. This knowledge is easiest obtained from the odd-A nuclei in this region.

The purpose of the present study has been to investigate the evolution of the shell structure and to determine the lowest quasiparticle excitations and to deduce the location of single particle levels in this region. Since reaction studies are not possible for these very neutron rich nuclei, the nuclear structure is studied mainly via β-decay properties. The isomeric states frequently occurring in these nuclei also provide an useful way to probe the structure of these nuclei.

Beta decay usually populates states with relatively low spin in the daughter nucleus. On the contrary, it has been known already for a long time that fission fragments may carry quite high angular momentum and it is also known that isomeric states with angular momentum up to 27/ 2 can be populated directly in fission (Lhe86). However, observation of isomeric states has been limited by their half-lives. The longest half-lives of isomeric decays observed in prompt γ-ray experiments have been typically of the order of several microseconds. On the other hand, the shortest half-lifes of isomeric states observed in mass separated sources are typically of the order of 100 ms or longer. As a rapid method, the IGISOL offers an appropriate approach to investigate isomeric states populated directly in fission down to the submillisecond region.

Use of the electron transporter ELLI (ELectron Lens for IGISOL) connected on-line with the mass separator (Par91), has made it possible to identify transitions with isomeric nature. Furthermore, ELLI was utilized in deducing the multipolarity of several transitions via observation of their internal conversion coefficients. This data and the observed β-decay properties have been used to deduce spins and parities of states.

Towards higher neutron excess, the data obtained in the present measurements become less and less detailed. However, even though it does not provide much information of nuclear structure and location of single quasiparticle states, it is not out of value. The data can be used, for example, in determination of fission product yield distribution, as shown in (Lei91), (Jau92). Additionally, the data on β-decay half-lives provide important information on the reliability of β-decay models used for example in astrophysical calculations.

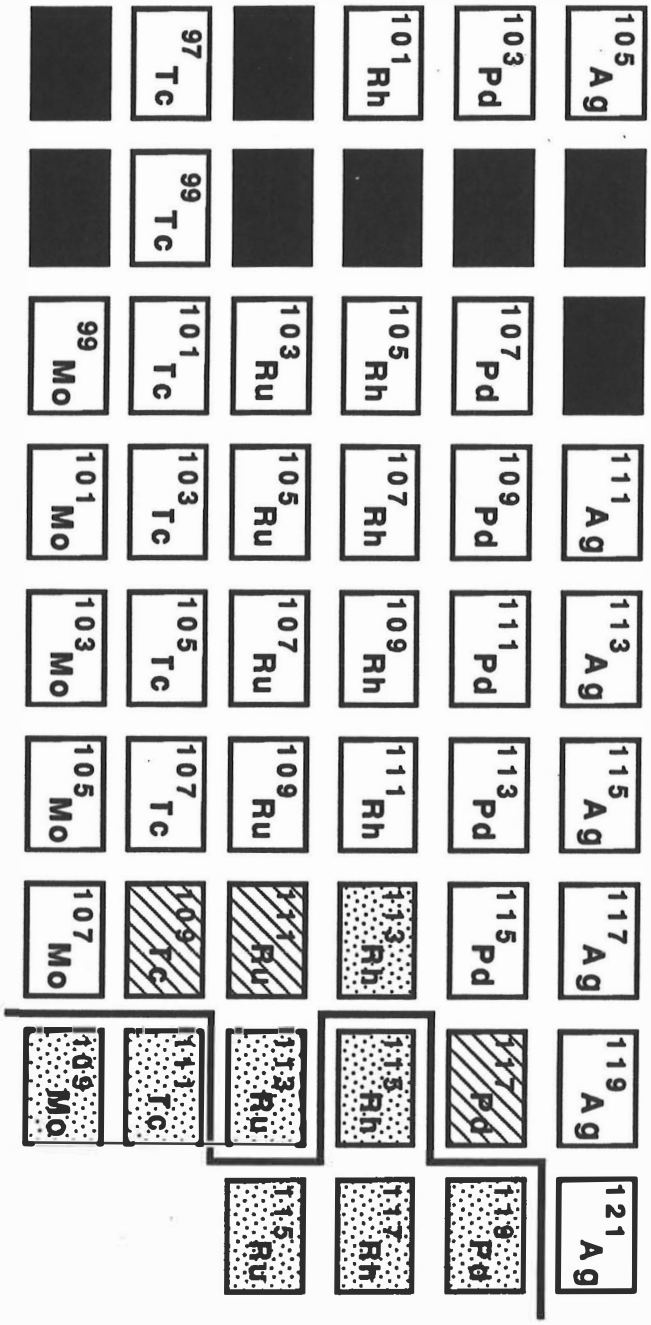

Figure 1.1. The region of the nuclei studied in this work. Stable isotopes are marked with black. The solid line shows the boundary of known isotopes prior to present study. The isotopes found in the present study are shaded. The shaded isotopes in the "previously known" region represent erroneously reported isotopes. Lighter shadow show the isotopes previously identified indirectly but for which the present study represents the first direct observation. Only the odd mass isotopes are shown.

The present work includes new results that are not published elsewhere. In order to completly rewiev the studies on neutron rich odd-A nuclei with the ion guide, this monography is partly based on the following published articles:

1) J. Äystö, P.Taskinen, M.Yoshii, J.Honkanen, P.Jauho, H.Penttilä and C.N.Davids, IDENTIFICATION AND DECAY OF NEW NEUTRON-RICH ISOTOPES ^{115}Rh AND ^{116}Rh, Phys. Lett. **201B**, 211 (1988).
https://doi.org/10.1016/0370-2693(88)90214-6

2) H. Penttilä, P. Taskinen, P. P. Jauho, V. Koponen, C. N. Davids and J. Äystö, HALF-LIFE MEASUREMENTS FOR NEUTRON-RICH Tc, Ru, Rh AND Pd ISOTOPES. IDENTIFICATION OF THE NEW ISOTOPES ^{111}Tc, ^{113}Rh AND ^{113}Rh, Phys. Rev. C **38**, 931 (1988).
https://doi.org/10.1103/PhysRevC.38.931

3) P. Taskinen, H. Penttilä, J. Äystö, P. Dendooven, P.Jauho, A. Jokinen and M. Yoshii, EFFICIENCY AND DELAY OF THE FISSION ION GUIDE FOR ON-LINE MASS SEPARATION, Nucl. Instr. and Meth. **A281**, 539 (1989).
https://doi.org/10.1016/0168-9002(89)91488-5

4) H.Penttilä, J.Äystö, P.P.Jauho, A.Jokinen, J.-M.Parmonen, P.Taskinen, K.Eskola, M.E. Leino, P. Dendooven and C. N. Davids, NEW NEUTRON-RICH NUCLEI AND ISOMERS PRODUCED IN SYMMETRIC FISSION, Physica Scripta **T32**, 38 (1990).
https://doi.org/10.1088/0031-8949/1990/T32/006

5) H.Penttilä, J.Äystö, K.Eskola, Z.Janas, P.P.Jauho, A.Jokinen, M.E.Leino, J. Parmonen, P.Taskinen, FIRST OBSERVATION OF THE BETA DECAY OF ^{117}Pd AND THE DISCOVERY OF A NEW ISOTOPE ^{119}Pd, Z. Phys. **A 338**, 291 (1991).
https://doi.org/10.1007/BF01288192

6) H. Penttilä, P.P. Jauho, J. Äystö, P. Decrock, P. Dendooven, M. Huyse, G. Reusen, P. Van Duppen and J. Wauters, IDENTIFICATION OF THE RARE NEUTRON-RICH ISOTOPE ^{117}Rh, Phys. Rev. C **44**, 935 (1991).
https://doi.org/10.1103/PhysRevC.44.R935

Previous results

The previous results in the studied mass region are, with only few exceptions, from three main sources. The earliest results were obtained in prompt fission fragment studies of spontaneous fission of ^{252}Cf (Joh70), (Hop72), (Hop73), (Che79) or ^{248}Cf (Hot91). These multiparameter coincidence measurements between gamma- and X-rays and the fission fragments were easy to perform for strongly fed nuclei, and were very suitable for detecting directly-in-fission-fed, isomeric states with half-lives up to several microseconds. However, the mass resolving power of such a system is rather modest. The mass assignment of the fission fragments was based on the energy signals from fragment detectors and the width of the deduced mass distribution was of the order of four mass units (Hop72). Results observed with this method have lead to some misassignments of decays, especially among the odd-A fission products.

The second group of studies was performed by the research group of the University of Uppsala which employed the OSIRIS isotope separator in Studsvik (Rud76). Using the plasma ion source ANUBIS (Jac87) located near the reactor core they were able to produce mass separated sources of short-lived Pd isotopes up to ^{116}Pd via thermal neutron induced fission of ^{235}U. For heavier Pd isotopes, short half-lives compared with the diffusion time of the ion source made their investigations impossible. For odd-A Ag isotopes up to ^{115}Ag they have observed a beautiful systematics.

A few occasional studies concerning these nuclei have been performed via chemical means. The only systematic series of studies in this region, which forms the third main source of information, is the research collaboration in the University of Mainz, which utilizes a rapid chemical separation technique SISAK for fission products of thermal neutron induced fission (Ska80). This research has partly taken place simultaneously with the present work; the decays of ^{109}Tc, ^{111}Ru and ^{117}Pd have been observed independently in Mainz and at JYFL (Alt90), (Rog90a), (Rog90b).

The fourth possible method to study nuclei in this region is the primary fission fragment separation (Mol75), (Bor87). However, except one experiment (Gra89) performed at LOHENGRIN fragment mass separator, studies at these facilities have concentrated on lighter nuclei (see e.g. (Lhe86)).

A = 109. The levels of ^{109}Rh can be investigated via ^{110}Pd(d,^{3}He)^{109}Rh reaction, and the structure of ^{109}Rh is indeed studied in detail via this reaction and via the β-decay of 34.5 s ^{109}Ru (Kaf87).

The observation of the β-decay of 109Tc is based on chemical separation of Tc, and its half-life 1.4 (4) s was determined from the growth-in component in the decay of the 206 keV gamma transition assigned to the β-decay of ^{109}Ru (Tra76). No gamma transitions assigned directly to the decay of ^{109}Tc was given. The half-life of 1.4 (4) s was also adopted in (Gra89), in which 13 gamma transitions were connected with the β-decay of ^{109}Tc. The experimental β-decay energies connected to nine of these gamma transitions are also given. The gamma transitions assigned to ^{109}Tc β-decay are 194.6 keV, 137.7 keV, 295.7 keV, 331.9 keV, 531.3 keV, 628.2 keV, 964.6 keV, 1073.5 keV, 1159.2 keV, 1268.1 keV, 1502.6 keV, 1632.6 keV and 1964.3 keV.

The β-decay of ^{109}Mo has not been observed, but in the measurements of prompt gamma rays from fission fragments of ^{252}Cf spontaneous fission five gamma transitions of 69.4 keV, 115.1 keV, 119.7 keV, 123.2 keV and 125.3 keV energies were assigned as transitions in ^{109}Tc (Bla84). In the same studies gamma rays at 74.2 keV, 98.3 keV, 131.8 keV, 172.3 keV and 374.2 keV were proposed as transitions in ^{109}Ru (Hop72), (Hop73). A level scheme for ^{109}Ru was proposed (Hop73) but it was never adopted by the evaluators of Nuclear Data Sheets. Furthermore, gamma transitions of 60 keV, 96 keV, 98 keV and 132 keV have been reported as transitions in ^{109}Ru (Bla84). The 96 keV gamma ray is connected with a lifetime of 550 ns (Joh70).

A = 111. The decay of ^{111}Rh (Kaf84) is relatively well established since besides the β-decay of a chemically separated Rh source (Kaf84) the levels of ^{111}Pd can also be reached via the reaction ^{110}Pd(d,p)^{111}Rh (Led78), (Bla90).

The decay of ^{111}Ru has been observed only indirectly by chemical means. A chemical study of Fettweis and del Marmol (Fet75) gives a half-life of 1.5 (3) s for ^{111}Ru. Their result for the half-life was based on delayed separation of Ru isotopes from fission of ^{235}U and on beta counting of their palladium granddaughters. Another chemical separation study of Matschoss and Bächmann (Mat76) introduces a novel method, chemical separation of ^{252}Cf fission products in gas phase. In this study, a half-life of 2.1 (6) s for ^{111}Ru was deduced from the growth-in component of the decay curve of the 275 keV gamma ray in ^{111}Rh decay. Franz and Herrmann (Fra78) used rapid chemical separation of fission products from thermal neutron induced fission reactions. They obtained a half-life of 3 (1) s from the growth-in

component of the decay curve of the 275 keV gamma ray in ^{111}Rh decay. Thus, no direct observation of the β-decay of ^{111}Ru was reported prior to the present studies.

In a prompt fission-fragment gamma ray coincidence measurement gamma rays with energies of 58.4 keV, 62.7 keV, 103.9 keV, 150.3 keV, 166.7 keV and 357.6 keV were reported as possible transitions in ^{111}Ru (Hop73) and also a decay scheme was proposed. In contrary to the case of ^{109}Ru, this level scheme was adopted by the evaluators of Nuclear Data Sheets. The β-decay of ^{111}Tc has not been reported prior to the present studies.

A = 113. The β-decay of ^{113}Pd has been studied by Fogelberg et al. (Fog88). The isomeric state expected to appear in ^{113}Pd on the basis of the systematics was not observed, and a question arises if it exists or not and what would cause this exception from the systematics of isomers known for lighter odd-A Pd isotopes.

The decay of ^{113}Rh was reported in a study of fission fragments produced in ^{252}Cf spontaneous fission (Wil69). The decaying source was produced in ^{252}Cf spontaneous fission with no separation. The half-life of ^{113}Rh was based on a 0.91 (8) s decay of a 128.51 keV gamma transition, which was assigned to decay of Rh via X-ray coincidences (Wil69).

The decay of ^{113}Ru with a half-life of 3.0 (7) s was reported in a study performed by chemical separation of fission products (Fra78). The identification was based on a 303.6 keV gamma transition, which was assigned to A = 113 on the basis of fission fragment study (Joh70). In fact, the mass assignment in (Joh70) was not exclusive since it also allowed an A = 112 assignment. The 303.6 keV gamma transition was assigned to the decay of Ru on the basis of X-ray coincidences in another fission fragment study (Hop72).

A = 115. The β-decay of ^{115}Pd was reported in (Fog88). In this study a β-decaying isomeric state in ^{115}Pd was also observed. This isomeric state was also observed to decay via an 89.4 keV E3 transition to the ground state of ^{115}Pd. From the β-decay properties of the two β-decaying states in ^{115}Pd the ground state was assigned with $I^{\pi} = 5/2^{+}$ (or $3/2^{+}$) and the isomeric state with $11/2^{-}$ ($9/2^{-}$).

A = 117. The β-decay of ^{117}Pd was for the first time indirectly observed by Weiss et al (Wei68). The observation was based on chemical separation and the half-life $5.0^{+0.7}_{-0.5}$ s was deduced from the ^{117}Cd activity after a delayed chemical separation of Pd. No gamma rays

were observed. In (Brü75) a 5.0 (4) s decay of a 247.1 keV gamma transition was reported, and assigned to the β-decay of ^{117}Pd or ^{118}Pd on the basis of chemical separation of neutron induced ^{249}Cf fission products. No direct observation of the decay of ^{117}Pd was thus reported prior to the present studies.

Independently of the present work the Mainz group has assigned the 247.5 keV, 323.9 keV and 402.5 keV γ-transitions to the β–decay of ^{117}Pd on the basis of a rapid chemical separation and determined a half-life 4.4 (2) s from the decay of these γ-transitions (Rog90b).

A = 119. Prior to the present studies, the most neutron rich isotope with A = 119 was ^{119}Ag, whose decay to the levels of ^{119}Cd was studied in (Kaw75). In this work, only one β-decaying isomer was observed. $I^{\pi} = 7/2^{+}$ was suggested for the observed state.

2. Theory

The atomic nucleus, although very small, is still far from being a point-like object. It has dimensions in space, and its shape has significant effect on the properties of nucleus. This is clear if one compares spectra of a nearly spherical nucleus like ^{128}Sn and a prolately deformed nucleus like ^{164}Er. However, the shape of the nucleus is not invariant but rather one of the dynamical properties of the nucleus. An excited nucleus can have a very different shape compared with the shape in the ground state. This does not mean that the shape would be a function of excitation energy: states with almost the same excitation energy can be related to different shapes. This coexistence of shapes was originally suggested for ^{16}O in the 50's (Hey83). The possibility of coexistence of shapes in heavy nuclei was also proposed, and it was experimentally confirmed when complete bands of levels built on different shapes were discovered in ^{72}Se and ^{184,186,188}Hg (Ham89).

The properties of a nucleus are described by two kind of models. In macroscopic models the nucleus is treated as a droplet of continuous, incompressible nuclear matter. In microscopic models the motion of individual nucleons is taken into account. A real microscopic calculation, however, would require solving a quantum mechanical many-body problem starting from the nucleon-nucleon interaction, which is not known exactly. Besides, such a calculation requires huge computational capacity. The general approximation is known as the single particle model. In this approach the single particle spectrum of an individual nucleon is calculated by solving the Schrödinger equation

$$H\Psi_\nu = \varepsilon_\nu \Psi_\nu \qquad (1)$$

in the average potential well which results from the interactions with the other nucleons. The Hamiltonian H is assumed to be of the form

$$H = V(r,\theta,\phi) + \frac{\hbar}{2M}\nabla^2 \qquad (2)$$

where $V(r,\theta,\phi)$ is the average potential and $\frac{\hbar}{2M}\nabla^2$ represents the kinetic energy of a nucleon with mass M. The solutions ε_ν, Ψ_ν depend on the potential $V(r,\theta,\phi)$. The potential used has been e.g. either the one with infinite walls like the harmonic oscillator (HO) or the modified harmonic oscillator (MHO), or the one with finite depth like a folded Yukawa

potential, or a Woods-Saxon (W-S) potential. Because the nuclear force has a short range, the shape and the size of the average potential are assumed to correspond to the shape and size of the nucleus. The possible deformation of the nucleus is included in the shape of the average potential. A traditional parametrization of the nuclear shape is the use of spherical harmonic functions $Y_{\lambda\mu}$, but other parametrizations of the nuclear shape exist (Nil55), (Pau73). In the present work the shell model calculations are performed in an axially deformed Woods-Saxon potential (Dud81), (Cwi87), as will be described in more detail below. In the W-S potential the axial symmetry can also be broken (triaxially deformed W-S potential).

However, the calculated single particle spectra do not reproduce the experimental magic numbers, as can be seen in figure 2.1. This is because of the velocity-dependent forces present in the nucleus. These forces are taken into account by introducing a spin-orbit correction term V_{so} in the potential V. This term is

$$V_{so}(r,\theta,\phi) = -\lambda\, \mathbf{L}\cdot\mathbf{S} \qquad (3)$$

where **L** is the angular momentum and **S** the spin of the nucleon. Potential $V(r,\theta,\phi)$ then reads

$$V(r,\theta,\phi) = V_c(r,\theta,\phi) + V_{so}(r,\theta,\phi) + V_{coul}(r,\theta,\phi) \qquad (4)$$

where V_c is the chosen central potential (HO, Yukawa, W-S), V_{so} is the spin-orbit potential, and V_{coul} is the Coulomb potential for protons. With these refinements the correct magic numbers are produced, as shown in figure 2.1.

The strong spin-orbit force is a unique feature of the nuclear system, and its strength has to be determined experimentally. It is immediately seen in figure 2.1 that the spin-orbit strength parameter λ is the most crucial to produce the correct order of single particle levels as well as the correct level spacings. The dependence on the central potential V_c is not that sensitive, since the changes of the central potential depth or radius do not change the order of single particle levels, as can be shown using variational calculus (Pau73).

In the single particle model particle orbits are calculated in an average potential. Deviations of the average potential are treated as residual interactions. The most important residual force is pairing. The nucleons filling time-reversed orbits, i.e. moving in the same orbit but in opposite directions, are on the average closer to each other than to the other nucleons. This results in an additional attractive force between the nucleons, which locally deepens the nuclear potential. Because of the strong pairing force, all even-even nuclei have $I^{\pi} = 0^+$ ground states without a single exception. The strong pairing also generates the 0^+–2^+energy gap in the even-even nuclei.

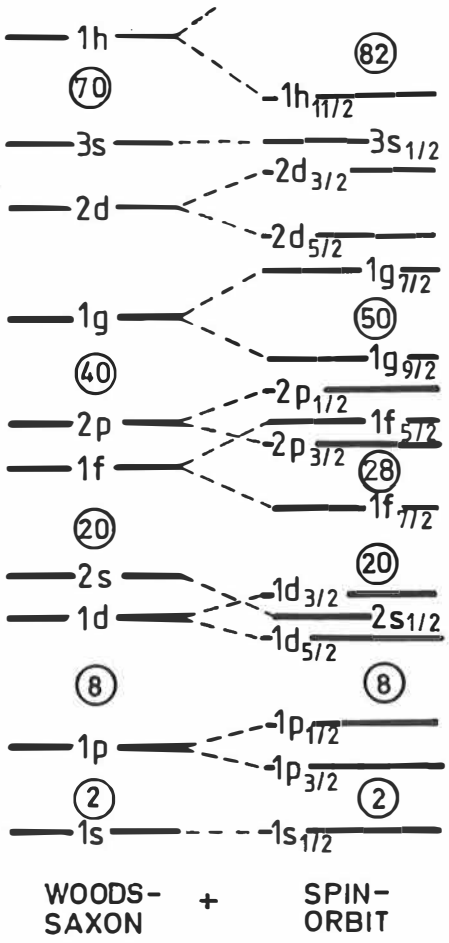

Figure 2.1. The effects of spin-orbit coupling to the single-particle spectrum in the spherical case. The circled numbers correspond to the calculated magic numbers with and without the spin-orbit coupling.

The effects of deformation on the single particle motion was studied theoretically by J. Rainwater (Rai50) and A. Bohr (Boh52). These studies were continued by S.G.Nilsson (Nil55). In his calculations in an axially deformed harmonic oscillator potential, the quadrupole deformation included. The deformed single particle model is also known as the Nilsson model and the plots of single particle spectra as a function of deformation are known as Nilsson diagrams. An example of a "Nilsson diagram" is shown in figure 2.3. The Nilsson model results in the breaking of degeneracy of the spherical shell model states. In deformed nuclei, the quantum mechanical angular momentum j is not any more a constant of motion whereas its projection Ω on the symmetry axis of the nucleus is. This explained the ground state spins and parities of well deformed odd-A nuclei in the rare earth and actinide regions which could not be explained by the spherical shell model.

The coexistence of different shapes can be easily understood starting from the Nilsson model. If the sum of the energies of the occupied single-particle orbits as a function of deformation has two equal minima, coexistence of shapes corresponding to these minima may result.

However, the single-particle energies do not represent the total energy of the nucleus. The method of calculating the total energy of the nucleus is known as the Strutinsky shell correction method (Str67). In this approach the microscopic and macroscopic models are combined in such a way that the smooth part of the summed discrete single-particle energies is replaced by the liquid drop energy of the nucleus. This procedure results in the total energy of the nucleus. The coexistence of shapes can now be understood as minimization of total energy of the nucleus, as is shown schematically in figure 2.2. If a Nilsson orbital, which energy decreases towards larger deformation, is occupied by valence nucleons, the total energy of the nucleus also becomes smaller at larger deformation. Since the energy of a liquid drop increases with increasing deformation, a minimum value of the total energy is achieved at some finite deformation.

In the present work neutron rich odd-A Pd nuclei are studied from this point of view using a nuclear model described in some detail below.

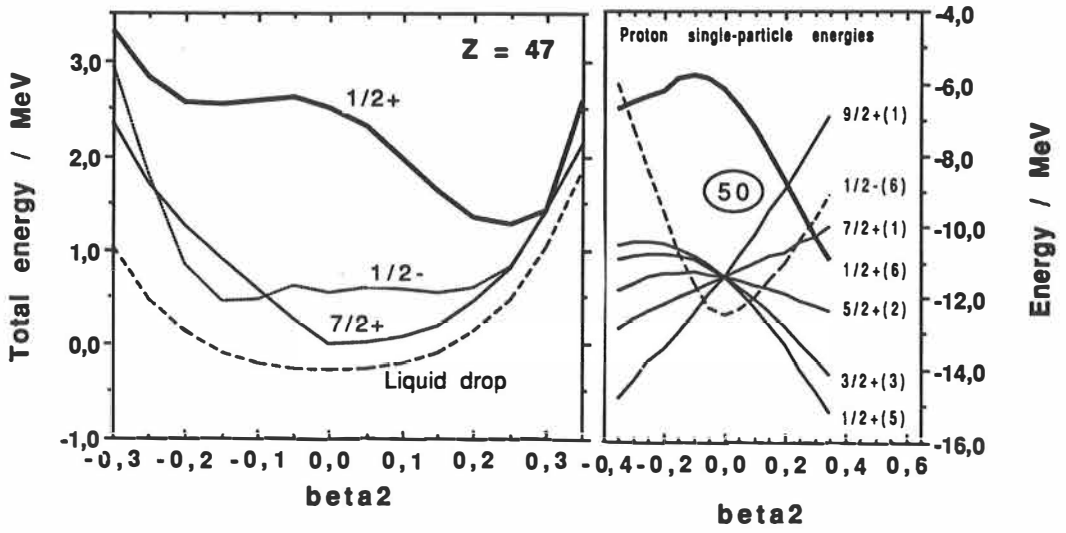

Figure 2.2. Schematic representation of the origin of shape coexistence starting from the deformed shell model. The $7/2^+$ state originating from the $g_{9/2}$ spherical shell model orbital has minimum energy with nearly spherical shape, whether the $1/2^+$ state originating from the $d_{5/2}$ orbital intrudes across the Z = 50 shell closure and has minimum at $\beta_2 \approx 0.25$. The $1/2^-$ state corresponding to the spherical $d_{1/2}$ orbital has oblate minimum.

Deformed macroscopic-microscopic model

The macroscopic-microscopic model calculations in this work are based on the Strutinsky approach in which the total energy of an axially deformed nucleus is calculated as a sum of a macroscopic term, a shell correction term and a pairing correction term:

$$E_{tot} = E_{macr} + E_{shell} + E_{pair} \tag{5}$$

Since the studied nuclei are located in the transitional region, they are expected to be soft against deformation and small changes in the shell correction term can push the nucleus towards different shapes. The concept of the calculations is to search for the minimum of the total energy of the nucleus as a function of deformation for each (single-quasiparticle)-state separately. The lowest value is expected to correspond to the ground state of nucleus.

The macroscopic energy term is calculated using the mass formula of Möller and Nix (Möl88). The shell energy corrections are based on single particle levels calculated in an axially deformed Woods-Saxon potential using the computer code "WSBETA" (Cwi87).

Pairing is taken into account in the calculations using the BCS equations

$$N_n = 2 \sum_{k=1}^{N_{states}} v_k^2 \tag{6a}$$

$$\frac{2}{G_n} = \sum_{k=1}^{N_{states}} \sqrt{(\varepsilon_k - \lambda)^2 + \Delta_n^2} \tag{6b}$$

$$v_k^2 = \frac{1}{2}\left[1 - \frac{\varepsilon_k - \lambda}{\sum_{k=1}^{N_{states}} \sqrt{(\varepsilon_k - \lambda)^2 + \Delta_n^2}}\right] \tag{6c}$$

where N_n is the number of (free) nucleons, and N_{states} is the number of single-particle states included in the calculation, v_k and ε_k are the occupation number and energy of the k:th state, λ is the fermi energy and G_n and Δ_n are the pairing strength and the pairing gap. In the present calculations, equations are solved using the average pairing gap method.

The average pairing gap $\tilde{\Delta}$ is first calculated using the formulas given in (Jen84). In the present work calculations are performed for nuclei with up to 14 neutrons more than the nearest stable isotopes. Thus, no experimental data of odd-even mass differences for calculating the pairing gap is available, and a semiempirical formula of ref. (Jen84) has to be

used. The average pairing gap can also be calculated from the formula of Madland and Nix (Mad88). The difference between these two models in this mass region is less than 10 %. The pairing strength G_n is obtained by solving the BCS equations using the average pairing gap $\tilde{\Delta}$ as Δ_n. For the actual calculations, the pairing strength G_n is fixed and λ, Δ_n, and v_k are calculated at different deformations from the BCS-equations (6). The single-particle energies ε_k are calculated for each deformation with in axially symmetric Woods-Saxon potential with the computer code "WSBETA".

The Woods-Saxon potential. The deformation of a nucleus can be defined by the nuclear surface S through the equation

$$S(r,\theta,\beta) = c(\beta)\, R_0 \left[1 + \sum_{\lambda \geq 2} \beta_\lambda\, Y_{\lambda 0}(\cos\theta) \right] \qquad (7)$$

where $\beta = \beta_2,\beta_3,\beta_4,...$ is a set of deformation parameters β_λ, which are defined as expansion coefficients of spherical harmonic functions in the above equation. $Y_{\lambda 0}(\cos\theta)$ are spherical harmonic functions, in which the axial symmetry of the studied nuclei is assumed. $R_0 = r_0\, A^{1/3}$ is the radius of the corresponding spherical nucleus, and $c(\beta)$ is a scaling factor determined from the condition that the volume of the nucleus is equal to the volume of corresponding spherical nucleus independently of deformation (constant volume condition).

The Woods-Saxon potential used in calculations is of the form

$$V(r,\beta) = \frac{V_0}{1 + e^{[\delta_S(r,\,\beta)/d]}} \qquad (8)$$

where $\delta_S(r, \beta)$ is equal to the distance between the point r and the nuclear surface defined by the surface S, d is the diffuseness parameter and V_0 is the central potential defined as

$$V_0 = V\left(1 \pm \kappa \frac{N - Z}{N + Z}\right) \qquad (9)$$

where the + -sign holds for protons and the – -sign for the neutrons. The parameters V, κ, the radius parameter r_0 (which can be chosen separately for protons and neutrons) and diffuseness parameter d used in the present calculation are selected according to Rost (Ro68) so that V = 49.6 MeV, κ = 0.86, r_0(protons) = 1.275 fm, r_0(neutrons) = 1.347 fm, and d = 0.70 fm. The choice of the central potential parameters is "arbitrary" in the sense that the calculation of single particle levels is not sensitive to minor changes of the central potential parameters. The choice of proper spin-orbit potential parameters is very crucial instead, as will be discussed below.

The spin-orbit potential is assumed to be of the form

$$V_{so} = \lambda \left(\frac{\hbar}{2Mc} \right)^2 \left(\nabla \frac{V_0}{1 + \exp[\delta_{S_{so}}(r, \beta)/d_{so}]} \right) \cdot (\sigma \times p) \qquad (10)$$

where λ denotes the strength of the spin-orbit potential (Cwi87). S_{so} is an auxiliary surface having similar shape as the nuclear surface and its location is determined by a radius parameter $(r_0)_{so}$ separately for protons and neutrons. The diffuseness parameter d is assumed to be the same for the central and the spin-orbit potential. M is the nucleon mass. The vector operator σ is connected with the nucleon spin operator **s** by the usual relation $\mathbf{s} = \frac{1}{2}\sigma$, and **p** is the linear momentum operator. This form of the spin-orbit potential arises from the fact that the only possible orientation inside the nucleus is the direction of the gradient of nuclear density near the nuclear surface. The effects and the selection on the spin-orbit potential are discussed below and also in (Dud80).

In addition to these, a Coulomb potential for protons is taken into account. The Coulomb potential is assumed to result from the nuclear charge of (Z – 1)e which is uniformly distributed inside the nuclear surface S. Details of the method of solving the Schrödinger equation in the described potential are given in (Cwi87).

An example of the calculated single-particle orbits is shown in figure 2.3. It is worth stressing that even though the plot in figure 2.3 may be called as a "Nilsson diagram", the corresponding energy levels are not Nilsson states. Therefore they are not labeled with asymptotic Nilsson quantum numbers Ω^π [N n_z Λ], but with Ω^π and an ordinal number only. Thus $7/2^+(2)$ means the second lowest single-particle orbit with $\Omega^\pi = 7/2^+$ and so on. This may be confusing, if one has used to the general custom to label states with asymptotic Nilsson quantum numbers Ω^π [N n_z Λ]. However, the asymptotic quantum numbers [N n_z Λ] do not have physical meaning either, but are rather labels for bookkeeping. Anyway, the actual wave function has to be calculated for each specified deformation. To demonstrate this, the decomposition of the $5/2^+(4)$ state is calculated at different deformations using the Nilsson asymptotic wave functions as base functions, as shown in table 2.1. The state is relatively well described with $5/2^+$[4 1 3] Nilsson state at large deformations, but the amplitudes of $5/2^+$[4 1 3] and $5/2^+$[4 0 2] states are almost equal at lower deformations. The fourth column shows how adding of hexadecupole deformation again effects remarkably on the decomposition amplitudes.

Table 2.1. Decomposition of the $5/2^+(4)$ neutron state at different deformations. The non-neglible amplitude of states from different main shells results from the potential.

$\Omega^\pi = 5/2^+$	$\beta_2 = 0.15$	$\beta_2 = 0.25$	$\beta_2 = 0.35$	$\beta_2 = 0.35;\ \beta_4 = 0.08$
[2 0 2]	– 0.2679	– 0.3053	– 0.3023	– 0.2922
[4 0 2]	– 0.6821	– 0.7682	– 0.7886	– 0.7237
[4 1 3]	– 0.5414	– 0.3342	– 0.2411	– 0.4258
[6 0 2]	0.3146	0.3923	0.4059	0.3945
[6 1 3]	0.1172	< 0.1	< 0.1	< 0.1
[6 2 2]	– 0.1054	– 0.1454	– 0.1701	– 0.1015

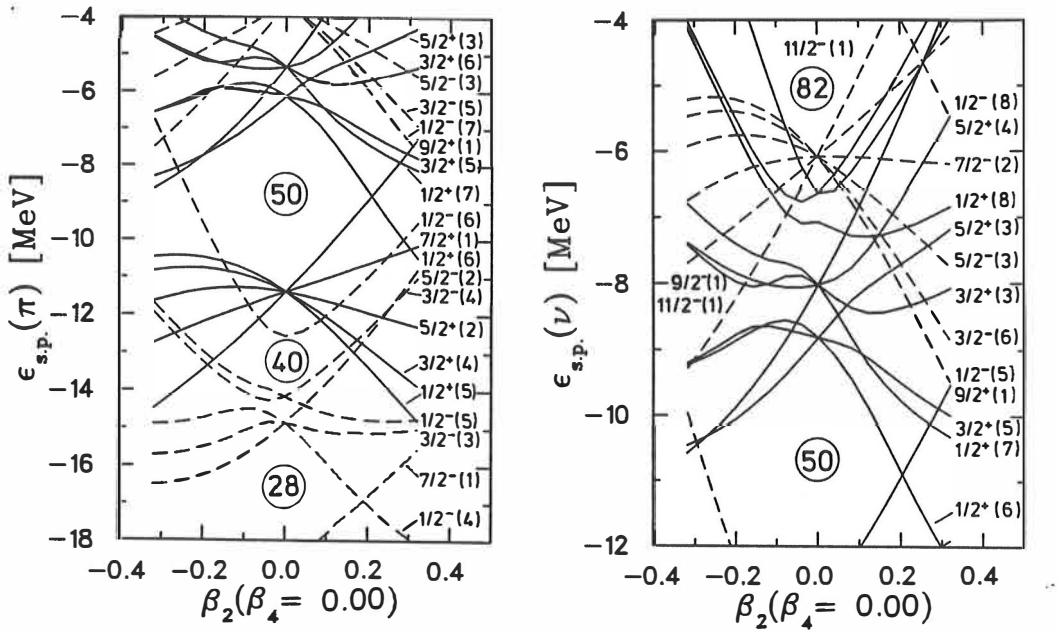

Figure 2.3. A "Nilsson diagram" in an axially deformed Woods-Saxon potential. The levels are calculated to correspond to ^{114}Pd using the "universal" set of parameters of the computer code "WSBETA". The calculation to the left is for protons and the one to the right for neutrons. The energy levels are labeled with Ω^π and an ordinal number. For details, see the text.

The spin-orbit potential. Since the location of the single-particle levels critically depends on the parameters of the spin-orbit potential, an effort was made to optimize these parameters in the studied region. The computer code "WSBETA" includes the possibility to select between five different parametrizations, most of which have been obtained by fitting calculated single particle spectra to experimental data on spherical nuclei, mostly ^{208}Pb. However, the code allows parameters defined by the user as well.

Different parametrizations are optimal in different regions and for different purposes. The so called "universal" set of parameters is generally accepted as the most reasonable choice, especially if the single-particle energies are calculated for an unknown region (see e.g. (Ryk89), (Möl90), (Vir89)). The "universal" set of parameters is originally based on the experimentally observed high spin states in the ^{208}Pb region (Dud81) and fine-tuned in ^{146}Gd (Dud82).

In purpose to test the applicability of the universal parameters in the $50 \leq N \leq 82$, $40 \leq Z \leq 50$ region, comparison of the calculated single particle spectra to the experimental data of odd-A Sn and Sb nuclei near Z = 50 and also of the N = 51 nuclei ^{89}Sr and ^{91}Zr was performed. These nuclei are known to be almost spherical at least at their ground states. For example, the experimentally determined electric quadrupole moments for the ground states of odd-A $^{115\text{ - }125}$Sb nuclei are ≤ 0.4 e^{2}b (Rag89). This corresponds to quadrupole deformation of the order of $\beta_2 \approx 0.02$. In the comparison, only the spin-orbit strength parameter λ and the spin-orbit radius parameter were varied, since changes of the central potential have very small effect. The spin-orbit potential was adjusted at the spherical limit mainly because there are more experimental data on these nuclei available, and scarce experimental data on nuclear deformation in the region of interest, the neutron rich transitional nuclei below Z = 50. The use of experimental bandhead energies from well deformed nuclei results also in some additional difficulties, that are described e.g. in (Rek76), in which reference the Nilsson model potential parameters are adjusted in a similar way.

There are also very little data on the odd-A Sn and Sb isotopes. The average excitation energies of the odd-A Sb nuclei were calculated as the weighted average of all states with the same I^{π}. The spectroscopic factors in one-particle transfer reactions from references (Bla87) for ^{117}Sb, (Aub79) for ^{119}Sb, (Tam79) for ^{121}Sb, (Tam80) for ^{123}Sb, (Tam81) for ^{125}Sb, (Has82) for ^{127}Sb, (Aub68) for ^{125,127,129}Sb were used as weights. Similar calculation was performed for ^{89}Sr (Sie89) and ^{91}Zr (Blo76), (Mül80). The average experimental excitation energies for $^{111\text{-}125}$Sn were taken from (Rek76).

The pairing correction for the single-particle levels was made using the equation

$$\varepsilon_k^* = \sqrt{(\varepsilon_k - \lambda)^2 + \Delta_n^2} - \Delta_n \qquad (11)$$

where ε_k^* is the excitation energy. The other symbols are as given above in the BCS-equations (6). Δ_n is taken from the average pairing gap $\tilde{\Delta}$ of (Jen84). The deduced experimental single particle energies are presented in table 2.2 for ^{89}Sr, ^{91}Zr and for $^{111\text{-}125}$Sn and in figure 2.4 for $^{117\text{-}129}$Sn.

As seen in figure 2.4, the experimental single-particle energies for the $^{117\text{-}129}$Sb isotopes behave in a peculiar way. In $^{121\text{-}129}$Sb the $d_{3/2}$ orbital comes far too close to its spin-orbit partner $d_{5/2}$. The 2d-orbit splitting can be compared to $g_{7/2}$ and $g_{9/2}$ spin-orbit partners, which are separating further from each other with increasing neutron number. In ^{117,119}Sb the d-orbital spin-orbit gap of about 2 MeV is reasonable. In these isotopes, the energy of the $d_{3/2}$ orbital is deduced as weighted average of four $3/2^+$ states populated in transfer reactions. In $^{121\text{-}129}$Sb, only one $3/2^+$ state can be found in the litterature. It is thus obvious that the low energy of the $d_{3/2}$ orbital results from insufficient data. Therefore, the $d_{3/2}$ orbital is not included in the calculations for the $^{121\text{-}129}$Sb isotopes.

Table 2.2. The experimental single-partigle energies (in MeV) for neutrons at N = 51 and N = 61 - 73 with Z = 50. The data is taken from references (Sie89) for ^{89}Sr, (Blo76), (Mül80) for ^{91}Zr and (Rek76) for $^{111\text{-}123}$Sn. The fermi energy in the BCS pairing calculation is assumed to coincide with the last filled single particle state.

SP-orbit	ENERGY [MeV]								
	^{89}Sr	^{91}Zr	^{111}Sn	^{113}Sn	^{115}Sn	^{117}Sn	^{119}Sn	^{121}Sn	^{123}Sn
$g_{9/2}$		– 3.6							
$d_{5/2}$	0.0	0.0	– 0.97	– 1.11	– 2.22	– 2.67	– 2.39	– 2.26	– 2.30
$s_{1/2}$	1.4	2.0	1.28	1.10	0.00	–1.10	– 0.73	– 0.77	– 0.76
$d_{3/2}$	2.4	3.3	1.53	1.56	1.34	0.50	0.55	0.58	0.70
$g_{7/2}$	2.8	3.5	0.00	0.00	– 1.82	– 2.23	– 1.99	– 1.99	– 2.16
$h_{11/2}$		3.2	2.22	1.92	1.25	0.00	0.00	0.00	0.00

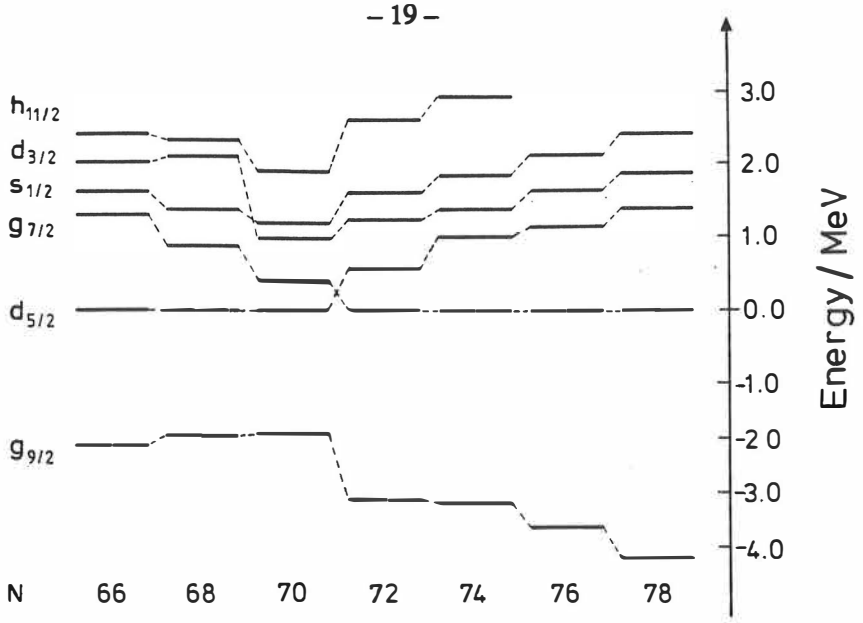

Figure 2.4. Experimental proton single-particle energies for odd-A Sb nuclei having one proton outside of Z = 50 shell closure. See text for the references.

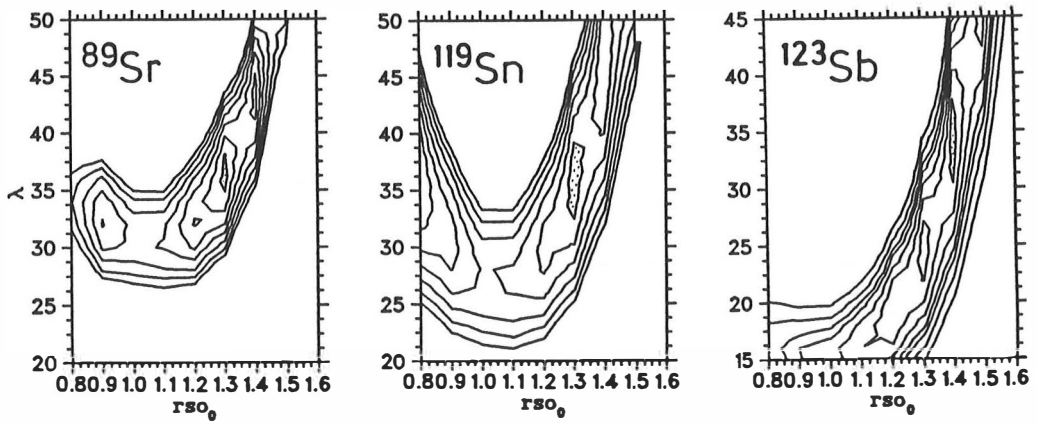

Figure 2.5. The contour plots of an auxiliary function δ, corresponding to the disagreement between the experimental and calculated single-particle levels.

The single-particle energies for a spherical nucleus were calculated with the code "SWBETA" for each nucleus separately varying the parameters λ and $(r_0)_{so}$. The calculated single-particle energies were compared to the experimental single particle spectrum using an auxiliary function

$$\delta = \sum_{sp} (\varepsilon_{sp}^{calc} - \varepsilon_{sp}^{exp})^2 ,$$

where ε_{sp}^{calc} and ε_{sp}^{exp} are the calculated and experimental single-particle energies, respectively.

The calculation was performed separately for neutrons and protons. Figure 2.5 presents the results of the calculations.

As seen in figure 2.5, there is not a well-located minimum for the auxiliary function δ, but rather a relatively deep and narrow valley in the $(\lambda,(r_0)_{so})$-plane. In practice this means that the change of the spin-orbit strength can be compensated by changing the spin-orbit radius and vice versa. This possibility is also discussed in (Dud81). From the figures one readily notices that all the optional $(\lambda,(r_0)_{so})$ parametrizations included in the "WSBETA" code lie in the valley of the $(\lambda,(r_0)_{so})$-plane. For the neutrons near N = 50, the deepest minimum corresponding to the best overall agreement between experimental and calculated single particle levels was found at $\lambda \approx 36$ and $(r_0)_{so} \approx 1.3$. Also, the odd-A Sn nuclei have local minima roughly at the same values. Even better agreement is achieved with parameter values of $\lambda \approx 36$ and $(r_0)_{so} \approx 0.8$, especially for the heavier Sn isotopes. However, such a low value for $(r_0)_{so}$ is clearly unphysical and rather result from purely coincidental agreement of the calculated single-particle spacings with the very limited number of experimental values; see also the discussion on the potential parametrization in (Pau73). For the protons, the odd-A Sb nuclei give the best agreement roughly with the values of $\lambda \approx 36$ and $(r_0)_{so} \approx 1.4$.

The results show that no attempt to really improve the "universal" set of parameters can be made with the incomplete experimental data available at present. However, the parameters of the Woods-Saxon potential need to be carefully investigated and are worth of a separate study. This is not meant to overlook the work in (Dud78), (Dud79), (Dud80), (Dud81), (Dud82), but rather recommend a proper reinvestigation using the most recent experimental data over the whole chart of nuclides and especially utilizing the remarkably improved calculation capability of present computers. The parameter optimization performed in the present work shows no reason to select any other parametrization but the "universal" one for the present calculations of transitional nuclei below Z = 50.

Calculations with the deformed macrocopic-microscopic model

The single-quasiparticle spectra were calculated for odd-A $^{103\text{-}115}$Rh, $^{105\text{-}117}$Pd and $^{107\text{-}119}$Ag nuclei. The quadrupole and hexadecapole deformations were taken into account in these calculations. The quadrupole deformation was allowed to vary from $\beta_2 = -0.36$ to $\beta_2 = 0.36$ with steps $\Delta\beta_2 = 0.04$ and the hexadecapole deformation was varied from $\beta_4 = -0.10$ to $\beta_4 = 0.10$ with $\Delta\beta_4 = 0.02$. The macroscopic energy was calculated using the mass formula of Möller and Nix (Möl88) and the pairing from the BCS-equations (6) using the average gap method and the mass formula from (Jen84). The single-particle orbits originating from the $2d_{5/2}$, $1g_{7/2}$, $2d_{3/2}$, $3s_{1/2}$ and $1h_{11/2}$ spherical neutron orbitals were taken into account for odd-neutron nuclei, and the single-particle orbits originating from the spherical $2p_{3/2}$, $2p_{1/2}$, $1g_{9/2}$, $2d_{5/2}$, $1g_{7/2}$ and $2d_{3/2}$ proton orbitals for odd-proton nuclei.

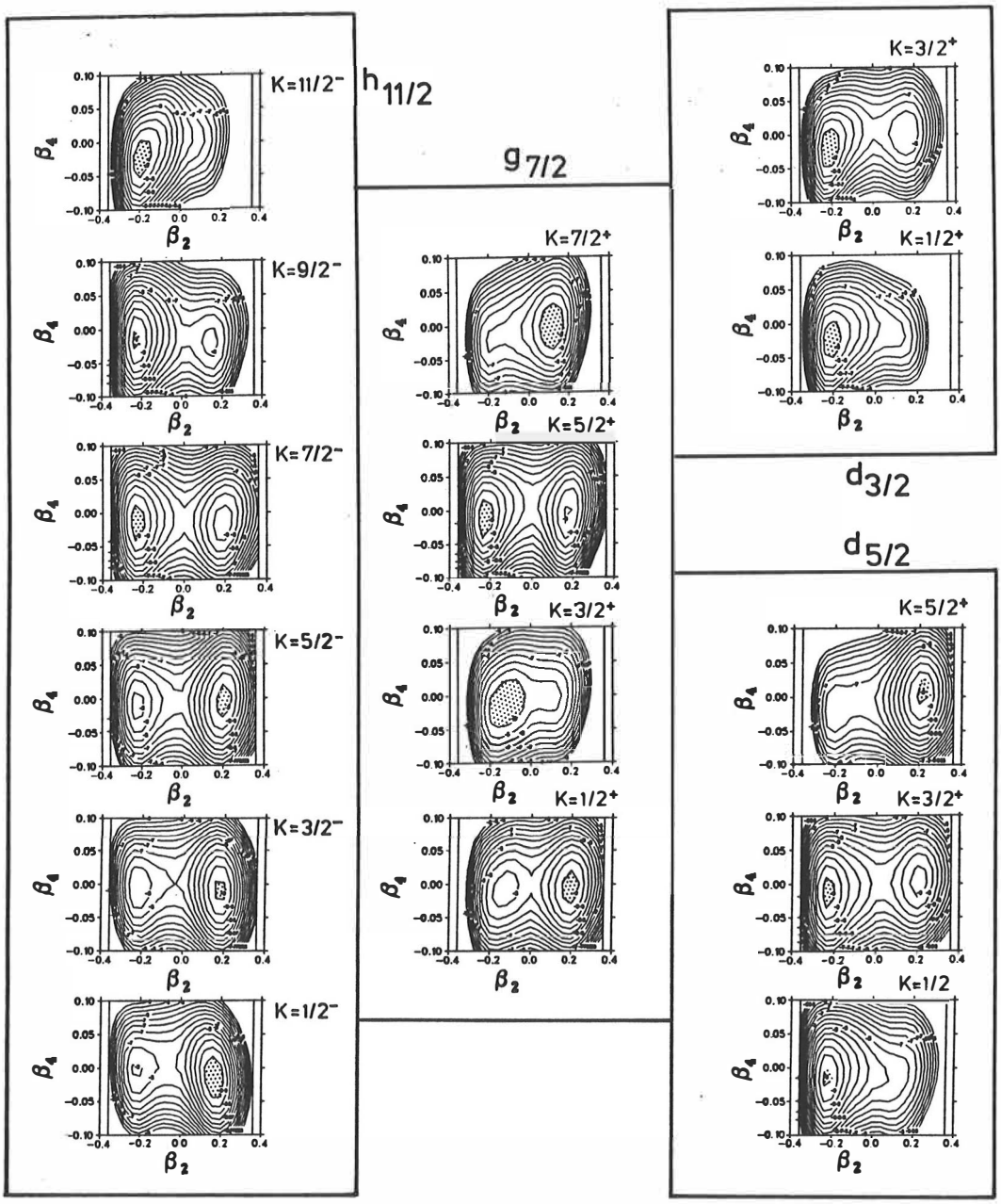

Figure 2.6. The calculated total energy surfaces in the (β_2, β_4)-plane for the neutron single-quasiparticle states. The separation of the contours is 250 keV. Plots are grouped according to corresponding spherical shell model state.

The calculated total energy surfaces in the (β_2, β_4)-plane for the neutron single-quasiparticle states originating from the $2d_{5/2}$, $1g_{7/2}$, $2d_{3/2}$ and $1h_{11/2}$ spherical neutron orbitals in ^{111}Pd are shown in figure 2.6. A general feature of these calculations is the oblate minimum in total

energy which appears to be roughly as deep as the prolate minimum for most states. In some cases the prolate minimum totally disappears. Since the nuclei in the studied region are supposed to be slightly prolate deformed, a question arises, if any states can be observed in the experimental spectra corresponding to these oblately deformed states. Comparison with the experimental spectra is done in chapter 5.

Triaxiality and core-coupled configurations

The macroscopic-microscopic model was used, because its concept is relatively straightforward and it is expected to be applicable to the transitional nuclei. The calculated states are single quasiparticle states, or Nilsson states, in an arbitrary deformed Woods-Saxon potential well. In well deformed nuclei there are always rotational bands build on these states. There are no collective rotations in spherical nuclei, but collective vibrations can couple to the motion of single nucleons. In transitional nuclei, where coexistence of shapes occur, both are possible. An example of rotational structure is the K=1/2 intruder band in odd-A Ag and Rh nuclei (Hey83), (Rog90). The low-lying $7/2^+$ state in the same nuclei can be explained within the Nilsson model, but its properties are probably best described as a three-hole cluster coupling to the vibrational core (Paa73), (Hey86). The $7/2^+$ state is also explained within the interacting boson-fermion model ((Hey86) and references given therein). In general, the collective excitations make the energy spectrum of these nuclei more complex, especially for the odd neutron nuclei, where there are more valence nucleons available than in the 3 or 5 proton hole nuclei Ag or Rh, respectively.

In the present macrosopic-microscopic calculations only the axially symmetric deformations were considered. However, it is experimentally known that axial symmetry is broken in neutron rich Ru nuclei (Äys90). In a recent theoretical study (Cha91) the expected ground state deformations in the transitional region were calculated. The lowest calculated total energy was observed to correspond to triaxial deformation for neutron-rich Ru nuclei. The neutron-rich Rh, Pd and Ag nuclei were calculated to have minimum total energy at axially symmetric deformations. The breakdown of axial symmetry results also in calculations employing nuclear supersymmetry, which means a unified treatment of odd-even, even-even and odd-odd nuclei (Fra87). This breakdown results in lowering of the energy of the second $5/2^-$, $3/2^-$ doublet in these nuclei. These states can also be explained as coupling of $p_{1/2}$ proton to the 2_2^+ state of the even-even core; the lowering of the 2_2^+ state reflects the triaxiality of the even-even core.

3. Experimental techniques

The main problem in the studies of radioactive nuclei produced in nuclear reactions is to separate the product of interest from other nuclei formed at the same time in the target with much higher yields. This is especially true for high-energy proton reactions, for fission and also for heavy-ion reactions. One of the most efficient methods, which allows the studies of particular product nuclei under sufficiently clean conditions, is the on-line mass separator. Such an instrument consists essentially of a target, an ion source and an electromagnetic mass analyzer coupled in series. An isotope separator operates on-line, when the production and the separation of the studied nuclei are both continuously performed (Rav89).

On-line mass separation is especially suitable to study nuclei far from beta stability. In some cases nuclei up to the nucleon drip-lines can be studied with on-line separators. However, the short half-life of the studied nuclei may cause severe losses of nuclei due to their decay. The reaction products formed in the target have to be thermalized in the system, transported to the ion source from which they are injected into the acceleration stage of the mass separator. In a conventional ion source the reaction products are stopped on a hot cathode or in a plasma and are ionizated by heating. The delay time in the ion source thus critically depends on the element to be ionized. The decay losses can be kept reasonably small even for very short-lived isotopes of some elements (Rav89), but in many cases the delay in the ion source dramatically reduces the efficiency for nuclides with half-lives below 1 s. A direct recoil separation technique (Mol75), (Bor87) removes these limitations. Such a separator is very fast; separation times are on the order of microseconds. However, they suffer from low intensities and have rather modest mass resolution.

3.1. The ion guide (IGISOL) method

The IGISOL, Ion Guide Isotope Separator On Line, is an approach that combines both of the mentioned methods. In principle, it can be used for radionuclides of all elements with a separation time of the order of a millisecond. The method is based on thermalizing the primary recoil ions from the target as single charged ions in helium and guiding them with helium flow and electric fields to a conventional mass separator. The idea of separating primary ions stopped in gas is not new (Ste70) but the first successfully operating device was developed in

Jyväskylä, first with a ^{227}Ac source (Ärj81a), (Ärj81b) and later in connection with the JYFL MC-20 light ion cyclotron (Äys84), (Ärj85), (Ärj87), (Äys87).

The primary ions from nuclear reactions are thermalized in flowing helium. In helium the initially high charge state of the ions is reduced via charge exchange reactions with helium atoms. Within a few microseconds the thermalized ions possess a +1 charge state. The high ionization potential of helium does not allow neutralization of ions in collisions with helium atoms. The time the ions remain singly charged after thermalizing is experimentally shown to be of the order of milliseconds or more (Tas89). The main neutralization mechanism is a three-body collision with an ion, a neutral atom and an electron, which is produced by the projectile collisions with helium atoms. Other neutralization mechanisms are diffusion into walls and collisions with impurity molecules. Neutralization due to impurities has a remarkable effect on the yield of +1 ions even though the impurity level in the He gas used at the IGISOL is only tens of ppm, the main impurities being N_2 (< 10 ppm), O_2 (< 5 ppm) and H_2O (< 10 ppm). A simple gas purification trap based on a liquid nitrogen cooled surface and a carbon filter was thus installed at IGISOL to lower the impurity level. The use of the purification trap improves the yields of +1 ions on average by a factor of two.

After their thermalization, the singly charged ions are transported by helium flow from the high-pressure region ($p_{He} \approx 100$ mbar) of the ion guide through an exit aperture (diameter 0.8 – 1.5 mm) into a low pressure region ($p_{He} \approx 0.1$ mbar). In this area the charged ions are guided by an electric field into the extraction stage of the mass separator through a conical skimmer electrode. Neutral He-gas is removed by a Roots blower. The electric field is typically 500 – 1000 V/cm, the distance of the skimmer and the exit hole is 5 – 15 mm and the hole at the tip of the skimmer electrode is 1.5 – 2.0 mm in diameter. High vacuum at the separator extraction and acceleration stages is achieved by high speed diffusion pumps.

The ion guide technique is very fast. The shortest-lived activity separated in test runs at the IGISOL is that of 64 μs ^{204m}Tl. The speed results from the very short delay time of the ion guide, which is of the order of 1 ms. Other advances of the ion guide are the non-selectivity with respect to chemical or physical properties of investigated ions and the operation at room temperature. The latter property quarantees that the method is very stable, which allows runs of the order of several days. This feature is important when nuclei produced with low cross section are investigated. The simple construction contains no parts which need replacement during the run.

The ion guide has been adopted in several experimental set-ups, covering a wide range in nuclear spectroscopy. It has successfully been used in spectroscopic studies of short-lived

mirror nuclei (Äys84), (Hon87), (Hon89), short-lived isomeric states (Lön84), β-delayed particle emitters (Äys88c), and in the production of short-lived actinides from radioactive Th targets (Huy88). The technique has also been used to mass separate fusion products in heavy ion induced reactions in combination with a gas filled recoil separator (Nom88) and mass separate fission products in light ion induced fission (Tas89), (Ast91).

3.2. The ion guide method and fission

The applicability of the ion guide method for all elements and the short delay time make the method an attractive approach to study neutron-rich fission products. The elements from Zr to Rh are still not available with conventional isotope separator ion sources. In the studies performed with the IGISOL the major drawback has been the low stopping efficiency for fission fragments in 100 mbar helium pressure. However, even with this practical limitation which is due to limited pumping capacity, a large number of new fission products have became available as mass separated ion beams with the IGISOL.

The neutron-rich nuclei studied with the IGISOL are produced via proton induced fission of ^{238}U. The fission process results in both asymmetric and symmetric mass divisions and it allows the study of the present frontier of the neutron rich nuclei between the mass numbers A = 80 and A = 160. Due to the high excitation energy of 25 MeV as compared to the thermal neutron induced fission, the proton bombardment of ^{238}U is a very competitive mean to produce neutron rich nuclei in the mass region A = 110 – 120 which corresponds to symmetric fission (Äys89).

Fission fragments differ considerably in their energy and angular distribution from the evaporation residues produced in light ion induced fusion reactions, previously studied with the IGISOL (Äys84), (Ärj84), (Lön84), (Ärj85), (Hon87), (Hon89). Thus, some redesign of the standard ion guide described in (Äys84), (Ärj85) was needed for the fission study application. The release of the total kinetic energy for the fragments is as high as 170 MeV in the proton induced fission of ^{238}U. To first order, the angular distribution of the fragments is isotropic (Coh55). Nearly isotropic angular distribution of fission fragments gives an additional degree of freedom in designing the ion guide. In the ion guide the main reason for the losses of thermalized +1 ions is the three-body collisions between ions, plasma electrons and neutral atoms, which is needed to carry away the momentum. The reduction of the amount of plasma electrons created by the projectile beam should raise the lifetime of ions in the helium gas and improve the efficiency of the ion guide. In the fission ion guide the projectile beam is isolated from the rest of the stopping chamber by a thin foil, as shown in figure 3.1. Some of

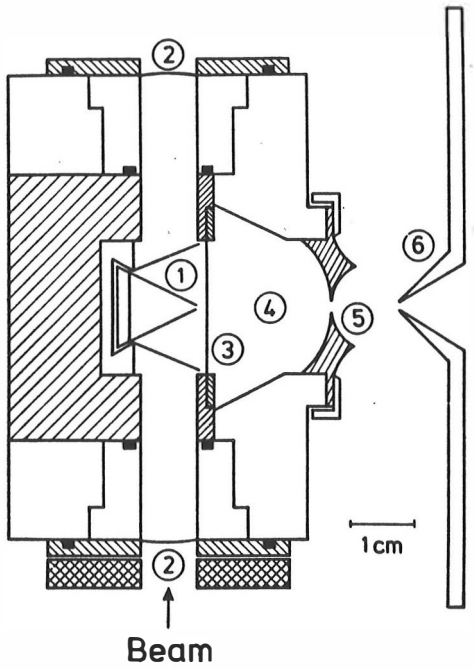

Figure 3.1. Design of the double chamber fission ion guide. (1) Uranium targets, (2) entrance and exit windows for the proton beam, (3) nickel foil, (4) stopping chamber, (5) exit hole, (6) conical skimmer electrode.

the isotropically distributed, initially very energetic fission fragments penetrate the 0.9 mg/cm^2 foil and enter the stopping chamber of the ion guide.The low-energy fraction of fission fragments is stopped in the helium gas in the stopping chamber. Since the helium in the stopping chamber is not ionized by the projectile beam, the fission ion guide can have a considerably larger effective volume than the standard design. To have a maximum opening angle for fission fragments from the four 15 mg/cm^2 ^{238}U targets, a curved foil is used to separate the targets from the stopping volume. A curved foil gives optimum laminar flow conditions for helium entering the stopping chamber surrounding the target area. The normal operating pressure of the IGISOL is about 100 mbar, giving a stopping efficiency of the order of 10^{-3} for the fission fragments.

The isotope separator coupled to the ion guide is of the Scandinavian type with a 55^o analyzing magnet. The beam of the mass separated radioactive ions is directed either into a counting station, consisting of a fast tape transport system and a conventional array of detectors for radioactivity studies, or to the source position of the electron spectrometer ELLI (Par91).

The mass calibration and the mass resolving power of the IGISOL are determined by introducing a trace amount of xenon in helium. The xenon atoms are ionized in collisions with the fission fragments in the stopping chamber of the ion guide. The Xe^+ ions transferred through the separator system give a perfect simulation to radioactive ions thermalized in the collection chamber. The intensity of Xe^+ ion beam is high enough to be detected by a conventional Faraday cup. The mass resolving power $R = M / \Delta M = B / 2 \Delta B = 330$ at FWHM is deduced from the A = 129 mass peak.

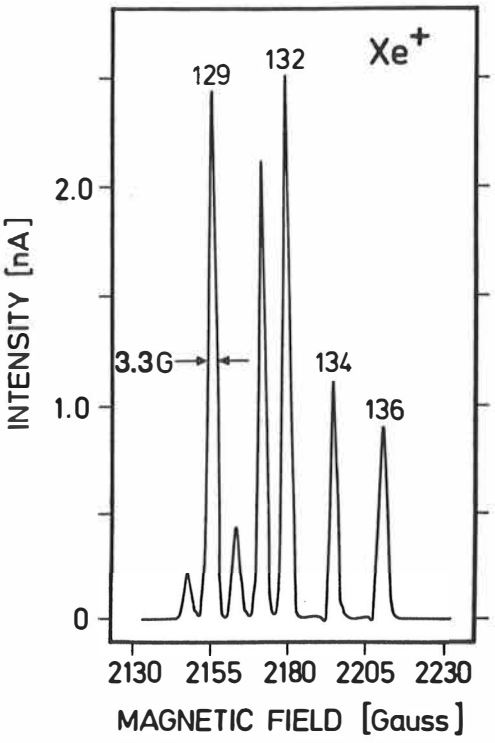

Figure 3.2. The figure shows a mass scan of stable Xe isotopes ionized by fission fragments using the double chamber fission ion guide and a helium pressure of 80 mbar. The spectrum is measured as a function of the magnetic field using a Faraday cup placed after a 1 mm wide vertical slit at the focal point of the analyzing magnet. The proton beam current on the four ^{238}U targets in this scan was 600 nA. The distance between neighbouring masses at A = 129 is about 14 mm.

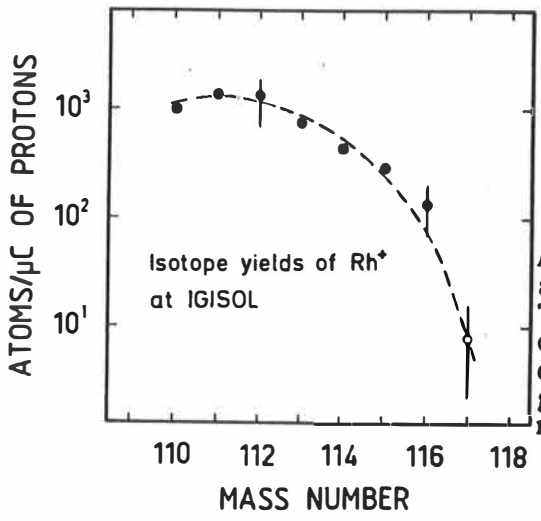

Figure 3.3. The cumulative yields of Rh atoms achieved with the fission ion guide. The yields of the given Rh isotopes are extracted from the saturation activities by correcting for the absolute efficiency of the gamma detectors as well as the branching ratios (Äys87), (Äys88a).

To show the capability of the fission IGISOL to produce neutron rich nuclei, the yields of neutron rich Rh isotopes are shown in figure 3.3. Prior to the studies with the IGISOL only the decay of ^{110}Rh was known in any detailed way.

3.3. Spectroscopy methods

The radioactive decays of the produced nuclei are studied with conventional spectroscopic methods. The collection station for gamma-ray, X-ray and β-particle spectroscopy consists of a narrow vacuum chamber and a moveable 1/4" wide collector tape in which the mass separated radioactive ion beam is stopped. The vacuum chamber has 10 mg/cm^2 thick plastic windows for measuring β-particles and low energy photons. The window material has about 90 % transmission for 20 keV X-rays and it is capable of holding a vacuum of 10^{-6} mbar. The windows are transparent, which makes it possible to check the collector tape without breaking the vacuum. A moveable mini Faraday cup is placed in front of the collector tape for final focusing of the separator beam with the Xe^+ ions.

The spectroscopy is performed at the point of implantation of the separator ion beam with various detector combinations. Counting at the implantation point is necessary in order to avoid decay losses of the studied radioactivity during the transportation of the source. The small size of the collector chamber allows counting with high geometrical efficiency. This is necessary, because the radioactive sources produced with the IGISOL are relatively weak. The lowest observed production rates for the most exotic nuclei have been of the order of 1 atom/s. The drawbacks of very close detector setups are summing of gamma rays and backscattering, the latter especially when detectors are facing each others.

In the present measurements, several detector combinations were used. A 1.4 cm^3, 7 mm thick planar Ge detector, or a larger, 10.0 cm^3, 10 mm thick planar Ge detector were used to observe characteristic X-rays and low energy gamma rays up to 400 keV. Larger coaxial high purity Ge detectors were used for gamma rays up to 2 MeV. The β-particles were detected with a ΔE_β detector, which typically consisted of 1.0 mm or 0.9 mm thick NE102 -type scintillation plastic sheet. The detector geometries used in the coincidence measurements are shown in figure 3.4. The set-up with the planar Ge detector, the large Ge detector and the ΔE_β detector was used for the elemental assignment of the observed radiations via the coincidences between characteristic X-rays and gamma rays. The (γ)(γ) coincidences at higher energies were measured by replacing the planar Ge detector with another large Ge detector, as is shown in figure 3.4. In the third geometry shown, altogether three Ge detectors were used. In this geometry the planar Ge detector was put as near to the source as possible, to reach maximum geometrical efficiency for characteristic X-rays. Two large Ge detectors were used to improve the geometrical efficiency for high energy gamma rays. An additional benefit was the lowered probability of coincidence summing in the large Ge detectors. Moreover, the (γ)(γ) coincidences between the large Ge detectors were recorded in the same run, and the beam time used for (γ)(X) measurement was maximized.

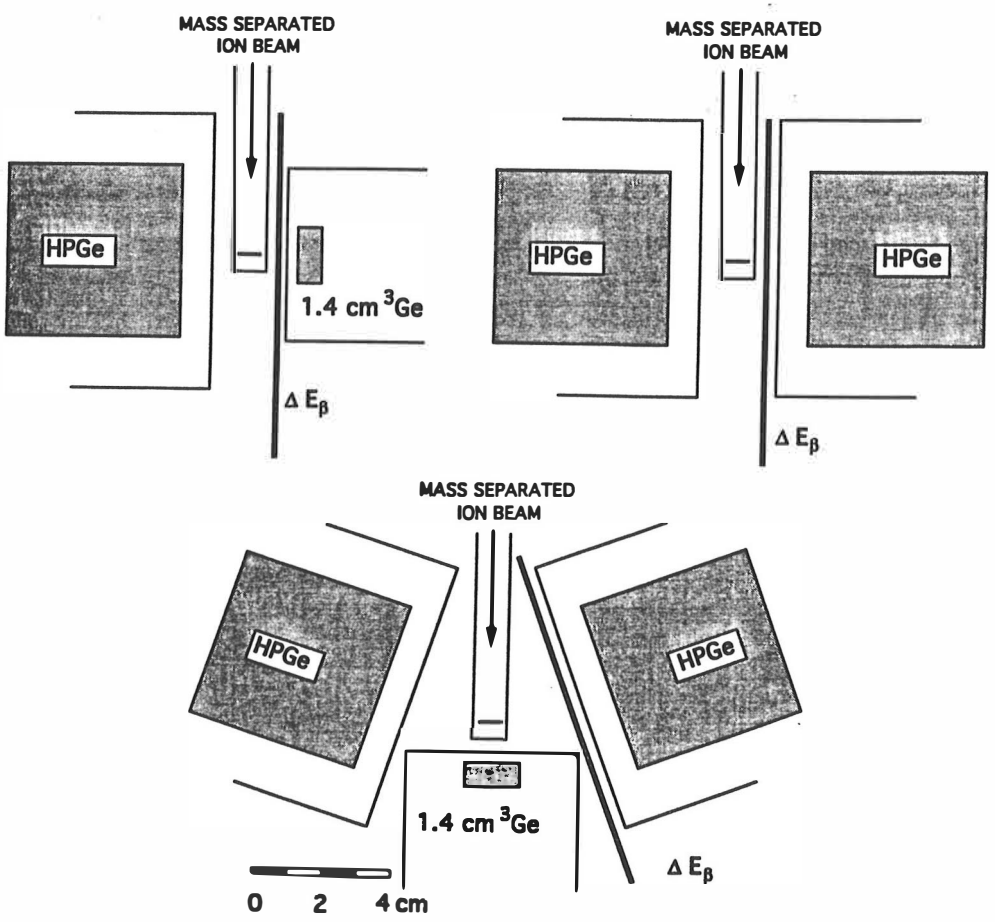

Figure 3.4. The X- and gamma-ray detector geometries used in the measurements with the fission IGISOL.

The scheme of a typical measurement is shown in figure 3.5. A sequence timer controls the ion source of the MC-20 cyclotron and the separator beam deflection. The clock also controls the tape unit and resets a time-to-digital converter (TDC) in the beginning of a collection cycle. The time information from this TDC is used for the half-life analysis of the studied nuclei. There is also another TDC, called a universal-time-TDC. This TDC is reset only in the beginning of each measurement. The coincident events are recorded event-by-event via a VME bus on a magnetic tape and the singles spectra on a computer disk. The energy signals from the detectors participating in the coincidence, and the readings of the two TDCs are written in each event. The parameter given by the universal-time TDC is often useful in the data analysis. In a run lasting several days one can expect difficulties such as separator high voltage or cyclotron breakdowns. Using the universal-time-TDC parameter the events recorded during such

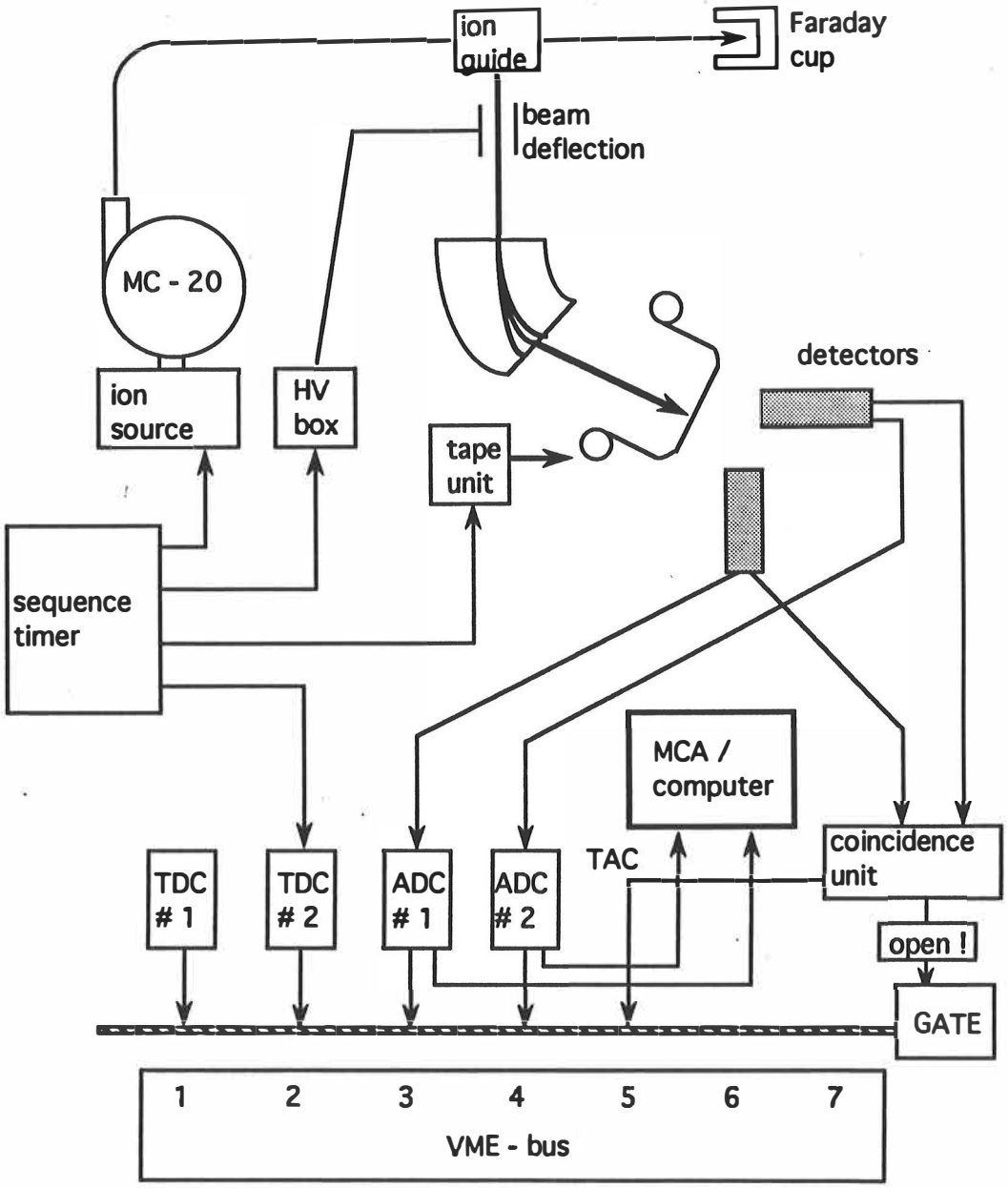

Figure 3.5. The flow chart of an IGISOL experiment. TDC#1 refers to the universal-time-TDC (see text).

periods can be easily omitted. With the help of this parameter also the possible gain shifts of detectors can be corrected in the off-line data analysis. The average yield of the mass separated ions of specified mass number with 1 μA proton beam current is of the order of 10^4 ions per second. This leads to counting rates of typically 10 – 100 coincident events per second.

There were only seven 4096 channel connections to the VME bus available. One of them was occupied by the universal-time TDC. The energy signals from each detector were recorded, which occupies three or four more connections. In addition, when the cyclotron and separator beams were pulsed, also the other TDC was connected to the VME bus. Thus, though the (γ)(γ)(t)- and (β)(γ)(t) coincidence time spectra were usually measured, their recording on the tape depended on the number of free connections to the VME bus.

The photopeak efficiency of the Ge detectors was measured in the counting geometry using calibrated gamma ray sources at the source position of the counting station. For the energy calibration of the Ge detectors, standard energy calibration sources as well as internal calibration were used. The summing of β-particles with gamma rays in the large Ge detector was avoided by setting the ΔE_β detector and gamma ray detector on opposite sides of the source. Absorbers for β-particles were used only in few cases.

Conversion electron spectroscopy. Internal conversion electron measurements are important for many reasons. Transitions at low energies are often highly converted and thus difficult to observe via other means. However, such transitions can be of key importance in constructing level schemes. Internal conversion coefficients (ICC) are also valuable for the multipolarity assignments of the transitions.

The short delay time of the ion guide allows studies of short-lived radioactive decays like the 1.50 (3) ms decay of ^{114m}Ag. Because of the short half-life also the conversion electron spectroscopy has to be performed at the point of implantation. Any mechanical transportation of such short-lived activities is out of question. Conversion electron measurements can be performed with a Si(Li) detector positioned near to the collector tape, but the background conditions are difficult. At the IGISOL facility this problem was solved by a magnetic electron transporter spectrometer, ELLI (ELectron Lens for IGISOL) (Par91). The ion beam of the IGISOL is implanted directly in the source position of the spectrometer. A magnetic field is used to transport electrons from the implantation point to a Si(Li) detector cooled to liquid nitrogen temperature. Since there is no need to mechanically transport the activity, the excellent time characteristics of the IGISOL can still be profited.

Elemental identification. The assignment of the gamma transitions to a specific nucleus was based on coincidences with characteristic X-rays, as shown in figure 3.6. X-rays in coincidence with gamma rays are produced via the internal conversion of other transitions in cascade with the observed one. The presence of low-energy, strongly converted transitions in the nuclei favors the use of the method in this region of transitional nuclei below Z = 50. The measured average yield of characteristic K X-rays in neutron induced and spontaneous fission in this region is 0.1 X-rays per fission fragment (Rei71). Other gamma rays can be assigned via the (γ)(γ) coincidences, as shown in figure 3.6.c).

A significant limitation in the (γ)(X) coincidence method is that those gamma transitions which are not in coincidence with any other gamma transition cannot be assigned. The first possible such a case is a situation in which an excited state, populated directly in the β-decay, decays via a single transition to the ground state. Typical examples are the 275.4 keV transition in the decay of ^{111}Ru and the 348.9 keV transition in the decay of ^{113}Rh. Such gamma transitions can be assigned trough the β-decay half-life if the half-life of the parent nucleus is otherwise known. The second case appears in single transitions between an isomeric state and the ground state. In both these cases the single transition can be identified in conversion electron measurements via the coincidences of conversion electrons with the characteristic X-rays, as shown in figure 3.6.d). X-ray coincidence is an effective method to assign conversion electrons, since the emission of a conversion electron is usually associated with a characteristic X-ray. The method is especially suitable for isomeric transitions, since those often have a high multipolarity and thus a large ICC. In this work the 194.9 keV transition in ^{109}Ru, the 348.9 keV transition in ^{113}Pd, the 71.4 keV transition in ^{117}Pd and the very important isomeric 81.3 keV transition in ^{113}Pd were identified using (e^-)(X) coincidences.

Beta decay half-life measurements. At the end of each implantation period the separator beam was deflected away by electrostatic plates to allow for a decay period. The ion source of the MC-20 cyclotron was also shut off for the decay period in order to lower the background due to the neutrons. The long-lived background activities, partly produced and mass separated simultaneously with the short-lived ones and partly being their daughter activities, were carried away from the detector by moving the collector tape at the end of each decay period. The β-decay half-lives were deduced from the decay of gamma rays observed in coincidence with β-particles. In some cases the characteristic X-rays, produced via internal conversion, provided the best statistics. In such cases the β-decay half-life was deduced from characteristic X-rays observed in coincidence with β-particles.

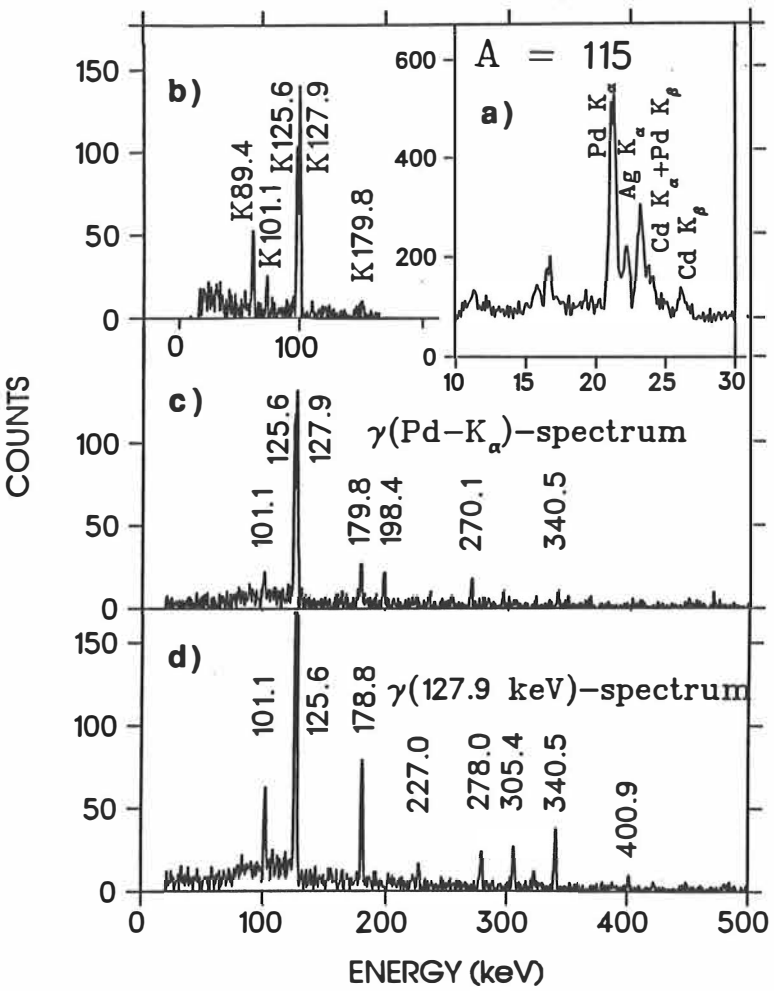

Figure 3.6. **An example of elemental identification of γ– and converted transitions.**

A typical X-ray spectrum detected in coincidence with γ–rays is shown in figure a). This spectrum at mass number A = 115 was recorded in 21 hours using the (γ)(X) set-up shown in figure 3.3. The 20 MeV proton beam was pulsed for the β-decay half-life analysis in cycles of 2.5 s on for producing activity and 5.0 s off for measuring the decay of the produced source. The yield of ^{115}Rh atoms was about 100 atoms/s during the beam on period, which leads to the total intensity of 4500 counts in K_α peak of the characteristic X-rays of Pd. The electron spectrum and the γ–ray spectrum seen in coincidence with the characteristic K_α X-rays of Pd are shown in figures b) and c). The energy scale of the conversion electron spectrum is shifted by 24.25 keV, the K-shell binding energy of Pd, to align the corresponding γ– and conversion electron transitions. More transitions are assigned via (γ)(γ) coincidence relations, as shown in figure d). Note that the K-89.4 keV peak due to the isomeric E3 transition to the ground state of ^{115}Pd can be assigned only via (e^-)(X) coincidences.

Half-lives of isomeric decays. The half-lives of isomeric states were deduced from the gamma rays assigned to the isomeric decay. The multispectrum method was usually used; in some cases, however, singles gamma ray events with the TDC time information were recorded on magnetic tape. For the shortest isomeric half-lives the decay and implantation periods were of the order of 100 ms or less. In these cases it was not practical to transport the source away with the collector tape at the end of each decay period. The source was moved away only from one to four times per minute; the proper time interval depended on the half-lives and the production rates of both the studied and the contaminating long-lived activities. Also, in the experiments performed with a continuous separator beam, the collector tape was used to transport the long-lived activities away to optimize the relative intensity of radioactive decay of interest.

Lifetime measurements of excited states. The delayed coincidence spectra were normally recorded in the measurements. However, some of the large Ge detectors had quite poor timing properties for the electronic lifetime measurements, especially at low energies. A more serious problem in lifetime measurements was the low production rate of the most exotic nuclei. $(\gamma)(\gamma)(t)$ spectra have often extremely low statistics. Thus, in most cases the $(\beta)(\gamma)(t)$ measurement provides better statistics and is used instead. It is, however, more sensitive to errors and requires a detailed knowledge of the decay scheme. In these measurements, it was possible to deduce some lifetimes, but due to above difficulties, the results are not very precise.

ICC measurements. The measurements of internal conversion coefficients were performed with the ELLI spectrometer by measuring the conversion electron spectra and the gamma ray spectra simultaneously. The gamma ray detectors used for this purpose were a 20 % coaxial Ge detector with a special design for the magnetic field, and the planar 1.4 cm^3 and 10.0 cm^3 Ge detectors mentioned above. Planar Ge detectors were in the first place used to observe coincidences between conversion electrons and characteristic X-rays. However, they have good energy resolution and their efficiency for low energy gamma rays is almost comparable to the 20 % Ge detector; moreover, the planar Ge detectors are relatively small and hence insensitive to both background neutrons and background beta radiation from the source. The lower efficiency of the planar Ge detectors as compared with the 20 % Ge detector is thus compensated by the favorable peak-to-background ratio at low energies. In most cases the gamma ray spectrum used to deduce the the internal conversion coefficients was observed using the planar Ge detectors. Even though their efficiency rapidly decreases above 200 keV, it did not cause major difficulties in measurements of odd-A nuclei, because the highest observed conversion electron energy was below 400 keV.

The set-up has to be calibrated in each measurement, because the efficiency of the ELLI is very sensitive to the position of the source (Par91). The focussing of the mass separator, achieved with Xe^+ ions and a mini Faraday cup, was confirmed with the A = 99 mass having a copiously produced 97.8 keV E2 transition in the decay of ^{99}Nb (Mül86). This, and three E2 transitions, 118.6 keV and 212.5 keV in ^{100}Zr and 159.5 keV in ^{100}Mo at A = 100 mass (Sin90) were used to normalize the gamma ray efficiencies for the Ge detectors and the conversion electron transmission for the ELLI. The experimentally known α_K values, if available, were used as internal calibrators to check the normalization in each run.

The α_K values were in the first place deduced from simultaneous measurement of conversion electron and gamma ray singles spectra. The K/L ratios deduced from the electron singles spectra can be used to distinguish between L = 1 and L = 2 transitions. Especially the M1 and E2 transitions can be separated this way. The background conditions can be significantly improved using gated spectra. A β-gated gamma ray spectrum from another measurement often gives much better statistics to determine the intensities of gamma transitions. Beta gated conversion electron spectra were also taken in these measurements. When the converted transition and the gamma transition intensities were measured separately, they had to be normalized to each other using transitions with known α_K values. Normalization has to be made separately for each nucleus to avoid effects of different half-lives on the relative transition intensity. Thus, at least one α_K for each nucleus has to be measured in a simultaneous measurement of conversion electrons and gamma rays.

The electron transition intensity can also be deduced from an electron spectrum gated by characteristic K X-rays. The multiple lines in the singles electron spectrum can be separated in this way. The normalization is then performed for each nucleus separately. In the use of X-ray coincident electron spectra some care is needed. A characteristic X-ray in coincidence with conversion electrons can be produced via another transition in cascade with the observed one; the intensity of the electron transition is thus increased which has to be taken into account. Also, the statistics in the X-ray gated gamma spectrum is low as compared with the β-gated electron spectrum. Therefore, the X-ray gated spectrum was used only in the most difficult cases.

The internal conversion of a transition can also be deduced from the yield of the characteristic X-rays. The amount of X-rays produced by a transition can be observed by gating with a proper transition in cascade with the studied one. The level scheme has to be known accurately to separate all contributions to the observed intensity of X-rays in the gated spectrum. For some transitions in this work the conversion coefficient α_K was deduced using this method.

Data analysis. The common analyzing programs available at JYFL were used in the data analysis. The programs include standard matrix sorting and matrix gating programs as well as programs for sorting spectra directly from the event tapes.

For the analysis of gamma ray and conversion electron spectra several programs were used. In every program, however, similar fits were performed. For gamma rays, a gaussian shape fit with or without tail was used. In conversion electron spectra the peaks have much stronger distorted gaussian component, especially at low energies (Trz89). A shape fit with a gaussian, a distorted gaussian and a step function components was thus used. The intensities of the gamma transitions were deduced from a gamma ray spectrum observed in coincidence with β-particles. The effects of (γ)(γ) coincidence summing to first order have been taken into account. The adopted intensity values in this work are typically weighted averages of different measurements with different gamma detectors. The intensity errors given in the tables include statistical and fit error.

3.4. Experiment at Louvain-la-Neuve

The production rate for ^{116}Rh, the heaviest known Rh isotope (Äys87) prior to the measurement described below, was about 50 - 100 atoms/s normalized to 1 μA proton beam intensity (Lei91). The studies of heavier isotopes were hampered by their low production rate. The main difficulty was the limited beam intensity at the MC–20 cyclotron, which was of the order of 1 μA at maximum with 20 MeV protons. Thus, the experiment to search for the ^{117}Rh decay was performed with the ion guide set-up of the LISOL facility located at the CYCLONE heavy ion cyclotron laboratory in Louvain-la-Neuve.

The nuclei studied were produced with 23 MeV proton induced fission on ^{238}U. Four targets with a total thickness of 40 mg/cm^2 were used. The isobaric chain with A = 117 was mass separated and implanted in a moveable collector tape. The radioactivity of the produced nuclei was detected at the point of implantation with a 70 % n-type Ge detector, a 500 mm^2, 10 mm thick planar low energy Ge detector and a 1 mm thick NE-102 type plastic detector operating as a ΔE_β detector for β-particles. Only double or triple coincidence events were recorded together with the cycle time information from a TDC. The cyclotron beam was pulsed to create an implantation and decay period. One cycle consisted of a 1.5 s implantation period followed by a 3.0 s decay period. The background produced by the long-lived radioactive nuclei in the same isobaric chain was reduced by transporting the source away after each ten collection cycles. In this measurement the lower limit of the production rate of ^{117}Rh was observed to be about 5 ions/s normalized to 1 μA proton beam intensity.

4. Experimental results

Fifteen new isotopes have been found in the studies of fission products with the ion guide technique. The decays of the new odd-A isotopes, shown also in figure 1.1, i.e. ^{109}Mo, ^{109}Tc, ^{111}Tc (Pen88), ^{111}Ru, ^{113}Ru (Pen88), ^{113}Rh (Pen88), ^{115}Rh (Äys88a), ^{117}Rh (Pen91b), ^{117}Pd (Pen91) and ^{119}Pd (Pen91), are reviewed in this chapter. The other new isotopes with the even mass number, reported elsewhere, are ^{118,120}Pd, (Kop89), (Jan91), ^{116}Rh (Äys88a), ^{112,114}Ru (Pen88), (Jok91) and ^{112}Tc (Äys90). These isotopes were discovered in Jyväskylä, with the exception of ^{117}Rh, which was found at LISOL facility in Louvain-la-Neuve, Belgium.

4.1. Elemental identification

The elemental identification of the produced radioactive isotopes was based on the X-ray coincidence method, as described in chapter 3. (γ)(X) coincidence measurements were performed in the case of six odd mass numbers from A = 109 to A = 119 using the experimental set-ups shown in figure 3.4. The acquisition time required for each measurement varied from 20 hours for A = 111 to 48 hours for A = 119. The number of γ-transitions observed in coincidence with characteristic X-rays for different isotopes varied between one and 22. A typical yield of K_α X-rays was 5 – 10 % of the amount of β-decays. The γ-transitions assigned using (γ)(X) coincidences are given in table 4.1.

A series of conversion electron measurements was performed using the magnetic conversion electron spectrometer ELLI (Par91),and (e^-)(X) coincidence measurements were performed for the same six odd mass numbers as the (γ)(X) measurements. In these measurements 30 conversion electron transitions were identified via their X-ray coincidences. These transitons are given in table 4.1. Seven transitions were assigned only via their conversion electron decays.

The elemental identification in the (e^-)(X) studies was limited to the characteristic K X-ray coincidences. In the present measurements the applicable energy region begins 10 – 15 keV above the K-electron binding energy of each element due to the noise level in the conversion electron detector. However, highly converted transitions of low energy may become of key importance in the structure of many nuclei. (e^-)(L X) coincidence measurements would provide a powerful spectroscopical tool at low energies. In future experiments, the possibility of detecting L X-rays in coincidence with low energy conversion electrons should be carefully investigated.

Table 4.1. The elemental identification of the observed transitions (D stands for doublet). The gamma ray energies are from the (γ)(X) coincidence spectra. The energies may, in some cases, due to low statistics, differ up to 0.6 keV from the values determined from the (γ)(β) spectra. The β-coincident γ-transition energies are given in tables 4.3 – 4.4, 4.6 – 4.19 in chapter 4.2. K-conversion electron energies refer to the transition energy.

	GATE	GAMMA RAYS [keV]	K-CONVERSION ELECTRONS [keV]
A = 109	Tc K_α	289.1	
	Ru K_α	58.4, 68.7, 69.1, 96.2, 98.5, 117.7, 122.5, 128.7, 138.2, 171.7, 186.9, 208.0, 267.3, 278.8, 289.6, 300.3, 323.7, 336.6, 376.7, 445.8, 490.1, 589.7	69 (D), 96.2, 98.5, 128.7, 138.2, 186.9, 195.0
A = 111	Ru K_α	267.0	147.1, 150.4
	Rh K_α	78.5, 114.5, 136.8, 189.4, 211.7, 250.8, 280, 303.9, 1265.5, 1515.7	78.4, 91.3, 136.8, 189.4, 211.7, 303.8
A = 113	Rh K_α	185.6, 206.0, 211.0, 227.6, 263.5, 338.3, 353.0	
	Pd K_α	79.4, 84.0, 116.3, 120.3, 135.2, 137.1, 151.3, 157.0, 189.8, 217.2, 220.8, 252.3	79.3, 81.3, 135.2, 189.8, 348.9
A = 115	Pd K_α	101.1, 125.6, 127.9, 179.9, 198.4, 227.0, 270.1, 305.6, 340.5	89.4 , 125.6, 127.9, 179.9
A = 117	Pd K_α	34.5, 97.1, 131.8, 168.6, 481.6	71.4, 168.6
	Ag K_α	76.6, 247.1, 401.8, 521.8	76.5, 247.3, 323.1
A = 119	Ag K_α	256.3	

4.2. The experimental β-decay half-lives

The β-decay half-lives were measured as described in chapter 3. Half-lives are usually based on the decay curve of γ-rays in a daughter nucleus observed in coincidence with β-particles. If several transitions are used in the analysis, the final half-life is the weighted average of the individual half-lives. In the cases of ^{109}Mo and ^{117}Rh the characteristic X-rays observed in coincidence with the β-particles have been used. The measured β-decay half-lives are given in table 4.2. Each decay is discussed in more detail below.

^{109}Mo

A 289.1 keV γ-transition appeared in coincidence with the characteristic K X-rays of Tc, giving the first evidence of the β-decay of ^{109}Mo. This γ-transition was also observed in coincidence with a 65.1 keV γ-transition. No sign of the previously reported 69.4 keV, 115.1 keV, 119.7 keV, 123.2 keV and 125.3 keV γ-transitions in ^{109}Tc (Bla84) were found. Instead, γ-transitions with similar energies, namely 69.1 keV, 117.7 keV, 122.4 keV and 128.6 keV, were observed to belong to the β-decay of ^{109}Tc.

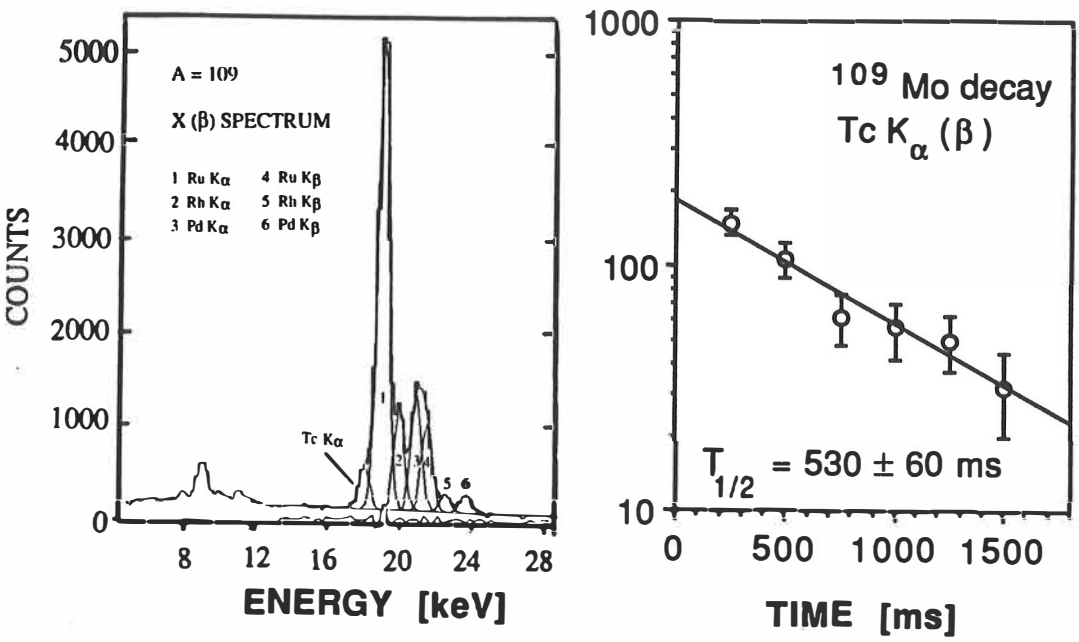

Figure 4.1. The figure on the left shows the characteristic X-ray spectrum at mass number A = 109 observed in coincidence with β-particles. The figure on the right shows the decay of the characteristic K_α X-rays of Tc, following the β-decay of ^{109}Mo.

Table 4.2. The observed β-decay half-lives for the studied odd-A nuclei.

Decaying nucleus	T 1/2 [s]	Deduced from	T 1/2 [s]	Previous value [s]
^{109}Mo	0.54 ± 0.06	Tc K X-rays*)	0.59 ± 0.11 0.53 ± 0.06	
^{109}Tc	0.87 ± 0.04	96.1 128.7 195.0	0.83 ± 0.08 0.89 ± 0.09 0.87 ± 0.04	1.4 ± 0.4 [1]
^{111}Tc	0.30 ± 0.04	150.4	0.30 ± 0.04	
^{111}Ru	2.11 ± 0.08	211.7 303.8	2.13 ± 0.11 2.10 ± 0.10	2.2 ± 0.7 [2]
^{113}Ru	0.80 ± 0.06	88.3 211.7 263.3	0.92 ± 0.13 0.66 ± 0.18 0.79 ± 0.06	3.0± 0.7 [3]
^{113}Rh	2.80 ± 0.12	84.9 117.0 137.5 189.8 348.9	2.68 ± 0.44 2.84 ± 0.29 3.00 ± 0.45 2.78 ± 0.25 2.79 ± 0.17	0.91 ± 0.08 [4]
^{115}Rh	1.02 ± 0.03	127.9 *)	0.99 ± 0.05 1.04 ± 0.03	
^{117}Rh	0.44 ± 0.04	Pd K X-rays	0.44 ± 0.04	
^{117}Pd	4.3 ± 0.2	247.3	4.3 ± 0.2	5.0 ± 0.4 [5] $5.0\ ^{+0.7}_{-0.5}$ [6]
^{119}Pd	0.92 ± 0.13	256.6 326.1	0.88 ± 0.18 0.95 ± 0.19	

*) Values from two different runs.

[1]) (Tra78); [2])Value adopted by Nuclear Data Sheets; unweighted average of (Fet75), (Mat76) and (Fra78); [3]) (Fra78); [4]) (Wil69); [5]) (Brü75); [6]) (Wei68).

Unfortunately, a 289.6 keV γ-transition appears in the decay of ^{109}Tc, and it was impossible to separate the 289.1 keV and the 289.6 keV γ-transitions by any means for half-life determination. Furthermore, the half-lives of ^{109}Mo and ^{109}Tc appeared to be so similar that the ^{109}Mo half-life cannot be separated in a two-component fit to the decay curve of this doublet. The intensity of the 65.1 keV γ-transition was too low for a half-life measurement. Finally, the β-decay half-life of 0.54 (6) s was determined from the characteristic K X-rays of Tc gated by β-particles, as shown in figure 4.1. The adopted value is the average of the results from two different runs. Most of the characteristic X-rays are due to the internal conversion of the 65.1 keV transition. Its E2 multipolarity was deduced from the yield of the characteristic K X-rays. The internal K-conversion coefficient was obtained to be $\alpha_K = 5$ (3). This result could not be confirmed by a conversion electron measurement, because of the low yield of ^{109}Mo and the presence of the converted 69.1 and 68.7 keV transitions in ^{109}Ru and the 68.1 keV transition in ^{109}Rh.

^{109}Tc

Altogether 22 γ-transitions appeared to be in coincidence with the K X-rays of Ru. Nine additional γ-transitions were assigned via their (γ)(γ) coincidences. The most intense transition, 195.0 keV, does not show up in coincidence with X-rays or other γ-rays. Its belonging to this decay was confirmed via (e^-)(X) coincidences, as shown in figure 4.2. In (Alt90) this γ-transition was reported to appear in coincidence with a 138 keV γ-transition, but this was not confirmed in the present work. Three γ-transitions with the best statistics in the β-coincident spectrum were used for the half-life analysis. A half-life of 0.86 (3) s was adopted for ^{109}Tc, which is the weighted average of three half-life values shown in figure 4.4. The adopted value clearly differs from the value of 1.4 (4) s observed indirectly by a radiochemical study (Tra76).

In (Gra89) 13 γ-transitions were proposed to belong to the decay of ^{109}Tc. The present work confirms directly only the 137.7 keV and the 194.6 keV γ-transitions. In addition, the 331.9 keV, 1159.2 keV and 1268.1 keV γ-transitions were assigned to the β-decay of ^{109}Tc on the basis of their decay properties, even though they could not be placed in the level scheme. The 531.2 keV and 1073.5 keV γ-transitions were not observed in the present measurement. The 295.7 keV and 964.6 keV transitions were excluded to belong this decay on the basis of the half-life analysis. The 295.7 keV transition probably belongs to the laboratory background; 964.6 keV is unknown, but it is very long-lived. The 1502.6 keV γ-transition seems to belong to the β-decay of ^{109}Ru (Kaf87). The 1964.3 keV γ-transition was not observed in the present measurement, which might also be due to low counting statistics.

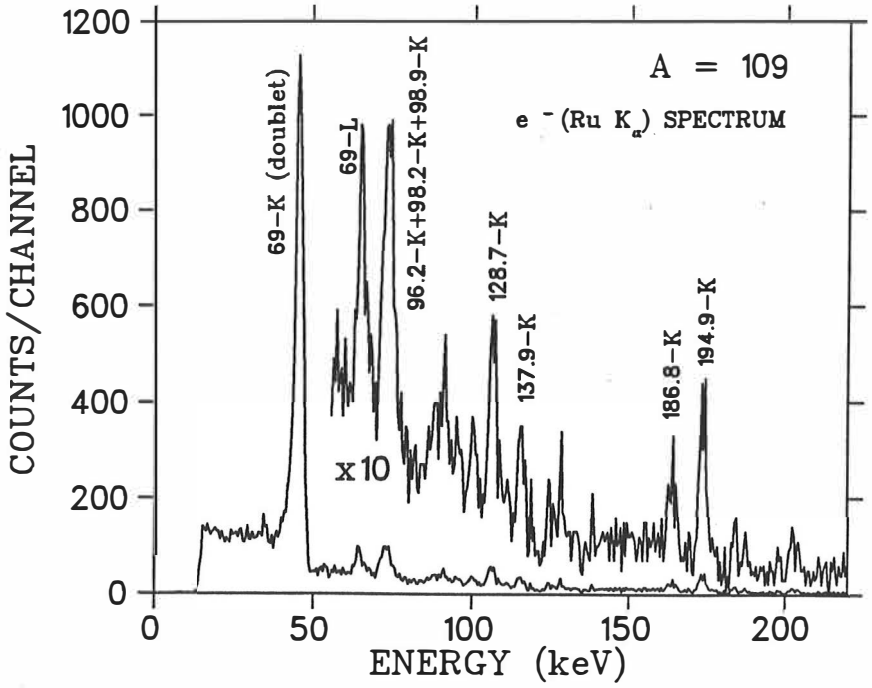

Figure 4.2. The conversion electron spectrum of A = 109 fission products obtained in coincidence with characteristic K_α X-rays of Ru. The L conversion electrons are seen in coincidence with K X-rays because the 68.8 keV and the 69.1 keV transitions in ^{109}Ru are in cascade.

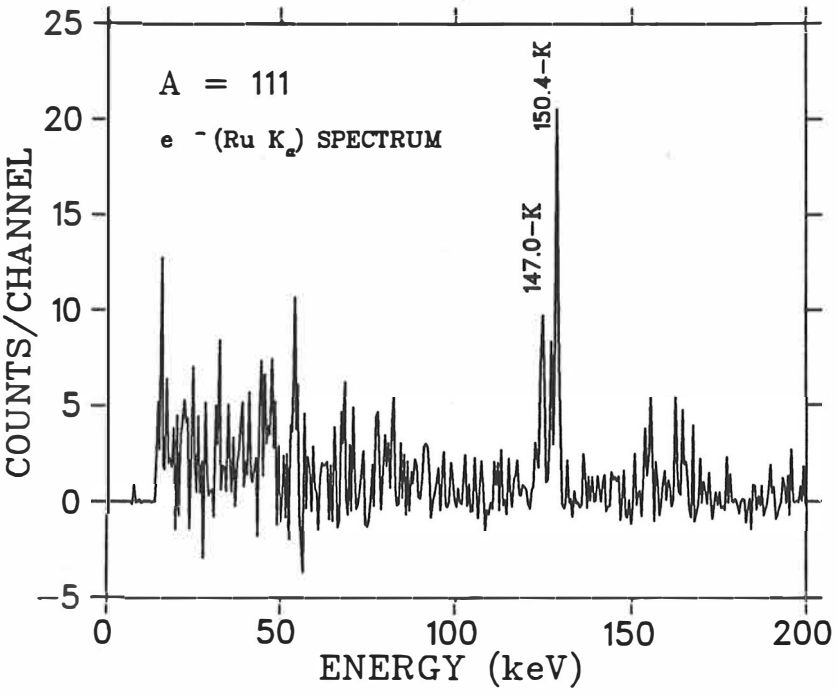

Figure 4.3. The conversion electron spectrum of A = 111 fission products in coincidence with the characteristic K_α X-rays of Ru.

^{111}Tc

In the (γ)(X) coincidence measurement at the mass number A = 111 a 267.0 keV γ–transition and traces of 147.0 keV and 150.4 keV γ-transitions appeared in coincidence with characteristic K X-rays of Ru. In the conversion electron measurement the K-conversion electrons from the latter two transitions appeared in coincidence with K X-rays of Ru, as shown in figure 4.3. Additionally, 103.9 keV, 175.0 keV and 368.0 keV γ-transitions were assigned to belong to this decay on the basis of half-life analysis. The adopted β-decay half-life of 0.30 (4) s for ^{111}Tc is based on the decay of the 150.4 keV γ-rays as shown in figure 4.4. The other mentioned γ-transitions were observed to decay with a similar half-life.

^{111}Ru

Ten γ-transitions appeared in coincidence with characteristic K X-rays of Rh. Fifteen γ-transitions were assigned to this decay on the basis of their (γ)(γ) coincidence relations. The two strongest γ-transitions, 211.7 keV and 303.7 keV, were used for the half-life analysis, as shown in figure 4.4. The weighted average of 2.12 (7) s of the observed values was adopted.

The average value of the previous, indirect values (Fet75), (Mat76), (Fra78) agrees with the present one. No direct measurement of the β-decay half-life of ^{111}Ru has been reported prior to the present studies. In fact, the gamma rays following the β-decay of ^{111}Ru were observed in a radiochemical study (Fra78), but the decay was erroneously assigned to the β-decay of ^{113}Ru, as described below.

^{113}Ru

Seven γ-transitions were observed in coincidence with the characteristic K X-rays of Rh. Ten additional γ-transitions were assigned via their (γ)(γ) coincidence relations. The β-decay half-life was deduced from the 88.3 keV, 211.7 keV and the 263.5 keV γ-transitions. Their decays are shown in figure 4.4. The weighted average of 0.80 (6) s was adopted for the β-decay half-life of ^{113}Ru.

This is the first time when the β-decay of ^{113}Ru is observed. The previous half-life assigned to ^{113}Ru, based on the 3.0 (7) s decay of a 303.6 keV γ-transition (Fra78) is in error. The 303.6 keV γ-transition belongs to the β-decay of ^{111}Ru instead. In (Fra78) the 303.6 keV γ-transition was assigned to the decay of Ru using chemical separation, but the A = 113 assignment which was based on an earlier study of prompt γ-rays (Hop72), was in error.

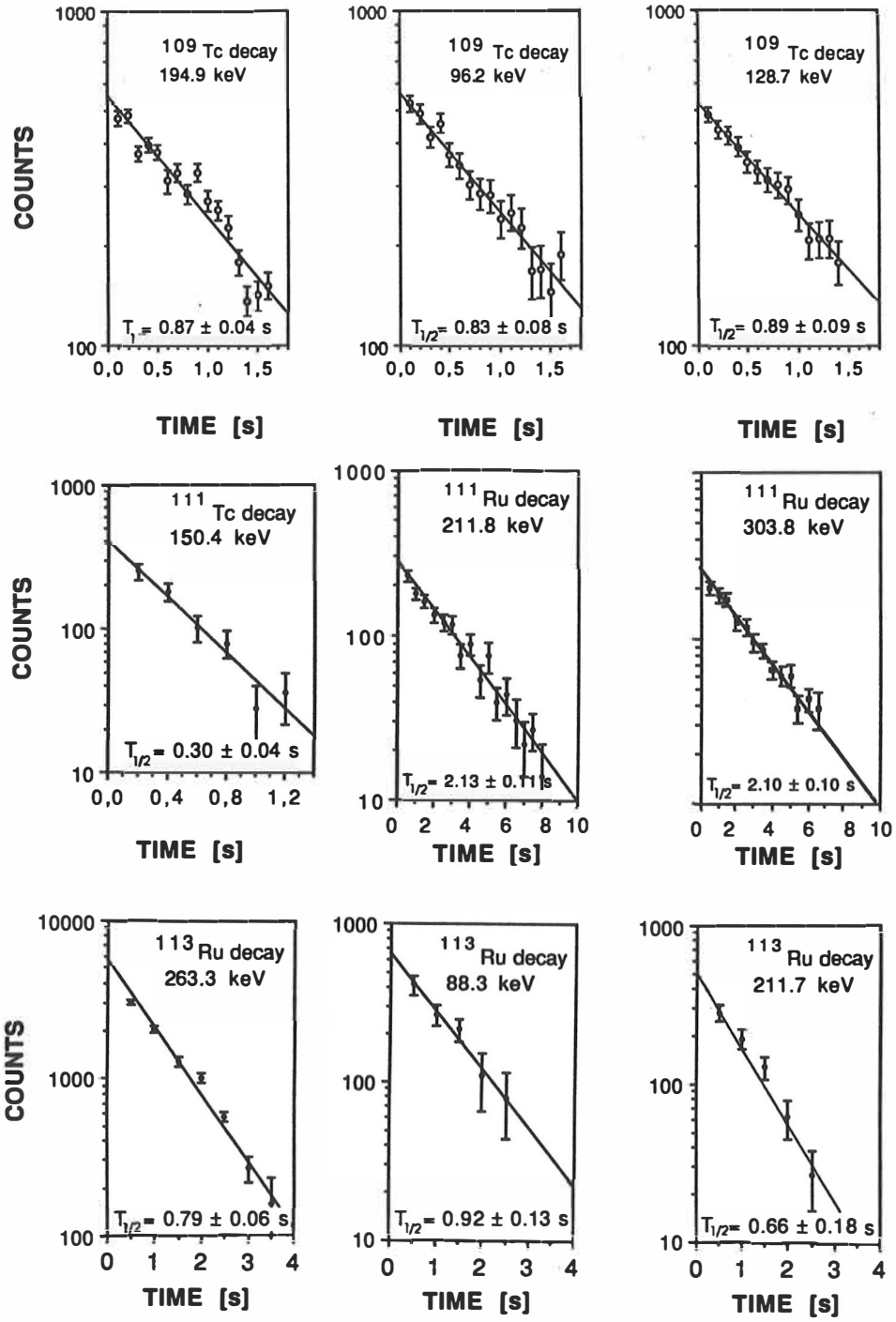

Figure 4.4. The decay curves of β-coincident γ-transitions used in the β-decay half-life analysis of ^{109,111}Tc and ^{111,113}Ru.

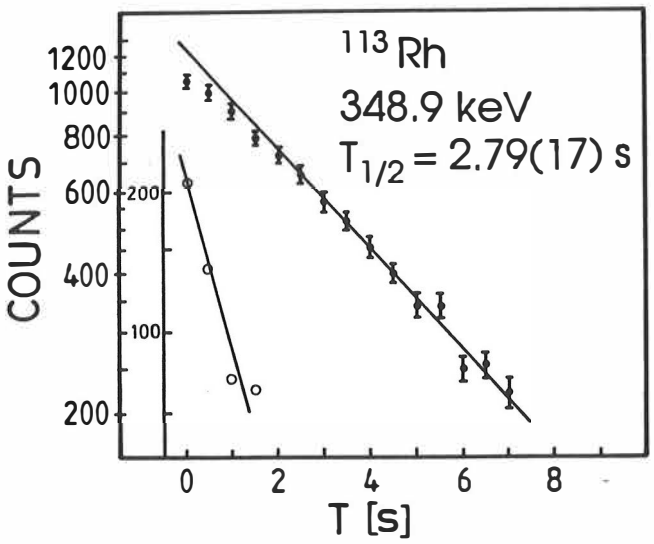

Figure 4.5. The β-decay of ^{113}Rh. The growth-in component is due to the β-decay of ^{113}Ru.

^{113}Rh

Twelve γ-transitions and five K-conversion electron transitions were observed in coincidence with characteristic K X-rays of Pd. Twenty-five additional γ-transitions were assigned on the basis of their (γ)(γ)-coincidence relations and six γ-transitions on the basis of their decay properties. For the β-decay half-life analysis five γ-transitions, 84.9 keV, 116.8 keV, 137.5 keV, 189.8 keV and 348.9 keV, were used. A two-component fit was used because of the growth-in component due to the 0.80 s decay of ^{113}Ru, as shown in figure 4.5. The weighted average of 2.80 (12) s was adopted for the half-life of ^{113}Rh. These results show that the previous assignment of the 128.5 keV γ-transition to this decay was in error. These γ-rays could result from the 127.9 keV transition belonging to the decay of ^{115}Rh, as described below. Thus, the β-decay of ^{113}Rh was observed for the first time in the present measurements.

^{115}Rh

Nine γ-transitions were observed in coincidence with the characteristic K X-rays of Pd. Three of these transitions were observed in coincidence with K X-rays of Pd as conversion electron transitions also. In addition, a K-conversion electron transition corresponding to the 89.4 keV γ-transition energy was observed via (e^-)(X) coincidences. This transition originates from the decay of an isomeric state to the ground state in ^{115}Pd with a half-life of 50 s (Fog88). Thirteen other transitions were assigned via their (γ)(γ) coincidence relations. For the half-life analysis, the 127.9 keV γ-transition observed in coincidence with β-particles was used. The β-decay half-life of 1.04 (3) s was observed, as shown in figure 4.6. An earlier run resulted in a half-life of 0.99 (5) s (Pen88). The weighted average of 1.02 (3) s has been adopted.

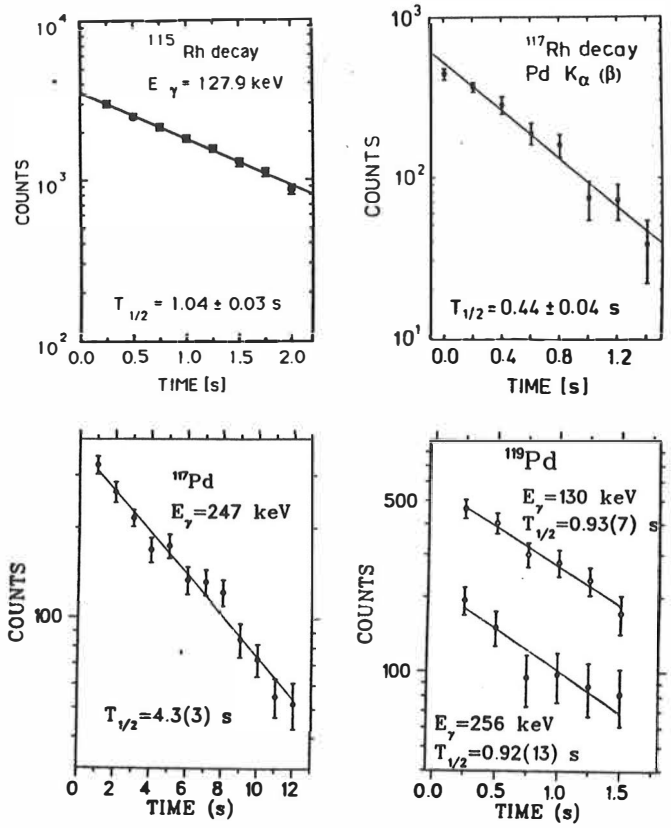

Figure 4.6. The decay curves of β-coincident transitions used in the β-decay half-life analysis of ^{115,117}Rh and ^{117,119}Pd.

^{117}Rh

In the measurements performed in Louvain-la-Neuve for the mass number A = 117 five γ-transitions were observed in coincidence with the characteristic K X-rays of Pd. The 34.6 keV, 97.1 keV, 131.7 keV and 168.6 keV γ-transitions were previously observed in connection with the decay of the 19.1 (7) ms isomeric state in ^{117}Pd, as described below and in (Pen91). The 481.6 keV γ-transition has not been observed in the measurements at JYFL. In the LISOL experiment, the 34.6 keV, 97.1 keV, 131.7 keV and 481.6 keV γ-transitions, as well as the K X-rays of Pd, were observed in coincidence with β-particles, as shown in figure 4.7. A half-life of 0.44 (4) s was determined from the observed decay of the β-gated K X-rays of Pd, produced mostly by the internal conversion of the 34.6 keV transition. The decays of the β-gated 34.6 keV and 131.7 keV transitions followed the same decay pattern. In the vicinity of the 481.6 keV γ-transition there is also a 482.2 keV γ-transition that results from the β-decay of ^{117}Pd. For this doublet, the total intensity as a function of time was fitted assuming two components. The results obtained for the half-lives were ≈ 5 s and ≈ 0.5 s. These half-lives are comparable to the obtained β-decay half-lifes of 4.3 (2) s and 0.44 (4) s of ^{117}Pd and ^{117}Rh.

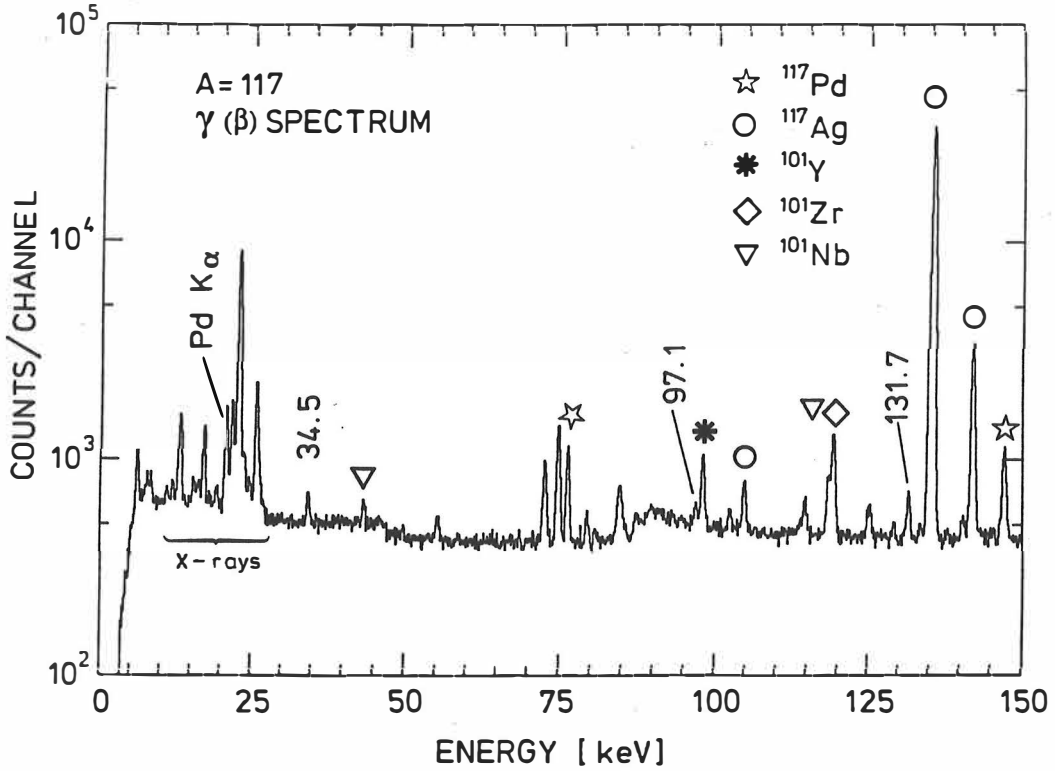

Figure 4.7. The low-energy part of the gamma spectrum observed at mass A = 117 in coincidence with beta particles.

^{117}Pd

A 247.3 keV γ-transition was observed in coincidence with the characteristic K X-rays of Ag. A conversion electron transition corresponding to the same γ-transition energy was also observed in coincidence with the K X-rays of Ag. In the measurements at JYFL two additional γ-transitions, 76.5 keV and 323.8 keV, were assigned to this decay. In the experiment at LISOL, which was primarily devoted to the observation of the β-decay of ^{117}Rh, 17 additional γ-transitions were assigned to the β-decay of ^{117}Pd via their (γ)(X)- and (γ)(γ)-coincidence relations.

The β-half-life of 4.3 (2) s for ^{117}Pd was obtained from the decay of the 247.3 keV γ-transition observed in coincidence with β-particles. This was unquestionably the first direct observation of the β-decay of ^{117}Pd. The other assignments were based on chemical separation, but the observed half-lives $5.0^{+0.7}_{-0.5}$ s (Wei68), 5.0 (4) s (Brü75) and 4.4 (2) s (Rog90b) are not in disagreement with the present result.

^{119}Pd

At the mass number A = 119 a 256.6 keV γ-transition was seen in coincidence with the characteristic K X-rays of Ag. A 69.9 keV γ-transition was observed in coincidence with the 256.6 keV γ-transition. Both of these and a 326.1 keV γ-transition, corresponding to the sum of the the two, were observed in coincidence with β-particles. Additionally, a 129.9 keV γ-transition was observed to decay with the same half-life as the transitions mentioned. Due to the low production rate of of ^{119}Pd, no conversion electron transitions assigned to this decay were observable in the present measurements.

The β-decay half-life was determined from the decays of the 256.6 keV and 326.1 keV γ-transitions, as shown in figure 4.6. The deduced values were 0.88 (18) s and 0.95 (19) s. Their weighted average of 0.92 (13) s is adopted for the β-decay half-life of ^{119}Pd. Additionally, a half-life value of 0.93 (7) s was observed for the 129.9 keV γ-transition. No evidence for an isomeric transition, which might be expected on the basis of the systematics of lighter odd-A Pd isotopes, was observed for ^{119}Pd.

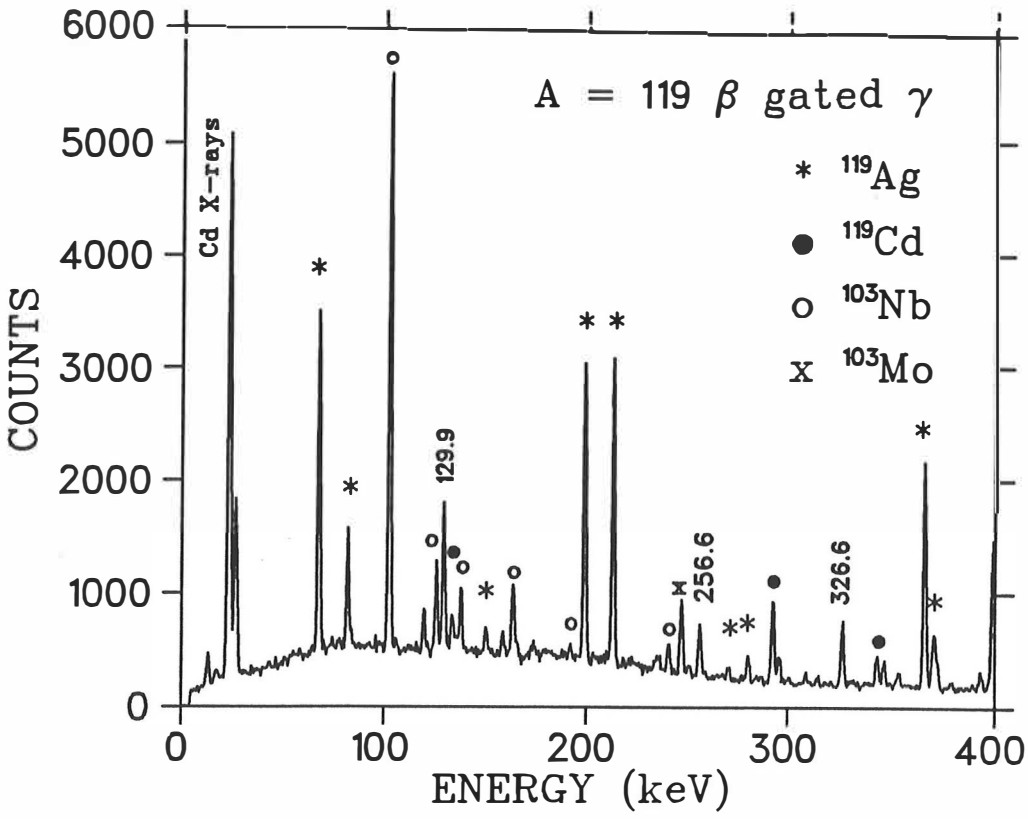

Figure 4.8. The beta gated low-energy gamma spectrum observed at mass number A = 119.

4.3. The half-lives of isomeric decays

^{113m}Pd

A relatively long-lived isomeric state at low energy was expected to exist in ^{113}Pd on the basis of the existing odd-A Pd systematics (see chapter 4.4.). However, no isomeric state had been found in the previous experiments (Fog88), (Pen90). A 0.4 (1) s isomer was discovered in the $(e^-)(X)$ coincidence experiment by observing a 57.0 keV K-conversion electron transition, corresponding to the 81.3 keV transition energy, in coincidence with the characteristic X-rays of Pd, as shown in figure 4.9. The half-life 0.4 (1) s for the isomeric state was deduced from the decay of the 81.3 keV γ-transition in the low energy singles gamma spectrum, as shown in figures 4.9 and 4.10.

This isomer was not observed in (γ)(X)- or (γ)(γ) coincidence experiments, because the 81.3 keV γ-transition is not in coincidence with any other γ-transition. Neither the 81.3 keV γ–transition nor the corresponding conversion electron transition was observed in coincidence with β-particles, which implies the isomeric nature of the transition. The observed half-life differs significantly from the β-decay half-life of 2.8 s of ^{113}Rh, which implies that the isomeric state in ^{113}Pd is populated directly in fission.

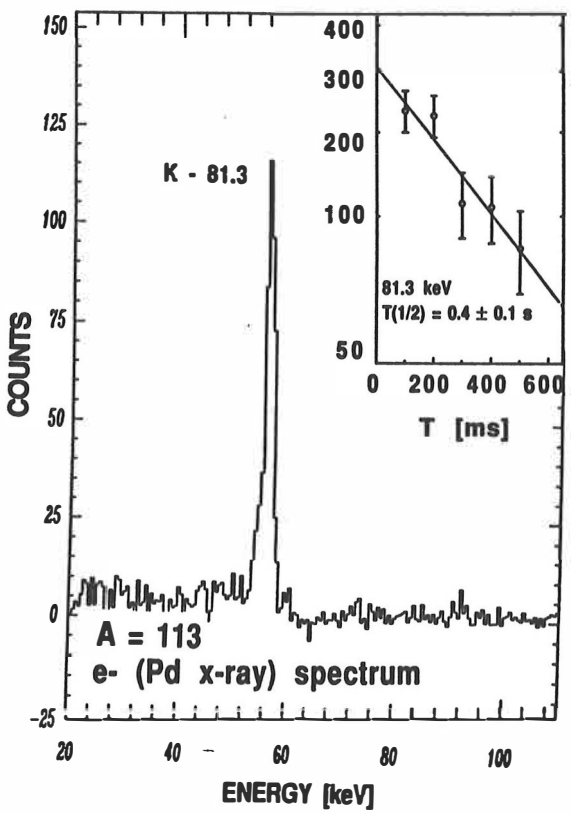

Figure 4.9. Discovery of the isomeric decay of ^{113m}Pd. The data for the half-life analysis seen in inset is taken from the decay of the 81.3 keV singles gamma transition, shown in figure 4.10.

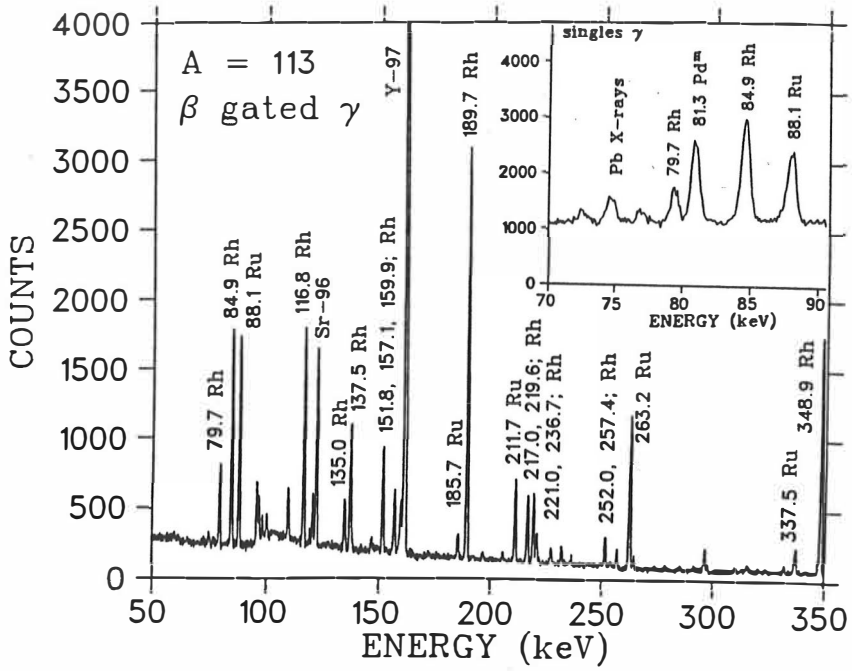

Figure 4.10. Low energy (γ)(β) spectrum at mass number A=113. The presence of ^{96}Sr and ^{97}Y contaminations is due to $(SrOH)^-$- and $(YO)^-$-ions, respectively. The isomeric 81.3 keV M2 transition is not seen in the (γ)(β) spectrum. The inset shows a part of the γ-singles spectrum, in which the 81.3 keV transition is observed.

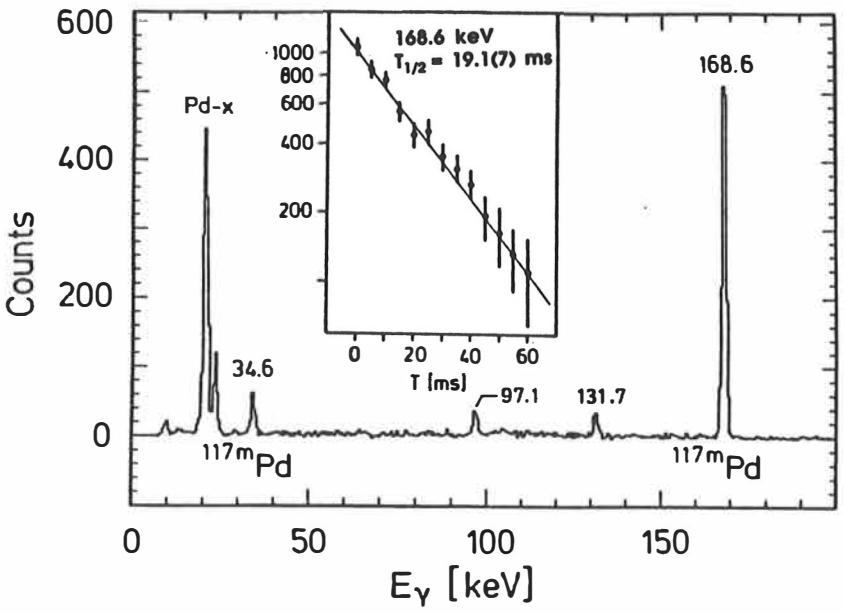

Figure 4.11. Discovery of the isomeric decay of ^{117m}Pd. The gamma ray spectrum seen in coincidence with characteristic K X-rays of Pd. The inset shows the decay of the 168.6 keV gamma rays.

^{117m}Pd

Four low energy γ-transitions, 34.6 keV, 97.1 keV, 131.7 keV and 168.6 keV were observed in coincidence with K X-rays of Pd, as seen in figure 4.11. In the measurements at JYFL only some traces of the 34.6 keV γ-transition were observed in coincidence with β-particles. Later in the LISOL experiment, the 34.6 keV, 97.1 keV and 131.7 keV γ-transitions, and the K X-rays of Pd, were found to appear in coincidence with β-particles, following the 0.44 s β-decay of ^{117}Rh. The 168.6 keV γ-transition, on the other hand, was not observed in coincidence with β-particles in any measurement, which implies that the 168.6 keV transition is de-exciting an isomeric state. The other mentioned γ-transitions are more complex. They are de-exciting states that are populated partly in the isomeric decay of ^{117m}Pd, partly in the β-decay of ^{117}Rh. A more detailed level scheme of ^{117}Pd is given in chapter 4.4. The isomeric half-life was deduced from the decay of the 168.6 keV γ-transition in the singles γ-spectrum. The analysis resulted in a half-life of 19.1 (7) ms. Since no longer half-life component was found in the decay of the 168.6 keV γ-transition, the isomeric state in ^{117}Pd is deduced to be populated not in the 0.44 s β-decay of ^{117}Rh but directly in fission.

4.4. The level schemes

The level schemes of the studied nuclei were deduced on the basis of the intensities and the (γ)(γ) coincidence relations of the observed transitions. Figures 3.6, 4.16 and 4.22 show some typical (γ)(γ) spectra.

The deduced internal conversion coefficients were used for the multipolarity assignments of the transitions by comparison with theoretical ICC values based on (Rös78). Since the original computer codes were not available, the α_K values were calculated from tabulated values using a simplified computer code (Kan89).

In the presented level schemes, the internal conversion is included to the intensities of the transitions. If the experimental conversion coefficient α is not available, but the multipolarity of the transition can be deduced from the level scheme, the corresponding theoretical conversion coefficient is used. If nothing else is known of the transition, M1 multipolarity is assumed. This is because if a low energy transition has higher multipolarity than M1 or E2, it would have been possible to determine its conversion in most of the cases. The difference between the conversion of M1 and E2 transitions is neglible in the studied nuclei, if compared to the overall uncertainties. Thus, no fatal error is made, if the total conversion coefficient

corresponding to an M1 transition is used to calculate the total intensity of an E2 or an M1/E2 transition. The largest error results, if a low energy E1 transition is treated as M1. At high energies, the conversion does not effect remarkably on the intensity of low multipolarity transitions.

For the log *ft* values, experimental β-decay energies were available for the ^{109}Tc and ^{115}Rh β-decays (Gra89), (Äys87). For consistency, the mass formula of Möller and Nix (Möl88) was used to calculate the unknown Q_β values. The log *f* values were taken from (Gov71). The ground state branching of the β-decay was determined experimentally for the β-decays of ^{111}Ru, ^{113}Ru and ^{115}Rh. In the other cases, zero ground state branching was assumed.

The level scheme of ^{109}Ru

The level scheme of ^{109}Ru was constructed on the basis of (γ)(γ) coincidences given in table 4.3. Altogether 40 transitions were assigned to the decay of ^{109}Tc. Of these 27 were placed in the level scheme shown in figure 4.12. The α_K values were deduced for 11 transitions. These values are given in table 4.4. The K-68.8 keV and the K-69.1 keV peaks are mixed in the conversion electron spectrum, but the fluorescence yield of K X-rays shows the 68.8 keV transition to be a highly converted one.

The conversion of the 69.1 keV transition was, however, undeduceable. The K/L ratio was measured for the 195.0 keV transition, and for the 68.8 keV transition with the assumption that the conversion of the 69.1 keV transition is neglible. For the 68.8 keV transition, the value of 3.0 ± 0.2 implies L = 2 and multipolarity of E2; for the 195.0 keV transition, the value of 6.6 ± 2.0 cannot distinguish between M1 and E2. The conversion for the 98.2 keV, 98.9 keV doublet was α_K = 0.26 (5), which corresponds to M1 multipolarity. However, the same α_K for this doublet results, within the experimental error, in an E1 assignment for the 98.9 keV transition and M1 for the 98.2 keV transition. Because the M1 assignment for the 98.9 keV transition would be in disagreement with the M1 assignment for the 195.0 keV transition, the multipolarity of E1 was adopted.

The conversion electron measurement also confirmed the 195.0 keV transition belonging to the decay of ^{109}Tc. The 195.0 keV gamma transition did not appear in coincidence with any other γ-transition. In (Alt90) this gamma transition was reported to appear in coincidence with the 138 keV γ-transition. This coincidence was not observed in the present work.

The 96 keV γ-transition had previously been connected to a half-life of 550 ns (Bla84). In the present work two lifetimes of excited states were deduced from the (β)(γ) TAC spectrum. The time calibration of electronics was checked with the 380 ns half-life of 113 keV transition in

Table 4.3. The γ-transitions following the β-decay of ^{109}Tc. The intensities are determined from the (γ)(β) spectrum and normalized to the 195.0 keV γ-transition intensity.

Energy / keV		Relative intensity	Coincident gamma rays / keV
35.7 (2)		4.6 (3)	96, 98.2
58.2 (2)		3.3 (4)	68.8, 128.7
68.8 (2)		33.5 (14)	69.1, 118, 122, 129, 208, 289 [1]
69.1 (2)		30.6 (15)	68.8, 118, 267
96.2 (2)		44.3 (9)	36, 98.2, 98.9
98.2 (2)		4.0 (3)	36, 96, 132
98.9 (2)		2.6 (4)	96
117.7 (2)		8.3 (8)	68.8, 69.1, 138
122.4 (2)		19.0 (10)	68.8, 208, 323.7
128.7 (2)		45.0 (10)	58, 68.8, 208, 300 [1]
131.8 (2)		5.2 (5)	63.1 [1,2], 96, 98.2, 195.4 [1]
137.9 (2)		24.0 (14)	118, 289 [1], 377
172.0 (3)	[1]	2.5 (6)	
186.8 (2)		13.3 (5)	68.8
195.0 (3)		100.0 (20)	
197.4 (3)		6.8 (10)	208
200.5 (4)	[1]	≤ 2.0 (6)	178.1 [1]
208.0 (2)		20.0 (9)	68.8, 92.4 [1,2], 129, 197
242.2 (3)	[1]	2.9 (5)	58, 68.8, 69.1
255.6 (3)		7.2 (5)	
267.7 (3)		3.6 (6)	68.8, 69.1, 138
278.8 (3)	[1]	3.7 (6)	96, 98.2
289.5 (3)	[1]	9.3 (7)	68.8, 69.1, 138
300.4 (3)	[1]	3.5 (5)	68.8, 129
324.0 (5)		≤ 1.8 (7)	
332.0 (3)	[1]	28.5 (9)	
336.9 (5)	[1]	1.2 (6)	
376.7 (3)		19.2 (8)	68.8, 69.1, 96, 138
445.8 (2)		22.7 (9)	68.8
490.2 (2)		19.1 (10)	68.8, 69.1, 138
514.5 (3)		25.3 (13)	
589.7 (3)		7.1 (7)	68.8, 69.1, 129, 138, 168.5 [1,2], 208
627.9 (3)		6.0 (7)	
739.4 (5)	1)	6.6 (8)	
804.0 (3)		6.9 (9)	68.8, 122
848.1 (5)	1)	11.4 (10)	
995.0 (5)		4.6 (8)	
1158.7 (5)	1)	36.3 (16)	
1267.8 (5)	1)	22.3 (14)	

[1] Not placed in the level scheme.

[2] Not seen in (γ)(β) spectrum.

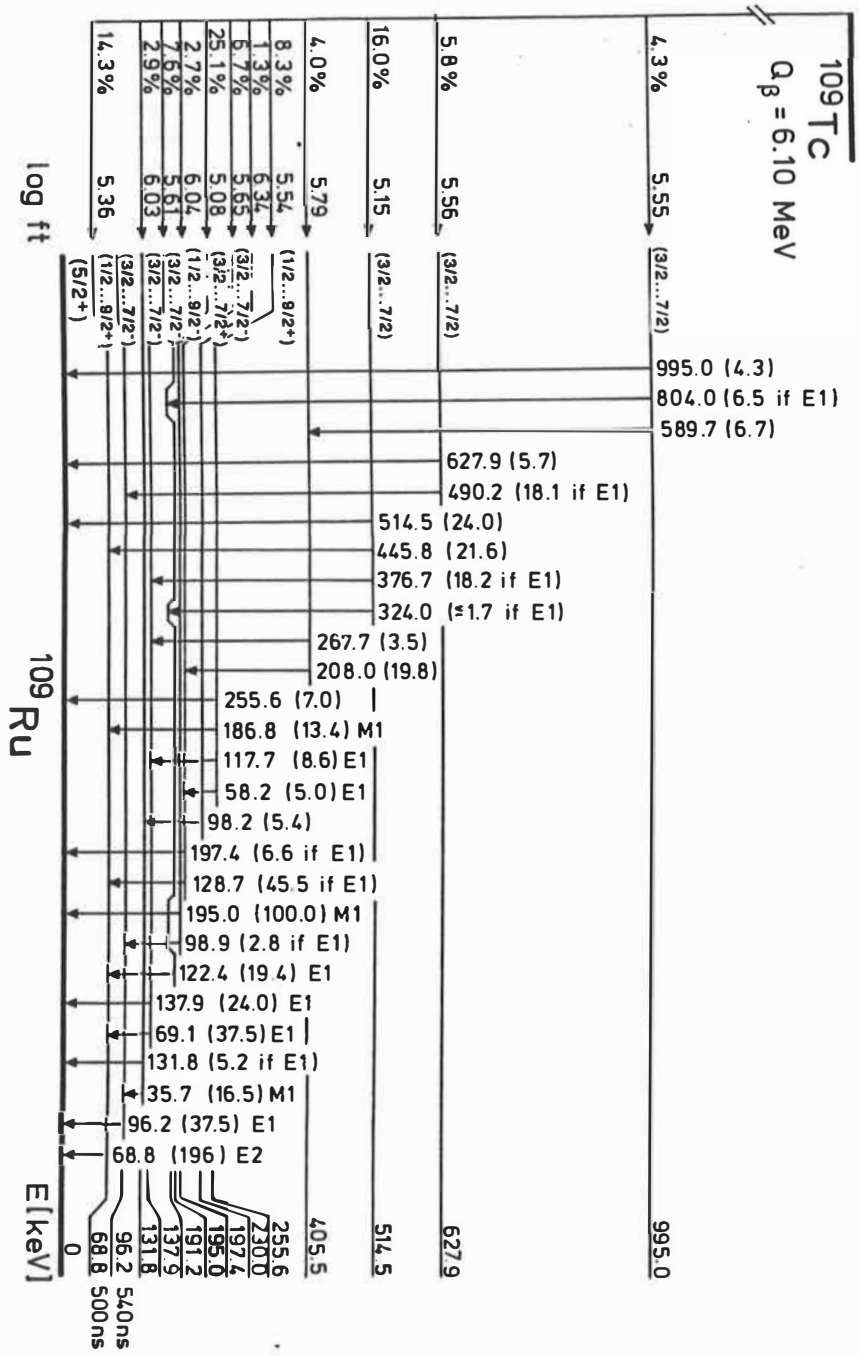

Figure 4.12. The level scheme of ^{109}Ru. For the 514.5 keV, 627.9 keV and 995.0 keV levels positive parity is assumed because of a log *ft* similar to the positive parity states at 68.8 keV and 195.0 keV.

Table 4.4. Internal K-conversion coefficients for transitions in ^{109}Ru.
D: simultaneous measurement of conversion electrons and gamma rays;
X: electron intensity measured from the Ru K_α X-ray coincident spectrum;
FX: calculation based on the fluorescence yield of the characteristic X-rays of Ru.

Transition / keV	α_K (exp)	Method	α_K (theor)	Multipolarity
35.7	5.2 (14)	FX	E1 2.193	M1
			M1 5.393	
			E2 23.26	
58.4	0.6(3)	X [1]	E1 0.564	E1
			M1 1.28	
68.8	≤ 2.5(5)	D	E1 0.355	E2
	3.5(9)	FX	M1 0.801	
			E2 3.49	
96.2	0.13(2)	D	E1 0.136	E1 (M1)
	0.22(11)	FX	M1 0.310	
98.2	0.26 (5)	D	E1 0.128	M1 for 98.2 keV
and 98.9			M1 0.293	E1 for 98.9 keV [2]
			E2 1.078	
117.7	0.09 (5)	X [1]	E1 0.0760	E1
			M1 0.176	
			E2 0.574	
122.4	0.080(14)	D	E1 0.0677	E1
			M1 0.158	
128.7	0.087(7)	D	E1 0.0587	E1 (M1)
			M1 0.138	
137.9	0.084(10)	D	E1 0.0482	E1 (M1)
			M1 0.114	
186.8	0.066(12)	D	E1 0.0206	M1
			M1 0.0512	
			E2 0.117	
195.0	0.039 (4)	D	E1 0.0181	M1
			M1 0.0451	
			E2 0.0995	

[1]) Normalized to the 128.7 keV and 137.9 keV transitions.
[2]) See the text.

^{109}Pd (Bar77), (Kan78) and the 1.6 μs half life of the 226 keV transition in ^{109}Rh (Kaf88). The results are given in table 4.5. If the half-life 0.5 (2) μs is connected to the 68.8 keV E2 transition, the partial γ-half-life for this level will be 3.1 (14) μs. This corresponds to 3.7 Weisskopf units, which means that the lifetime is rather close to the single particle estimate. The Weisskopf estimate for the 96.2 keV E1 transition is 0.34 ps which gives a hindrance factor of 18 000, which is typical for E1 transitions.

Table 4.5. The measured lifetimes of excited states in ^{109}Ru. The value for the 69 keV transition is rather connected with the 68.8 keV E2 transition from the 68.8 keV level than the 69.1 keV transition from 137.7 keV level.

Transition (keV)	Level (keV)	Half life (ns)
69 [1])	68.8 or 137.7	500 (200)
96	96	540 (170)

[1]) Doublet.

Spin and parity assignments.

The presence of E1 transitions implies both negative and positive parity states in ^{109}Ru. Assuming positive parity for the ground state on the basis of β-decay properties of ^{109}Ru (Kaf87), five states with negative and seven states with positive parity, shown in figure 4.12, can be deduced. The assumed negative parity states also tend to have higher log *ft* values than the positive parity states. If spin 5/2 is assumed for the ground state, again on the basis of the β-decay properties of ^{109}Ru, it becomes possible to give some spin assignments. The $5/2^+$ ground state assumption results in spin 3/2, 5/2 or 7/2 for all negative parity states except the 191.2 keV state, for which spin 1/2 and 9/2 cannot be excluded. If the first excited positive parity state is labeled with spin 1/2 in analogy with the $1/2^+$ state with $s_{1/2}$ single particle character in the isotone ^{111}Pd, the spin of the most negative parity states becomes 3/2. The 68.8 keV state has a half-life that corresponds to about three single-particle units, implying relatively large single-particle character. On the other hand, if ^{109}Tc has the $7/2^+$ ground state, as expected on the basis of experimental systematics, the large branching in β-decay does not support $1/2^+$ assignment for the 68.8 keV state. Furthermore, because ^{109}Ru has an odd neutron, the origin of the negative parity states has to be the $h_{11/2}$ orbital, which means that the negative parity states are expected to have a high spin.

The ground state branching was not determined for the ^{109}Tc decay. On the basis of systematics, $7/2^+$ can be expected for the ground state of ^{109}Tc. The strongest beta feeding goes to the 195.0 keV level, for which spin and parity $3/2^+$, $5/2^+$ or $7/2^+$ were deduced assuming $5/2^+$ ground state. Spin 3/2, 5/2 or 7/2 is then suggested also for the states with low log *ft* in the β-decay of ^{109}Tc, even though spin 1/2 or 9/2 cannot be totally excluded.

Comparison with the lighter odd-A Ru isotopes is difficult, since no spin and parity assignments are reported for ^{105,107}Ru (DeF86), (Bla91). However, some transition multipolarities in ^{107}Ru are reported: these are all either M1 or E2. The numerous E1

transitions were thus not expected, and an experimental error was suspected. The renormalization of the ICC values for transitions in ^{109}Ru by a factor of about 1.8 would result in an internally consistent result with M1, M1/E2 and E2 transitions only. In fact, the conversion electron experiment in question suffered very much from experimental difficulties, and as mentioned in chapter 3, the conversion electron measurements are very sensitive to the source size and position. However, the internal conversion coefficients deduced for transitions in ^{109}Rh in the same measurement are reasonable and seem to be rather a little bit too high than too low (table 4.6). It seems that a new series of experiments, possibly including mass numbers A = 105, A = 107 and A = 111 also, is needed to confirm the present tentative spin and parity assignments and clarify the situation in the odd-A Ru nuclei.

The level scheme of ^{109}Rh

A detailed level scheme of ^{109}Rh is given in (Kaf87). This level scheme was deduced from the decay of ^{109}Ru and it includes 53 levels. In the present work the multipolarities were deduced for seven transitions from the experimentally determined α_K values, as shown in table 4.6. In (Kaf87) only $\alpha_K = 13 \pm 4$ for the 31.8 keV M1/E2 transition was measured, using the fluorescent yield of K X-rays. This value could not be checked with a direct conversion electron measurement because of the low energy of the transition. The fluorescent yield measurement was repeated, but due to low statistics the previous value was not improved. The present measurement resulted in $\alpha_K = 17^{+10}_{-6}$.

Table 4.6. Internal K-conversion coefficients for transitions in ^{109}Rh. All the values are from simultaneous measurement of conversion electrons and gamma rays. In the last column the multipolarity assumed in ref. (Kaf87) is given.

Transition / keV	α_K (exp)	α_K (theor)	Multipolarity	Mλ in (Kaf87)
68.1	0.7 (2)	E1 0.366 M1 0.828 E2 3.62	M1	M1
183.9	0.13 (3)	M1 0.0524 E2 0.121	E2	E2
206.1	0.041 (7)	M1 0.0389 E2 0.0820	M1	M1
220.6	0.057 (11)	M1 0.0324 E2 0.0655	M1/E2	E2
226.0	0.062 (11)	M1 0.031 E2 0.061	E2	E2
245.1	0.07 (2)	M1 0.0247 E2 0.0452 M2 0.122	E2	M1
358.8	0.013 (3)	M1 0.0094 E2 0.0127	E2 (M1)	E2

The observed transitions in ^{111}Ru

The γ-transitions of 103.9 keV, 147.0 keV, 150.4 keV, 175.0 keV, 267.0 keV and 368.0 keV were assigned to the decay of ^{111}Tc. Their intensities are given in table 4.7. Only the 103.9 keV and 150.4 keV transitions were given in (Hop73). The internal conversion coefficients $\alpha_K = 0.107\ (13)$ for the 150.4 keV and $\alpha_K = 0.12\ (5)$ for the 147.0 keV transition were deduced from the simultaneous measurement of gamma rays and conversion electrons. The values imply multipolarity of M1 or E2 for both of the transitions. No level scheme can be deduced from the present data.

Table 4.7. The γ-transitions following the β-decay of ^{111}Tc. The intensities are determined from the (γ)(β) spectrum and normalized to the 150.4 keV γ-transition intensity.

Energy / keV		Relative intensity	Coincident gamma rays / keV
103.9 (2)		20 (3)	150
147.0 (3)		18 (4)	
150.4 (3)		100 (5)	104
175.0 (3)	1)	34 (4)	
267.0 (4)	2)	18 (6)	
368.0 (3)	1)	71 (6)	

1) Seen only in the (γ)(β)-spectrum.

2) Doublet resolved in low energy γ-spectrum.

The level scheme of ^{111}Rh

The level scheme of ^{111}Rh was constructed on the basis of the (γ)(γ) coincidence relations given in table 4.8. Levels of ^{111}Rh have been studied also in (Rog90a) via the β-decay of ^{111}Ru. The β-decay properties of ^{111}Ru are, however, not described in the study (Rog90a), which was concentrated on the search for the intruder states in ^{111}Rh. The level scheme of ^{111}Rh given in (Rog90a) agrees with the present one, given in figure 4.13. In the present measurement, three levels above 1 MeV were found. These levels were not given in ref. (Rog90a). On the contrary, the level scheme of (Rog90a) has additional levels at 568 keV, 733 keV, 860 keV and 977 keV. Their observation in the (Rog90a) experiment but unobservation in the present one is due to higher statistics in the chemical separation experiment.

Multipolarities were deduced for the seven transitions in ^{111}Rh the present work, see table 4.9. The K-78.5 keV transition intensity was deduced from the $(e^-)(\beta)$ spectrum. The electron

transition intensity for this transition could not be determined from the singles conversion electron spectrum because the 59.8 keV E3 transition in ^{111}Ag produced a huge amount of L-conversion electrons, which were inseparable from the K-78.5 electrons. Fortunately, the β-coincidence removed the conversion electrons due to the 59.8 keV transition from the spectrum, and the α_K for the 78.5 keV transition could be determined.

The ground state branching of ^{111}Ru. The ground state branching in the β-decay of ^{111}Ru can be deduced from the growth-in component in ^{111}Rh decay during the beam-off period (see Appendix). The fit to the data, from which a 60 % ground state branching was deduced, is shown in figure 4.14.

Table 4.8. The γ-transitions following the β-decay of ^{111}Ru. The intensities are determined from the (γ)(β)-spectrum and normalized to the 303.8 keV γ-transition intensity.

Energy / keV		Relative intensity	Coincident gamma rays / keV
78.5 (2)		26.4 (9)	251, 304, 554 [3]), 1265, 1516, 1651
91.3 (3)		2.1 (4)	304
136.7 (3)		14.4 (10)	114, 223, 304, 1463
186.1 (3)	[1])	4.9 (6)	304, 1274 [3])
189.1 (3)	[2])	16.6 (9)	189, 240, 295, 304, 342, 368
211.7 (2)		77.7 (15)	421, 827, 843, 1266, 1687, 1821
223.0 (3)		6.0 (6)	137, 304, 320
240.0 (3)	[1])	2.1 (6)	189
250.5 (2)		22.3 (8)	79, 304, 382, 1266
303.8 (2)		100.0 (23)	79, 91, 137, 157, 172 [3]), 189, 207, 223, 251, 280, 368, 604, 1266, 1404 [3]), 1516, 1592, 1729
382.0 (3)		41.3 (15)	171, 251, 1266, 1516, 1651
395.0 (3)		5.4 (7)	172, 221, 269
421.1 (3)		12.9 (9)	212, 1266
632.8 (3)		8.7 (10)	
843.7 (3)		27.7 (22)	212
1054.8 (4)		14.4 (30)	
1108.3 (4)	[1])	6.7 (16)	189, 304
1265.5 (4)		24.0 (40)	79, 212, 251, 304, 329, 382, 421
1400.8 (4)		11.0 (20)	212, 251, 382, 421
1463.3 (5)	[1])	5.5 (11)	137, 304
1515.9 (5)		28.0 (30)	79, 304, 382
1651.0 (5)		9.1 (14)	
1686.0 (5)		6.2 (11)	
1730.5 (5)		7.1 (14)	
1821.1 (5)		14.9 (15)	
1897.5 (5)		5.8 (12)	

[1]) Not placed in the level scheme.
[2]) Doublet.
[3]) Not seen in (γ)(β) spectrum.

Table 4.9. Internal K-conversion coefficients for transitions in ^{111}Rh.
D: simultaneous measurement of conversion electrons and gamma rays;
B: electron intensity measured from the β-coincident spectrum;
X: electron intensity measured from the Rh K_α X-ray coincident spectrum;
FX: calculation based on the fluorescence yield of the characteristic K X-rays of Rh.

Transition / keV	α_K (exp)	Method	α_K(theor)	Multipolarity
78.5	0.78 (13)	B[3]	E1 0.255	M1
	0.8 (4)	X	M1 0.612	
	0.6 (4)	FX	E2 2.320	
91.3	0.9 (6)	X	M1 0.396	M1 / E2
			E2 1.399	
136.7	0.12 (3)	D[1]	E1 0.0518	M1
			M1 0.129	
			E2 0.351	
211.7	0.037 (3)	D	M1 0.0399	M1
	0.039 (12)	X	E2 0.0778	
250.5	0.023 (10)	D[2]	E1 0.0094	M1
			M1 0.0257	
			E2 0.0436	
303.8	0.027 (4)	D	M1 0.0157	E2
			E2 0.0228	
382.0	0.011 (5)	D	M1 0.0087	E2 (M1)
			E2 0.0109	

[1]) If the 136.4 keV transition is not present in the decay of ^{111}Rh.
[2]) The L-230.8 (M1 in ^{111}Pd) intensity is calculated and subtracted from the electron intensity.
[3]) The conversion electron intensity is normalized to the K-303.8 intensity.

Spin and parity assignments.

The ground state. The 7/2$^+$ assignment for the ground state was deduced from the ^{111}Rh β-decay properties to the levels of ^{111}Pd, discussed in the next chapter. The main feeding in the ^{111}Rh β-decay goes to the 5/2$^+$, L = 2 level at 275 keV and 9/2$^+$ (7/2$^+$), L = 4 level at 412 keV. For the spin and parity assignments of these levels, see the next chapter. If the ground state branching is assumed to be zero, the log *ft* values for these branchings are 4.8 and 5.8. These log *ft* values correspond to allowed transitions, resulting in the 7/2$^+$ assignment. The level systematics of odd-A Rh nuclei also supports the 7/2$^+$ assignment. A triplet of 7/2$^+$, 9/2$^+$ and 5/2$^+$ levels is expected to appear at low energy in the odd-A Rh nuclei also on the basis of theoretical calculations (Bre89).

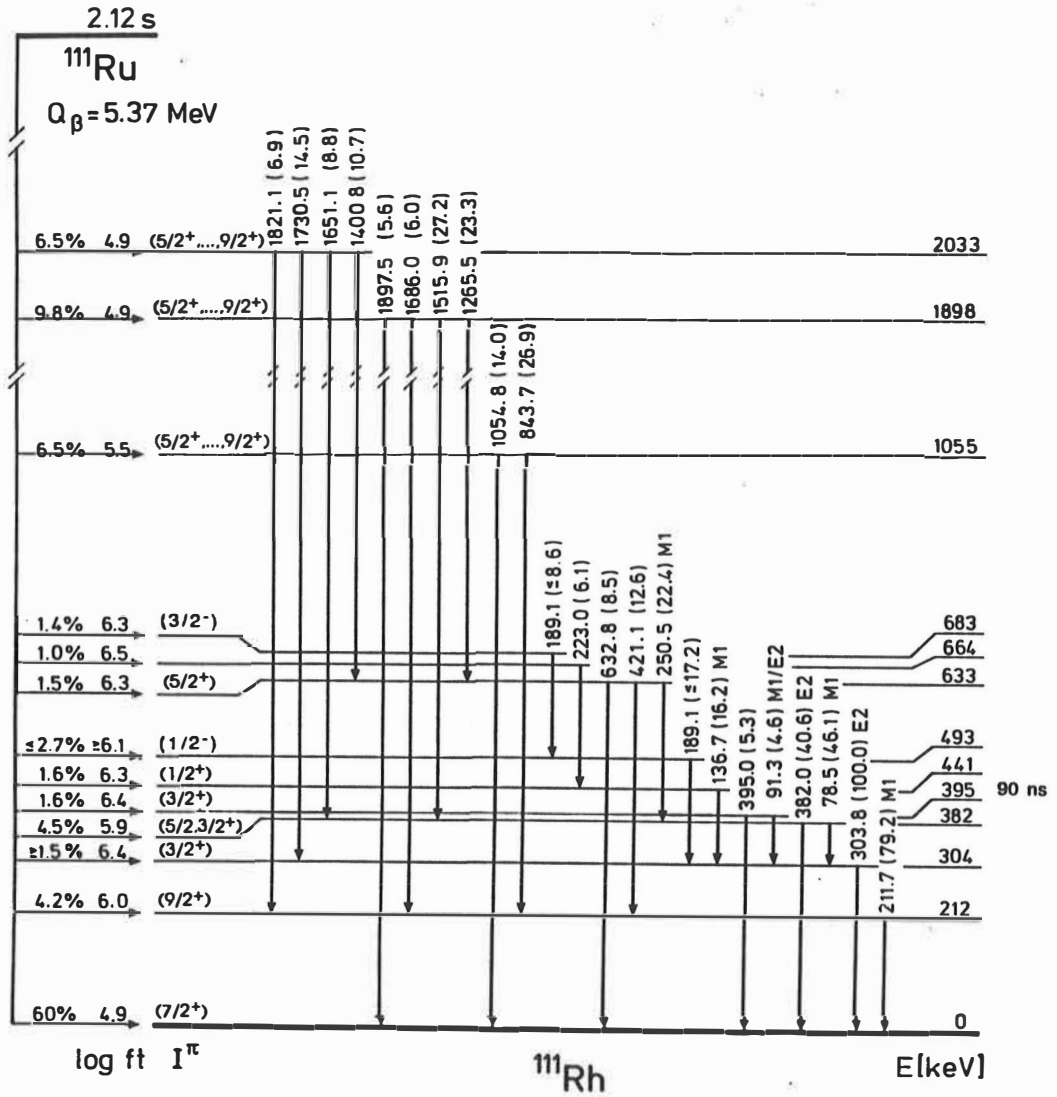

Figure 4.13. The level scheme of ^{111}Rh. The 1055 keV, 1898 keV and 2033 keV levels are not given in ref. (Rog90a).

The 211.7 keV level. This level is connected to the ground state with an M1 transition. The possible spin and parity assignments are therefore 5/2$^+$, 7/2$^+$ and 9/2$^+$. 9/2$^+$ is suggested because similarity with the decay scheme of ^{109}Ru (Kaf87) is expected. The 206 keV transition to the ground state in ^{109}Ru has multipolarity M1, and the log *ft* value for the 206 keV level in the β-decay of ^{109}Ru is of the same order as the log *ft* value of the 211.7 keV level populated in the β-decay of ^{111}Ru.

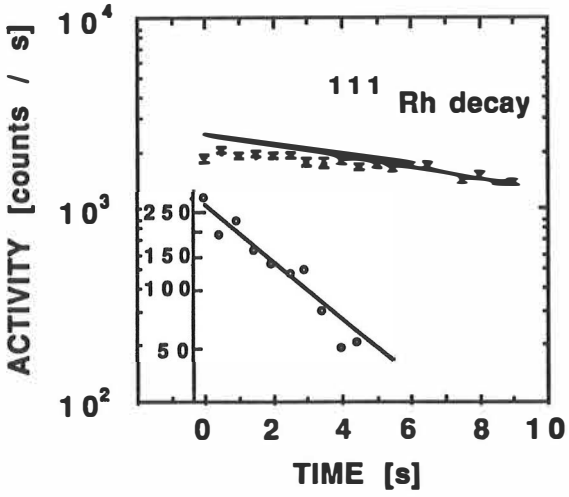

Figure 4.14. Determination of the ground state branching of the ^{111}Ru β-decay. The two component fit to the activity with fixed values of $\lambda_{Ru} = 0.33 \frac{1}{s}$ and $\lambda_{Rh} = 0.063 \frac{1}{s}$. The fit results in coefficients $C_1 = -538 \frac{1}{s}$ and $C_2 = 2468 \frac{1}{s}$, see Appendix.

The 303.8 keV level. The 303.8 keV transition to the ground state has E2 multipolarity. The possible spin and parity values are 3/2+, 5/2+, 7/2+, 9/2+ and 11/2+. There is no transition between the 303.8 keV and 211.7 keV levels, which may indicate large spin difference between the corresponding states. Hence, 3/2+ is assigned to this level.

The 382.0 keV level. The multipolarity assignment of M1 for the 78.5 keV transition is based on α_K which was deduced from the conversion electron peak intensity in the β-coincident electron spectrum. This assignment gives possible spin and parity assignments of 1/2+, 3/2+ and 5/2+ for the 382.0 keV level. For the 382.0 keV transition to the ground state a multipolarity of E2 was deduced. With the 7/2+ ground state assignment, this observation excludes 1/2+ for the 382.0 keV level. No transition to the 9/2+ level at 211.7 keV was observed, which would support a 3/2+ assignment. The β-decay properties, on the other hand, support a 5/2+ assignment. Spin and parity 5/2+ are suggested in (Rog90a), which is also consistent with the experimental systematics. Thus, spin and parity 5/2+ are preferred for this level, but the 3/2+ assignment cannot be excluded.

The 395.0 keV level. A M1 or E2 multipolarity or their mixture was observed for the 91.3 keV transition. The errors are too large to calculate meaningful mixing ratios. However, if there is any M1 mixing in the 91.3 keV transition, the possible spin values for the 395.0 keV level would be 1/2+, 3/2+ or 5/2+, but 7/2+ would be excluded. Again, there is no observable

transition to the 211.7 keV $9/2^+$ level, which implies low spin for the 395.0 keV level. On the other hand, low spin would hinder the transition to the $7/2^+$ ground state. The α_K of the 395.0 keV transition to the ground state corresponds to an E2 multipolarity, but M1 can not be excluded with the present uncertainty of the α_K value. Thus, $1/2^+$ can be excluded, but the $3/2^+$ and the $5/2^+$ assignments seem to be equally justified.

In (Rog90a) $3/2^+$ is suggested for the 395.0 keV level. This assignment is based on the assumption that this state is the lowest member of an intruder band. Such a band is known in ^{109}Rh and also in ^{113}Ag. In ref. (Rog90a) the half-life of the 395.0 keV state is measured to be 87 (8) ns. In the present measurement a half-life of 90^{+40}_{-30} ns can be deduced from the (β)(γ) TAC spectrum. The lifetime is one of the fingerprints of an intruder band. Hence, a $3/2^+$ assignment is finally adopted.

The 440.5 keV level. This level decays to the $3/2^+$ level at 304 keV via the 136.5 keV M1 transition. Decays to the other levels were not observed in the present measurements. Therefore, a low spin value is expected. The $1/2^+$ suggested in (Rog90a) is thus adopted. The level is a candidate for the intruder band member; because of the poor statistics the intruding states and their nature could not be studied in this work.

The 492.9 keV and 682.0 keV levels. These levels result from a cascade of two 189.1 keV transitions above the 303.8 keV level. Because no applicable crossing transitions to the 492.9 keV level were observed, the transitions were inseparable. The conversion electron transitions corresponding to these transitions were not observed with the present statistics, which could imply multipolarity of E1 at least for one of the transitions. In (Rog90a) the 492.9 keV and 682.0 keV levels are assigned to have spin and parity $1/2^-$ and $3/2^-$, respectively. These assignments are adopted in the level scheme.

The 632.8 and 663.5 keV levels. The 633.5 keV level is connected to the assumed $5/2(3/2)^+$ level at 382.0 keV via an M1 transition. The intensity ratio of the 250.5 keV, 421.1 keV and 632.8 keV transition supports $5/2^+$ assignment rather than an $1/2^+$ or a $3/2^+$ assignment. The 663.5 keV level is suggested to be an intruder band member (Rog90a).

The 1054.8, 1897.5 and 2033 keV levels: The low log *ft* values for these levels imply spins and parities similar to the ground state. Thus, $5/2^+$, $7/2^+$ or $9/2^+$ is suggested for these levels.

The level scheme of ^{111}Pd

Levels of ^{111}Pd have been studied using the ^{110}Pd(d,p)^{111}Pd reaction (Bla90). These levels have also been studied via ^{111}Rh β-decay in (Kaf84). However, the decay scheme given in (Kaf84) is tentative. In the present work the level scheme of ^{111}Pd was reconstructed using the observed data given in table 4.10. In the present work also the multipolarities were deduced for seven transitions on the basis of internal conversion coefficients. No experimental multipolarity assignments existed prior to the present study. A simultaneous intensity measurement of gamma rays and conversion electrons was possible for five transitions; for two transitions the gamma transition and the conversion electron transition intensities were measured separately and then normalized to the 275.4 keV transition. The K-conversion electrons of the 71.0 keV and 72.3 keV transitions produced a doublet in the singles electron spectrum. This doublet cannot be directly be resolved because of the 3.0 keV FWHM and strong tailing of these two peaks separated only by 1.3 keV and also because of high background compared to the peak intensities. Fortunately, the 72.3 keV transition was observed to disappear in coincidence with beta particles. This level was assigned to the $s_{1/2}$ single particle state, as an analogy to the 116 keV and 113 keV transitions in ^{107}Pd and ^{109}Pd with half-lives of 0.85 μs and 0.38 μs, respectively (Bla90). The Weisskopf estimate for a 72.3 keV E2 transition is 1.2 μs. The lifetime of this level could not be deduced due to poor statistics. However, its lifetime was utilized in deducing the conversion coefficients. The K-conversion of the 71.0 keV transition was deduced from the β-coincident conversion electron spectrum; the intensity of the K-72.3 keV transition was then taken from the electron singles spectrum by subtracting the calculated contribution of the 71.0 keV transition in the K-71.0/K-72.3 doublet. In order to determine the K-231.0 keV transition intensity, the calculated intensity of the L conversion electrons due to the 211.7 keV M1 transition in ^{111}Rh was subtracted from the intensity of conversion electrons corresponding to the K-231.0 transition. In addition, the K/L ratio of 8.0 ± 1.3 was observed for the 275.4 keV transition, which implies L = 1 for the transition. The α_K values and multipolarity assignments are given in table 4.11.

Five gamma transitions, 44.8 keV, 71.0 keV, 80.1 keV, 116.5 keV and 1202.2 keV, which were not reported in (Kaf84), were assigned to the ^{111}Rh decay. The 44.8 keV and 80.1 keV transitions were only observed in (γ)(γ) coincidence and low energy singles spectra. On the other hand, 15 gamma transitions reported in (Kaf84) were not observed, or their observation was uncertain. This was mainly due to the low statistics, with a few crucial exceptions. In (Kaf84), a 136.4 keV gamma transition with an intensity which is about half of the intensity of the 123.0 keV gamma transition was proposed to this decay. In the present studies

Table 4.10. The γ-transitions following the β-decay of ^{111}Rh. The intensities are determined from the (γ)(β) spectrum and normalized to the 275.4 keV γ-transition intensity.

Energy / keV		Relative intensity	Coincident gamma rays / keV
44.8 (4)	1,3)	0.14 (4)	
71.0 (2)	2)	0.94 (12)	116, 191, 580 2)
72.3 (2)	3)	1.36 (6)	
80.1 (3)	1)	0.26 (5)	
84.7 (2)		0.43 (9)	
116.5 (2)	2)	1.13 (11)	71, 97 2), 191
123.0 (2)		2.00 (9)	80, 256, 275, 594 2)
181.0 (3)		1.20 (13)	231
187.0 (3)		1.25 (7)	
191.2 (2)		1.95 (15)	71, 221, 259
195.2 (2)		1.4 (2)	80, 157 2)
220.5 (3)		0.26 (5)	
231.0 (2)		8.9 (5)	44, 181, 558, 832 2), 858, 1229 2)
255.0 (3)		0.47 (7)	
259.3 (3)		1.55 (18)	191, 402 2), 529, 830
275.4 (1)		100.0 (4)	814
411.8 (2)		9.42 (18)	
449.9 (3)		0.78 (16)	
529 (1)	1)		
558.3 (3)		1.7 (3)	191, 231
594.1 (4)	2)	1.5 (2)	
788.9 (3)		3.8 (5)	
813.6 (6)		0.4 (2)	
830.5 (5)		0.6 (2)	
1202.2 (6)	2)		259

1) Seen only in the gamma gated spectrum.
2) Not placed in the level scheme.
3) The intensity is determined from the low energy singles gamma spectrum.

a 136.7 keV gamma transition was observed, but it belongs to the decay of ^{111}Ru instead. Because of this 136.7 keV gamma transition it is impossible to totally deny the existence of the 136.4 keV gamma transition, but its intensity has to be considerably lower than suggested in (Kaf84). Furthermore, its placement in the previous tentative level scheme, which seems to be inspired by the 383 keV L = 2 state observed in the (d,p) reaction, is not confirmed in the present study. The 189.2 keV gamma transition was neither confirmed because of the presence of the 189.1 keV doublet in the ^{111}Ru decay. Not even the half-life analysis showed any longer-lived component in the decay of the 189.1 keV gamma transition, which was the case for the 136.7 keV gamma transition as well. The 189 keV gamma rays did not appear in coincidence with the 195.1 keV gamma transition in any measurement, which, together with the suspects on the 136.4 keV gamma transition, leads to the suggestion to exclude the 384 keV level from the β-decay scheme.

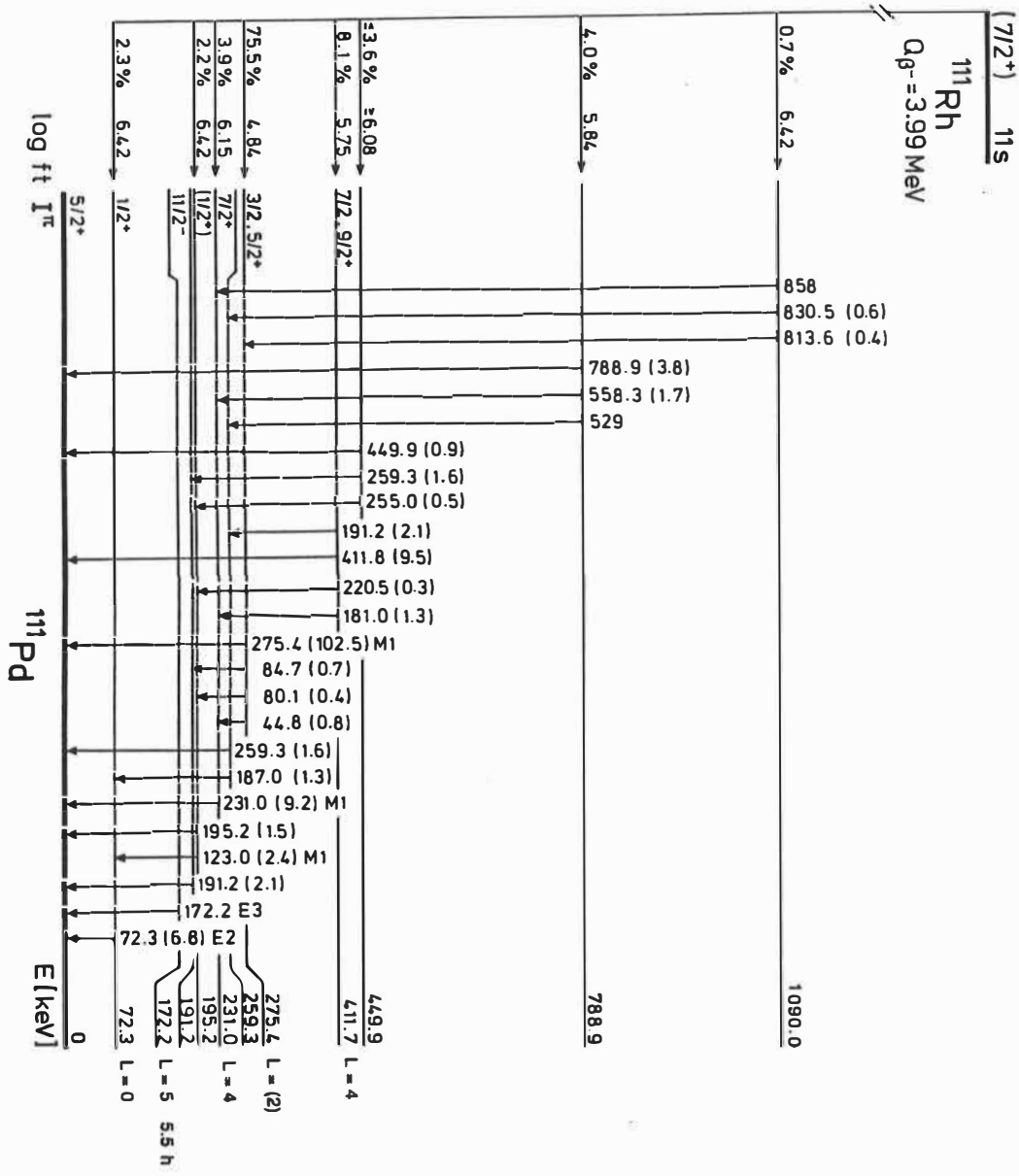

Figure 4.15. The level scheme of ^{111}Pd. Only the levels confirmed in this work and the 172 keV isomeric level (Sch69) are included. The 259.3 keV and 191.2 keV transitions are doubly placed and undivided intensity is given. In the beta feedings to the levels the intensity balances have been taken into account and the upper limits of the β-decay branching are given. The L assignments are taken from (Bla90).

The intensity of the 220.5 keV transition in the present measurement is considerably lower than in the previous one; however, its placement in the level scheme is the same as previously. The 529 keV gamma transition was observed only in the (γ)(γ) coincidence spectrum. As in (Kaf84), the 191.2 keV and 259.3 keV transitions are doubly placed in the level scheme to satisfy the observed coincidence relations. Deduced transition multipolarities support the previous spin and parity assignments of confirmed levels.

The 71.0 keV and 116.5 keV gamma transitions could not be placed in the level scheme. It should be noted that these transitions show similarity to the unplaced partial level scheme of ^{113}Pd, given in figure 4.15. These similarities are further discussed in chapter 5.

Table 4.11. Internal K-conversion coefficients for transitions in ^{111}Pd.
D: simultaneous measurement of conversion electrons and gamma rays;
DS: intensity of conversion electron transitions and gamma transitions deduced from singles spectra taken in separated runs;
B: electron intensity measured from the β-coincident spectrum;
FX: calculation based on the fluorescence yield of the characteristic X-rays of Pd.

Transition / keV	α_K(exp)	Method	α_K (theor)	Multipolarity
71.0	1.14 (17)	B	E1 0.255	M1/E2
	1.2(6)	FX	M1 0.612	
			E2 2.320	
72.3	1.8 (3)	D[1])	M1 0.856	M1/E2
			E2 3.058	
116.5	0.15 (4)	D	E1 0.0863	E1 or M1
			M1 0.223	
			E2 0.633	
123.0	0.123 (15)	D	E1 0.0737	E1 or M1
			M1 0.191	
231.0	0.032(8)	D[2])	E1 0.0124	M1
			M1 0.0349	
			E2 0.0605	
275.4	0.0231(5)	D	E1 0.0076	M1
			M1 0.0221	
			E2 0.0330	
411.8	0.010 (3)	DS	E1 0.00267	E2 (M1)
			M1 0.00807	
			E2 0.00917	

[1]) The K-71.0 keV intensity is calculated and subtracted from the electron intensity.
[2]) The L-211.7 keV (M1 in ^{111}Rh) intensity is calculated and subtracted from the electron intensity.

The level scheme of ^{113}Rh

In the construction of the level scheme of ^{113}Rh the (γ)(γ) coincidence relations given in table 4.12 were used. To give some insight to the quality of the (γ)(γ) coincidence data, the γ-spectrum gated by the 88.1 keV γ-transition is shown in figure 4.16. The γ-transitions without coincidences but corresponding to the energy of the cross-over transition to the ground state were placed in the level scheme. In general, the cross-over transitions were adopted in the level scheme onlu if they were assigned to the decay also on the basis of β-decay half-life. Multipolarities were deduced from the internal conversion coefficients for the 88.1 keV, 211.7 keV and 263.2 keV transitions, as shown in table 4.13. The low production rate of ^{113}Ru made it impossible to determine internal conversion coefficients for the other transitions. The deduced level scheme is shown in figure 4.17.

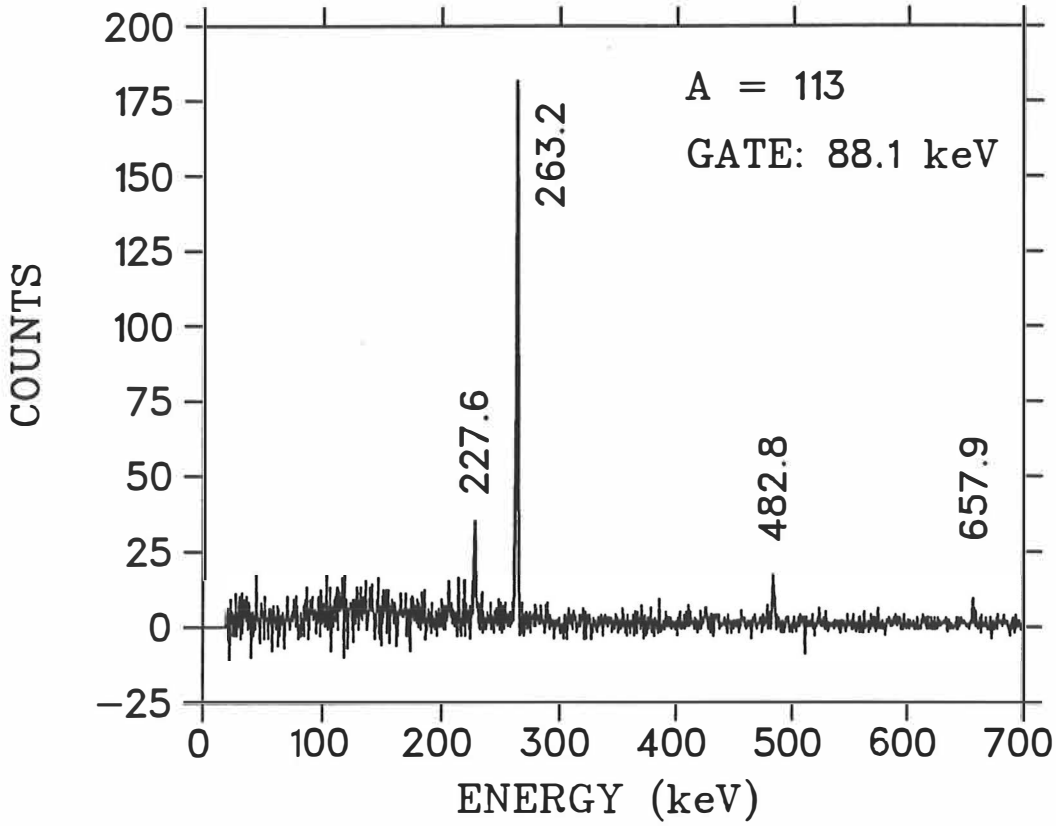

Figure 4.16. The gamma spectrum at mass number A = 113 gated by the 88.1 keV gamma transition.

Table 4.12. The γ-transitions following the β-decay of ^{113}Ru. The intensities are determined from the (γ)(β) spectrum and normalized to the 263.2 keV γ-transition intensity.

Energy / keV	Relative intensity	Coincident gamma rays / keV
88.1 (3)	22.4 (22)	228, 263, 483, 658
135.4 (5)	weak[1)]	
185.7 (3)	6.6 (8)	263, 337, 472 [2)]
206.1 (3)	2.4 (6)	
211.7 (3)	31.0 (15)	137, 232, 358 [2)], 367
227.6 (2)	6.4 (7)	88, 263, 351
232.3 (3)	6.1 (6)	136, 212, 298 [2)]
263.2 (3)	100.0 (40)	150 [2)], 186, 206, 228, 338, 424 [2)], 483, 499 [2)], 571, 715, 746
337.5 (3)	27.9 (24)	186, 233, 263, 358 [2)]
351.2 (4)	12.5 (32)	228
367.0 (4)	4.0 (6)	
443.7 (3)	5.4 (12)	
482.8 (3)	14.6 (27)	
571.0 (3)	4.3 (30)	
578.7 (4)	2.1 (6)	
600.2 (4)	5.2 (30)	
657.9 (3)	24.0 (18)	
714.9 (4)	6.2 (9)	
745.9 (5)	weak	
834.3 (4)	5.9 (16)	
1008.9 (4)	0.7 (4)	

1) Seen only in the coincidence spectrum.
2) Not placed in the level scheme.

Table 4.13. Internal K-conversion coefficients for transitions in ^{113}Rh.
D: simultaneous measurement of conversion electrons and gamma rays;
B: electron intensity measured from the β-coincident spectrum.

Transition / keV	α_K (exp)	Method	α_K (theor)	Multipolarity
88.1	0.46 (6)	D [1)]	E1 0.183	M1
	0.46 (8)	B [2)]	M1 0.439	
			E2 1.58	
211.7	0.06 (2)	B [2)]	M1 0.0399	M1 / E2
			E2 0.0778	
263.2	0.033 (5)	D	M1 0.0226	E2
			E2 0.0368	

1) Normalized to the 95.8 keV M1 transition in ^{111}Ag.
2) Normalized to the 263.2 keV E2 transition.

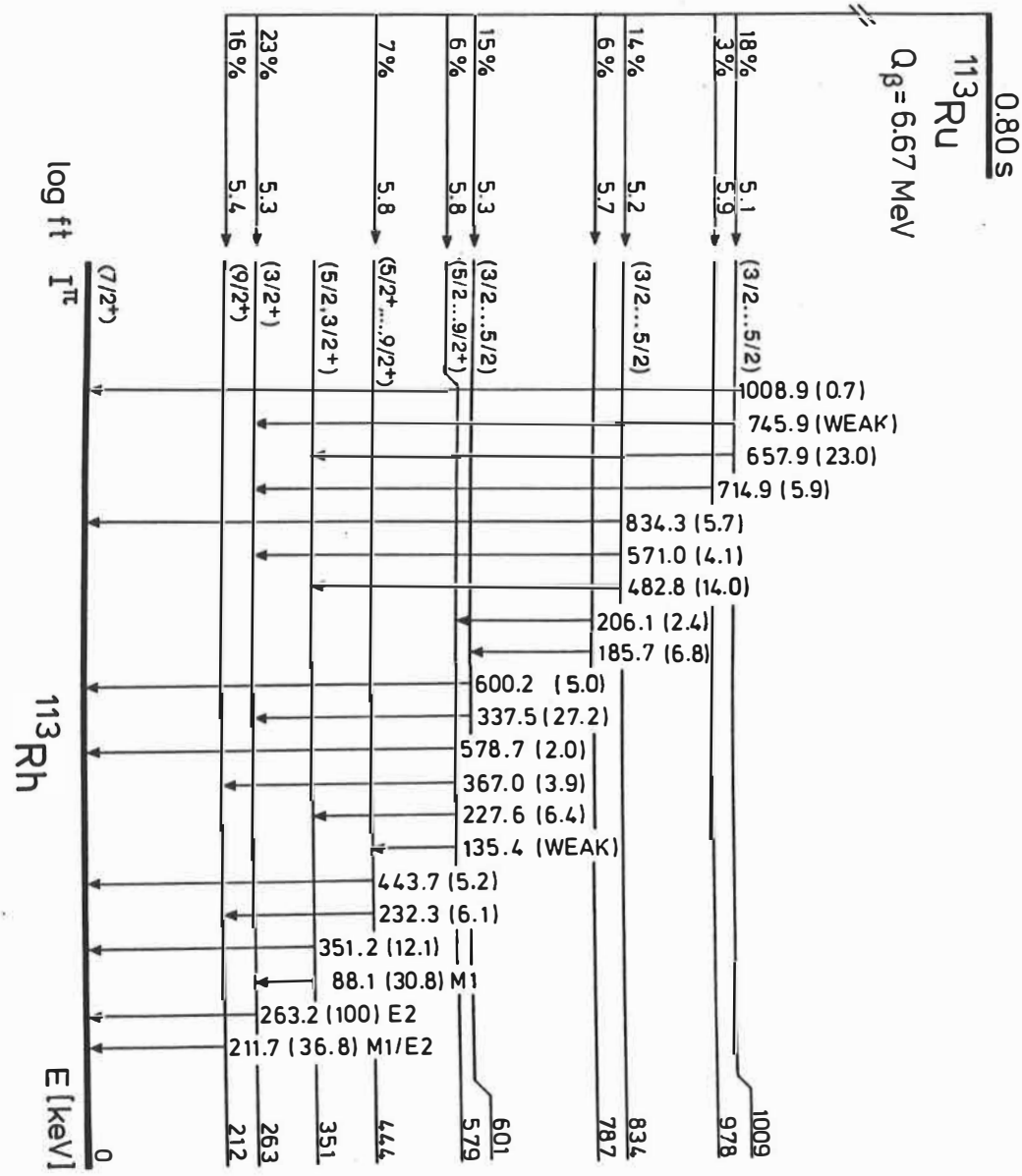

Figure 4.17. The level scheme of ^{113}Rh.

Ground state branching of the ^{113}Ru decay. The ground state branching in the β-decay of ^{113}Ru was determined in the same way as in the case of ^{111}Ru. However, the analysis of the data shown in figure 4.5, results in zero ground state branching. This result was unexpected, because a fast β-decay to the 7/2+ ground state of odd-A Rh is observed in the decay of lighter

odd-A Ru isotopes. It is possible that this reflects a change of the ground state I^{π} at ^{113}Ru as compared with the lighter Ru isotopes. There is, however, also some experimental uncertainty, and the deduced zero ground state branching in the decay of ^{113}Ru can also result from the used branching ratios in the β-decay of ^{113}Rh. The absolute branching of 0.38 γ-rays/decay for the 348.9 keV transition, which was used in calculation of the number of decayed ^{113}Ru nuclei, is deduced from the decay scheme given in figure 4.18. The absolute branching can, however, be considerably lower, if there is a lot of beta feeding directly to the ground sate of ^{113}Pd; in the present level scheme the ground state branching is assumed to be zero. The β-feeding to the excited levels that decay directly to the ground state and are not observed in the present studies have the same effect. However, so far, zero ground state branching in the β-decay of ^{113}Ru is adopted.

Spin and parity assignments.

The ground state. The spin and parity of the ^{113}Rh ground state were deduced from the observed β-decay properties. Most of the β-decay goes to the $5/2^+$ level at 348.9 keV and the $7/2^+$, $9/2^+$ level at 409.3 keV in ^{113}Pd, see figure 4.18. The spin and parity assignments of these levels will be discussed later. Thus, $7/2^+$ is suggested for the ^{113}Rh ground state. This is consistent also with theoretical calculations (Bre89) and with the systematics of the lighter odd-A Rh nuclei ^{107}Rh, ^{109}Rh and ^{111}Rh. The very low branching to the ground state in the β-decay of ^{113}Ru would then imply lower spin for the ground state of ^{113}Ru than 5/2 suggested for the lighter odd-A Ru isotopes.

The 211.8 keV level. This level is connected to the ground state with an M1/E2 transition. The possible spin and parity assignments are $5/2^+$, $7/2^+$ and $9/2^+$. In the case of ^{111}Rh the lowest transition seems to be pure M1. In ^{113}Rh the 211.8 keV transition seems to have at least some E2 mixing. From the systematics $9/2^+$ seems to be a reasonable choice. The relatively low log *ft* value is against this assignment, if the low branching to the ground state in the β-decay is accepted. This could result from unobserved, high energy gamma transitions to the 211.8 keV level. In the case of ^{111}Rh, there is a reasonable amount of feeding to the $9/2^+$ state from levels above 1 MeV; in the case of ^{113}Rh, these transitions are not observed, which may be due to low statistics. Thus, despite the relatively low log *ft* , $9/2^+$ is suggested for this level.

The 263.2 keV level. The 263.2 keV transition to the ground state has an E2 multipolarity, which reminds of the situation in ^{111}Rh. Neither is there any observable transition between the 263.2 keV and 211.8 keV levels. The strong β-decay feeding this level is different from that of the 303.8 keV level in ^{111}Rh, which is consistent with the low-spin assignment for the ground

state of ^{113}Ru. Spin and parity $3/2^+$ are thus suggested for this level, which is also supported by the level systematics.

The 351.2 keV level. The M1 multipolarity was deduced for the 88.1 keV transition feeding the $(3/2^+)$ state at 263.2 keV. This results in possible spin and parity values of $1/2^+$, $3/2^+$ and $5/2^+$. The feeding in the β-decay to this level is small, which could support a $5/2^+$ assignment. The level lifetime measurements at A = 113 showed no measurable lifetime for this level, within the limitations set by poor statistics. This result implies that the 351.2 keV state is not a member of the intruder band. This was expected, since the lowest member of the intruder band was observed at 395.0 keV in ^{111}Rh and the intruder band should appear at higher excitation energy in ^{113}Rh. Therefore, it can be deduced from the systematics that the 351.2 keV state can have the same origin as the $5/2^+$ (or $3/2^+$) state at 382.0 keV in ^{111}Rh.

The 443.7 keV level. This state decays both to the $9/2^+$ level at 211.8 keV and to the $7/2^+$ ground state. Even though the intensity of these transitions is low, high multipolarity would produce a measurable amount of conversion electrons. Thus, change of spin in these transitions is deduced to be ≤ 2 units, leading to possible spin values of 5/2, 7/2, 9/2, 11/2 and 13/2. Furthermore, no transitions to the $5/2^+$ level at 351.2 keV or to the $3/2^+$ level at 263.2 keV are observed. Thus, spin 9/2 is suggested, even though 5/2 or 7/2 cannot be excluded. Spin values of 11/2 or 13/2 are not probable, since the level is at least to some extent fed in the β-decay. The weak 135.4 keV transition from the 578.7 keV level, seen only in the coincidence spectrum, does not help in excluding any of these spin values.

The 578.7 keV level decays to all the levels below except for the $(3/2)^+$ level at 263.2 keV. Thus, a spin value of 7/2 or 9/2 is suggested for this level. The relatively high log *ft* supports this assignment.

The 600.2 keV level. This level is relatively strongly fed in the β-decay. This would imply a similar spin as that of the 263.2 keV level. The level has a stronger decay to the (3/2) state at 263.2 keV than to the $7/2^+$ ground state, which possibly implies spin 3/2 or 5/2. The level could then be the lowest member of the intruder band. The lifetime of this level could not be measured in the present studies, and the intruder band suggestion is based on low spin and extrapolation of level systematics. If the speculations are continued, the 185.7 keV transition could be an interband transition from the $7/2^+$ state at 787 keV, while the $5/2^+$ and $1/2^+$ states are not seen with the present statistics.

The 834.2 and 1008.9 keV levels are strongly fed in the β-decay. However, despite a larger Q_β window as compared with the ^{111}Ru decay, only levels below 1 MeV are populated. The low

yield of ^{113}Ru and low detection efficiency for high energy gamma rays may limit the possibilities of observing the β-decay to the levels at high excitation energy, and the absolute log *ft* values deduced from the present data may be in error. Spin 1/2, 3/2 or 5/2 is thus suggested for both of these levels, but these assignments have to be considered as preliminary.

Besides the intruder band, also negative parity states originating from the $p_{1/2}$ orbital are expected (Bre89), (Rog90c). Simple extrapolation from the lighter odd-A Rh isotopes gives the excitation energy of about 620 keV for the $1/2^-$ state. The properties of the 601 keV and 579 keV states do not fit this picture. The reasonable candidates for negative parity states are the 978 keV state and the 787 keV. The latter was also speculated to be the intruder band member. More experiments, especially concentrating on lifetime measurements, are clearly needed to identify the intruder band members.

The level scheme of ^{113}Pd

The level scheme of ^{113}Pd was deduced mainly from the (γ)(γ)-coincidence relations given in table 4.14. Multipolarity of 14 transitions was deduced from the internal conversion coefficients. At low energy, the copiously produced 43.2 keV $7/2^+$ isomer in ^{113}Ag tends to disturb conversion electron measurements. Fortunately, the conversion electrons due to this isomer disappeared in β-coincident electron spectra, as well as the conversion electrons due to the 81.3 keV M2 transition de-exciting the $9/2^-$ isomeric state in ^{113}Pd. For the determination of the ICC for the 81.3 keV transition, the calculated intensity of the K-conversion electrons due to the 79.7 keV M1 transition was subtracted from the intensity of the K-79.7/K-81.3 doublet in the singles conversion electron spectrum. The multipolarity of the 79.7 keV transition results from the ICC deduced from the β-gated spectra. The deduced K/L ratio for the 81.3 keV transition is 4.1 ± 1.2 which implies L = 2 for this transition. For the 34.9 keV transition, only L conversion electrons were possible to observe. The internal conversion coefficients and the deduced multipolarities of transitions are shown in table 4.15.

Spin and parity assignments.

<u>The ground state.</u> The spin and parity $5/2^+$ were uniquely assigned to the ground state of ^{113}Pd in (Fog88). The assignment was based on the observed β-decay properties of ^{113}Pd.

<u>The 34.9 keV level.</u> The observed (γ)(γ) coincidence data can be explained only by introducing a level at 34.9 keV, as seen in the level scheme given in figure 4.18. The 34.9 keV gamma transition did not appear in the (γ)(γ) spectra, but it was observed in the low energy gamma singles spectrum. More evidence of this transition was obtained from the singles electron

Table 4.14. The γ-transitions following the β-decay of ^{113}Rh. The intensities are determined from the (γ)(β) spectrum, except the intensity of transitions from isomeric states. The intensities are normalized to the 348.9 keV γ-transition intensity.

Energy / keV		Relative intensity	Coincident gamma rays / keV
34.9 (3)	1)	1.2 (2)	
79.7 (3)		2.7 (3)	97, 121, 138, 157, 609
81.1 (3)	1)	6.9 (4)	
84.9 (2)	2)	8.2 (5)	119, 135, 255, 980 2), 1053 2), 1124 2)
96.8 (3)		1.8 (3)	217, 252
100.4 (3)		0.7 (1)	
116.8 (2)		9.7 (5)	100, 197, 221, 258, 349
119.4 (3)	2)	0.5 (1)	
120.8 (3)		2.2 (3)	138, 217, 252, 358
135.0 (2)	2)	2.8 (3)	85, 119
137.5 (2)		7.8 (3)	80, 157, 237, 609
151.8 (3)		7.4 (4)	100, 197, 221, 258, 349, 358, 747.5 2)
157.1 (3)		5.7 (4)	80, 138, 217, 252
159.9 (3)		4.8 (5)	190
189.7 (2)		45.0 (8)	160, 220, 265, 311, 349, 542, 933 2), 1226 2)
197.0 (4)		0.9 (3)	117
217.0 (2)		9.1 (4)	97, 121, 157, 358, 609
219.6 (3)		10.3 (6)	190
221.0 (3)		4.3 (5)	117, 152, 358
236.7 (4)		0.9 (3)	
252.1 (3)		6.8 (5)	97, 121, 157, 609
254.8 (5)	3)	1.2 (4)	
257.5 (4)		2.7 (4)	117, 152, 333, 340, 672
265.0 (3)		2.8 (4)	190
310.8 (4)		1.2 (3)	190
332.7 (3)	2)	2.0 (3)	258, 340
339.1 (4)	3)	weak	258, 333
348.5 (6)	4)	2.2 (5)	117, 152
348.9 (5)	4)	2.1 (5)	190
348.9 (3)		100.0 (9)	
357.6 (3)		4.5 (3)	117, 121, 221, 252, 339
373.1 (4)		1.8 (4)	
409.3 (3)		42.2 (8)	
454.7 (4)		2.8 (4)	
500.3 (3)		5.5 (4)	
538.8 (4)		7.0 (5)	
543.0 (4)		3.8 (4)	
609.0 (3)		6.8 (5)	80, 138, 217, 252
671.1 (4)		2.3 (5)	
749.1 (4)		1.7 (4)	
932.7 (4)		3.8 (5)	
980.0 (5)		2.0 (4)	
1053.0 (5)		1.9 (4)	

1) Intensity from the singles spectrum.
2) Not placed in the level scheme.
3) Seen only in the (γ)(γ) spectrum.
4) Intensity deduced from the (γ)(γ) spectrum.

Table 4.15. Internal K-conversion coefficients for transitions in ^{113}Pd.

D: simultaneous measurement of conversion electrons and gamma rays;

DS: intensity of conversion electrons and gamma rays deduced from singles spectra taken in separated runs;

B: electron intensity measured from the β-coincident spectrum.

Transition/keV	α_K (exp)	Method	α_K (theor)	Multipolarity
34.9	α_L=29 (7)	D	α_L(M1)=1.5 α_L(E2)=40	E2
79.7	0.56(15)	B [1])	E1 0.254 M1 0.645 E2 2.235	M1
81.3	5.4(9)	D [2])	M1 0.610 E2 2.096 M2 7.043	M2
84.9	0.12(3)	B [1])	E1 0.212 M1 0.539	E1
116.8	0.31(3)	D	M1 0.220 E2 0.623	M1/E2
120.7	0.52(11) 0.57 (12)	D DS	M1 0.201 E2 0.557	E2
135.1	0.15 (5)	D	M1 0.147 E2 0.377	M1
137.5	0.16 (3)	D	M1 0.140 E2 0.355	M1
151.8	0.08(2)	D	E1 0.0403 M1 0.107	M1
189.7	0.063 (4)	D	E1 0.0215 M1 0.0586 E2 0.117	M1
217.0	0.05 (3)	DS	M1 0.0411 E2 0.0745	M1/E2
252.1	0.04 (3)	DS	M1 0.0278 E2 0.0445	E2/M1
348.9	0.0144(20)	D	M1 0.0121 E2 0.0152	M1/E2
409.5	0.020 (6)	DS	M1 0.00818 E2 0.00932 M2 0.0293	E2

[1]) Normalized to the 189.7 keV M1 transition in ^{113}Pd.

[2]) The K-79.7 (M1 in ^{113}Pd) intensity is calculated and subtracted from the electron intensity.

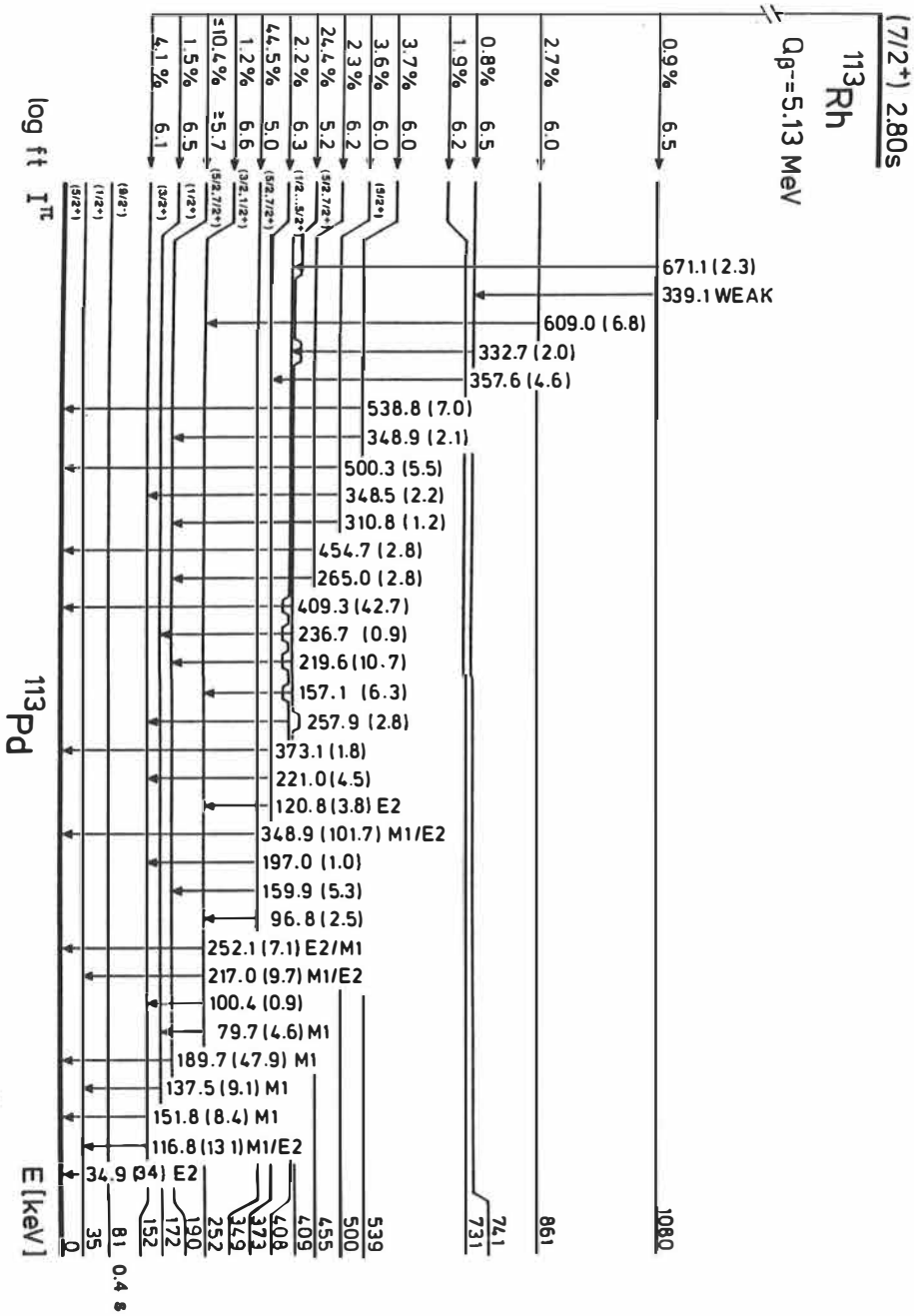

Figure 4.18. The level scheme of ^{113}Pd.

A peak in the singles conversion electron spectrum with an energy of 32.4 keV was observed, which corresponds to the L-34.9 transition in Pd. The K-conversion electrons have too low energy to be observed in the present measurements. Coincidence measurements between the conversion electrons and L X–rays which would possibly have confirmed the identification of the 32.4 keV conversion electrons were neither possible to perform. The deduced L conversion for the 34.9 keV transition implies an E2 multipolarity. An $1/2^+$ level at low energy is expected on the basis of the level systematics of the odd-A Pd nuclei ^{109}Pd and ^{111}Pd. Spin and parity $1/2^+$ were assigned for the 34.9 keV level. Furthermore, these can also be deduced from the multipolarities of the 116.8 keV, 137.5 keV and 217.0 keV transitions populating the 34.9 keV level. Due to the E2 multipolarity a relatively long lifetime of the corresponding state is expected. The non-observation of the 34.9 keV gamma transition in coincidence with β-particles also implies that the level has a lifetime much longer than the 1μs coincidence window used. The Weisskopf estimate for the half-life of a 34.9 keV E2 transition is 5 μs.

The 81.3 keV level. The isomeric state in ^{113}Pd was found as explained in chapter 4.3. The multipolarity of the transition was deduced to be M2. No coincidences were observed for the 81.3 keV gamma rays. Thus, there are two possibilities to locate the transition: above the ground state, or above the 34.9 keV level, which also may have a lifetime long enough to hinder coincidences. On the basis of the experimental systematics of the odd-A Pd nuclei a high spin is expected for the isomeric state. The systematics thus support the $1/2^+$ assignment for the 34.9 keV level and the location of the 81.3 keV transition above the $5/2^+$ ground state. If the 81.3 keV M2 transition is populating the $1/2^+$ state, the possible spins of the initial state would be 1/2, 3/2 or 5/2. A state with such a low spin could be expected to decay in very competitive way also to the ground state. The highest possible spin for the 81.3 keV level is 9/2 and this spin with negative parity is suggested for this level. On the basis of the systematics $11/2^-$ was expected. This exception from the systematics is discussed in chapter 5.

The 151.8 keV level is connected to the ground state via an M1 and to the 34.9 keV level via an M1/E2 transition. Spin and parity $3/2^+$ are thus suggested.

The 172.4 keV level. The placement of this level is fixed by the 236.7 keV gamma transition and the intensity ratio between the 79.7 keV and 137.5 keV transitions. Without the 236.7 keV transition the order of the 79.7 keV and 137.5 keV transitions could be switched. This level is connected to the $1/2^+$ level at 34.9 keV via an M1 transition and to the 252.1 keV level also via an M1 transition. Since no decay to the ground state is observed, a spin difference as large as

possible between the 172.4 keV level and the ground state is assumed and a spin and parity $1/2^+$ are suggested also for this level.

The 189.7 keV level is connected to the ground state via the second most intense transition in the whole decay. The M1 assignment of the 189.7 keV transition implies a spin and parity of $3/2^+$, $5/2^+$ or $7/2^+$ for this level. The relatively large β-decay branching to the 189.7 keV level implies a spin of 5/2, 7/2 or 9/2, if the ground state of ^{113}Rh is assumed to be $7/2^+$. Since no decay to the $1/2^+$ level at 34.9 keV is observed, $7/2^+$ is preferred over $5/2^+$.

The 252.1 keV level populates the $5/2^+$ ground state and the $1/2^+$ level at 34.9 keV via M1/E2 transitions. It is also connected via an M1 transition to the 172.4 keV level, for which spin and parity of $1/2^+$ were deduced. The $3/2^+$ assignment for this level is suggested. If the 252.1 keV transition is E2 with no M1 mixing, which is possible within the precision of the α_K measurement, an $1/2^+$ assignment becomes also possible.

The 348.9 keV level. The 348.9 keV gamma transition is the most intense in the decay of ^{113}Rh. It was assigned to this decay via $(e^-)(X)$ coincidences and its half-life.

The 348.9 keV level is de-excited by several gamma cascades to the ground state, as seen in the level scheme in figure 4.18. The intense 348.9 keV transition was also placed to de-excite this level. However, some weak coincidences between the 349 keV gamma rays and the 189.7 keV, 151.9 keV and 116.8 keV transitions were observed. These coincidences were far too weak to be coincidences between the intense transition from the 348.9 keV level to the ground state. The 189.7 keV transition is the second most intense transition in the β-decay of ^{113}Rh. Furthermore, the exact energy of the 349 keV γ-rays observed in coincidence with the 116.8 keV and 151.9 keV γ-transitions is 348.5 (6) keV.

The observed coincidences and intensities are explained by the multiple placement of 349 keV transitions. The 348.5 keV transition in coincidence with the 116.8 keV and 151.9 keV transitions fits energetically to the transition from the 500.3 keV level to the 151.9 keV level. Another 348.9 keV transition was placed above the 189.7 keV level, resulting in a level at 538.8 keV. This level is confirmed by a cross-over transition to the ground state.

Most of the observed gamma intensity in the 349 keV peak belongs to the transition from the 348.9 keV level to the ground state. No coincidences between this 348.9 keV gamma transition and other gamma transitions were observed. From the $(\gamma)(\gamma)$ coincidence spectra the intensities of the 348.5 keV transition and the 348.9 keV transition from the 538.6 keV level to the 189.7 keV level can be deduced to be 2.2 (5) and 2.1 (5), respectively, as compared with 100.0 (9) for the 348.9 keV gamma transition to the ground state. The angular correlation

effects are not taken into account in these numbers. Anyhow, they are believed to be neglible because of the used tight detector geometry.

The two low-intensity transitions were neglected in deducing of the α_K coefficient for the most intense 348.9 keV transition. Their effect is less than 5 % and it is taken into account in the error of the deduced α_K. The M1/E2 multipolarity for the 348.9 keV transition suggests a $3/2^+$, $5/2^+$ or $7/2^+$ assignment for the 348.9 keV level. If the ground state of ^{113}Rh is assumed to be $7/2^+$, the strong β-feeding to this level, which results in log *ft* of 5.0, implies possible spin values of 5/2, 7/2 and 9/2. The strong β-feeding gives reason to believe that spin and parity are similar to the other strongly populated levels at 189.7 keV and 409.3 keV, respectively. Thus, spin and parity values of $5/2^+$ or $7/2^+$ are preferred over $3/2^+$.

The 373.1 keV level is connected via a 120.8 keV E2 transition to the $3/2^+$ ($1/2^+$) level at 252.1 keV, implying positive parity for the 373.1 keV level. The multipolarity of the 221.0 keV from the 373.1 keV level transition was unmeasurable due to its low electron intensity. Since the 221.0 keV transition connects positive parity states, E1 is ruled out . The multipolarity of this transition has to be M1 or E2. If M1 is assumed, the $3/2^+$ assignment of the 151.9 keV level gives the possible spin and parity values of $1/2^+$, $3/2^+$ and $5/2^+$. Low β-feeding to this level supports an $1/2^+$ or a $3/2^+$ assignment over $5/2^+$.

No measurable lifetime was connected to this level. The Weisskopf estimate for the partial half-life of the 120.8 keV E2 transition is 385 ns. This should result in a lifetime of about 100 ns for the level when the gamma branchings are taken into account. The observed fast E2 transition may imply collectivity of the 373.1 keV state.

The 408.3 keV level is placed in the level scheme on the basis of the (γ)(γ) coincidence data. The 408.3 keV cross-over transition to the ground state was impossible to observe because of the strong 409.3 keV transition and the 407.0 keV gamma transition from the ^{97}Y decay. The 408.3 keV cross-over transition is thus not placed in the level scheme.

The 409.3 keV level decays to the ground state via an E2 transition. The deduced α_K coefficient given in table 4.15 is high for an E2 transition even within the quoted errors, but the intensity supports E2 assignment. Strong β-feeding to this level implies spin values similar to those of the other strongly populated levels at 189.7 keV and 348.9 keV, namely 5/2 or 7/2. A 9/2 spin assignment is not very probable for any of these levels. If M1 multipolarity is assumed for the 157.1 keV, 219.6 keV and 236.7 keV transitions, spin and parity $5/2^+$ results for the 409.3 keV level. The M1 assumption is reasonable according to the conversion electron yield

of these transitions, and it is also consistent with the previous spin and parity assignments for the levels at 172.4 keV, 189.7 keV and 252.1 keV.

The 500.3 keV level is another level resulting from the multiply placed 349 keV transition. A transition energy of 348.5 keV is adopted from the (γ)(γ) spectrum. The decay properties of the level to the levels below support a low spin assignment for this level. This fact combined with the relatively high β-feeding results in a $5/2^+$ assignment for the level.

The 538.8 keV level. The third 349 keV gamma transition was placed to de-excite this level. No spin or parity are suggested.

The 730.6 keV level results from the placement of the 357.6 keV transition. A 730.9 keV gamma transition is seen in the (γ)(β) spectrum, but there is no other evidence for this cross-over transition. Thus, the 730.9 keV cross-over transition is not placed in the level scheme.

The 741.0 keV level is based on the observation of the 332.7 keV and the 339.1 keV gamma transitions in coincidence with each other and also with the 257.9 keV gamma transition. The order of the 332.7 keV and 339.1 keV gamma transitions is based on the higher intensity of the 332.7 keV transition. No cross-over transitions from this level were observed.

The 861.2 kev level results from the placement of the 609.0 keV transition. A 861.2 keV gamma transition is observed also in the (γ)(β) spectrum, but its intensity is too low for a half-life analysis and it can be assigned to the level scheme by the energy only. Therefore, the 861.2 keV cross-over transition is not placed in the level scheme.

The 1080.1 keV level is fixed by the 671.1 keV gamma transition. The intensity of the 339.1 keV gamma transition could not be determined from the β-coincident spectrum, but it was placed in the level scheme on the basis of the (γ)(γ) coincidences.

The unplaced transitions. In figure 4.19 an unplaced partial level scheme of ^{113}Pd is given. The half-life of the 84.9 keV γ–transition observed in coincidence with β-particles show that these transitions are following the β-decay of ^{113}Rh. However, these transitions are not observed in coincidence with the other transitions belonging to the β-decay of ^{113}Rh. The 84.9 keV γ–transition is also connected with a lifetime of $T_{1/2}$ = 53 (4) ns, which is deduced from the (γ)(β)-TAC spectrum. It can be the same 84.9 keV transition reported in (Joh70), in which the 84.9 keV gamma transition was assigned to mass number A = 115 or A = 114 and connected with a half-life of 61 ns (± 25 %). The hindrance of this E1 transition as compared to the Weisskopf estimate is of the order of 10^5.

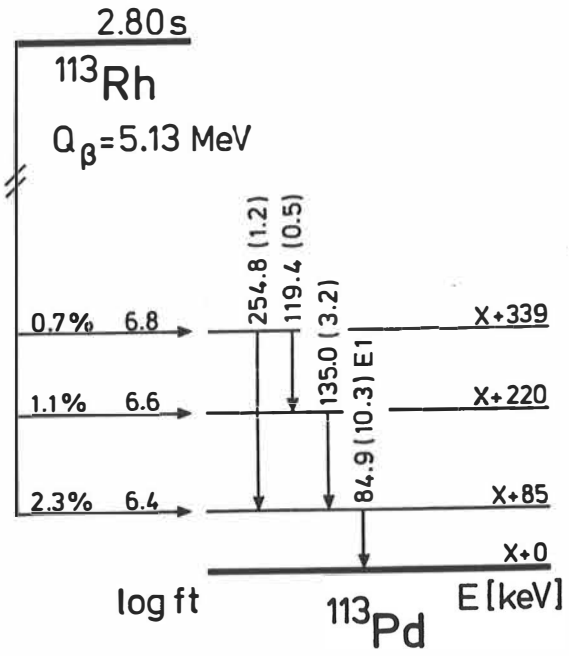

Figure 4.19. An unplaced partial level scheme of ^{113}Pd. The order of the levels is based on intensity balances.

The level scheme of ^{115}Pd

Altogether 23 gamma transitions were assigned to the β-decay of ^{115}Rh. Eighteen transitions were placed in the level scheme on the basis of the (γ)(γ) coincidences given in table 4.16. The deduced level scheme is shown in figure 4.20. A 89.4 keV E3 transition was observed only via (e^-)(X) coincidences. This transition is de-exciting a partly β-decaying negative parity isomeric state in ^{115}Pd, which decays with a half-life of 50 s (Fog88), (Fog90).

It was not possible to determine the ICC values in a direct simultaneous measurement of gamma rays and conversion electrons, because several strong converted transitions produced by the other activities – ^{115}Ag, ^{115}Cd, ^{99}Nb, ^{99}Zr – were present in the singles electron spectrum. The multiple peaks in the electron spectrum were impossible to be solved uniquely. However, the relative intensities of the converted transitions in ^{115}Pd can be deduced from the conversion electron spectrum gated by the K_α X-rays of Pd, in which the corresponding peaks showed up as seen in figure 3.6.d). On the other hand, the fluorescent yield of the characteristic X-rays due to the 127.9 keV transition can be deduced by gating the gamma spectrum by the 340.5 keV, 305.4 keV, 227.0 keV, 278.0 keV and 448.3 keV transitions. The α_K was deduced for the 127.9 keV transition on the basis of the yield of the characteristic K X-rays of Pd. The other α_K values given in table 4.17 are normalized to this experimental value.

Table 4.16. The γ-transitions following the β-decay of ^{115}Rh. The intensities are determined from the (γ)(β) spectrum and normalized to the 127.9 keV γ-transition intensity.

Energy / keV	Relative intensity	Coincident gamma rays / keV
38.5 (2) [1]	2.3 (5)	
101.1 (2)	6.6 (5)	126, 128, 164, 223, 254
125.6 (3) [3]	78.0 (35)	101, 128, 179, 223, 323, 498 [1], 882 [1], 1088, 247 [4]
127.9 (2)	100.0 (8)	101, 126, 179, 227, 279, 305, 323, 341, 401 [1], 423 [1], 450, 987, 1088, 1213
164.5 (2) [3]	17.0 (14)	101, 179
179.8 (3) [3]	19.2 (15)	126, 128, 164, 254, 416 [5]
198.4 (3) [1]	3.5 (4)	39 [1]
222.9 (3)	2.0 (4)	
227.0 (3)	2.9 (6)	
235.3 (3) [1]	10.6 (17)	
253.7 (3)	12.6 (22)	179
270.1 (3) [1]	11.4 (8)	
278.0 (3)	4.0 (7)	
296.3 (3)	23.8 (11)	138 [2], 172 [1], 281 [1]
305.4 (3)	4.9 (7)	128
322.9 (3)	3.6 (6)	
340.5 (3)	12.0 (8)	128, 205 [1], 462 [1]
400.9 (3) [1]	3.5 (6)	
423.6 (4) [1]	9.1 (8)	
448.8 (4)	2.5 (6)	
883.4 (5) [1]	4.7 (9)	
986.3 (4)	4.6 (8)	
1087.0 (5)	9.0 (13)	
1212.3 (6)	2.6 (6)	

[1] Not placed in the level scheme.
[2] Seen only in the gamma gated spectrum.
[3] Doublet; energy and intensity are deduced from the gamma gated spectrum.
[4] ^{115}Pd decay.
[5] ^{99}Zr decay.

An additional correction was needed to the relative intensities of the electron transitions deduced from the K X-ray gated spectrum, because the observed intensity of a transition is effected by the conversion of other transitions in the cascade. The X-rays produced by the conversion of a transition can be observed in coincidence with another converted transition in cascade with the first one. This effect is seen in figures 3.6.d) and 4.2. by the presence of L-conversion electrons that cannot otherwise appear in coincidence with K X-rays. Unfortunately, the intensity of L-conversion electrons in the conversion electron spectrum

gated by the K_α X-rays of Pd is so low that the effect cannot be deduced directly. Instead, the effect can be estimated using the branching ratios deduced from the level scheme and the conversion coefficient of the transitions. Because the correction effects on the electron transition intensities and thus on the conversion coefficients, making of the correction is, even though straightforwad, not a one step process. The effect was first calculated from the uncorrected intensities. The calculation was then repeated with the corrected intensities. After a few iteration the necessary correction was estimated to about 22% for the K-101.1 keV, about 25% for the K-125.6 keV, about 12% for the K-127.9 keV and about 22% for the K-179.8 keV transition.

Table 4.17. Internal K-conversion coefficients for transitions in ^{115}Pd.
X: electron intensity is obtained from the spectrum gated by the K_α X-rays of Pd;
FX: calculation is based on the fluorescence yield of the characteristic K X-rays of Pd.

Transition / keV	α_K (exp)	Method	α_K (theor)	Multipolarity
101.1	0.50 (18)	X [1]	E1 0.129	M1 / E2
			M1 0.329	
			E2 1.019	
125.6	0.18 (8)	X [1]	E1 0.0689	M1 (E2)
	0.15 (10)	FX	M1 0.179	
			E2 0.483	
127.9	0.20 (5)	FX	E1 0.0657	M1 / E2
			M1 0.171	
			E2 0.456	
179.9	0.054 (18)	X [1]	E1 0.0249	M1
			M1 0.0676	
			E2 0.140	
296.3	0.0097 (46)	X [1]	E1 0.00624	E1 (M1)
			M1 0.0184	
			E2 0.0258	

[1]) Normalized to the experimental $\alpha_K = 0.20$ (5) of the 127.9 keV transition.

In addition, the multipolarity of the 164.5 keV transition is indirectly deduced as E1, since the K-164.5 electron transition is not observed in the electron spectrum. If the 164.5 keV transition is M1, the K-164.5 keV transition intensity should be about the same as the intensity of the K-179.8 transition. The E3 multipolarity adopted for the 89.4 keV transition from (Fog88), (Fog90). The ICC of this transition was impossible to deduce in the present work, since the 89.4 keV gamma rays were not observed in the singles gamma ray spectrum. The background conditions in the present measurements were such that the upper limit of the intensity of the 89.4 keV γ-transition is 0.7% of the intensity of the 127.9 keV γ-transition. This results in $\alpha_K \geq 11$ for the 89.4 keV transition.

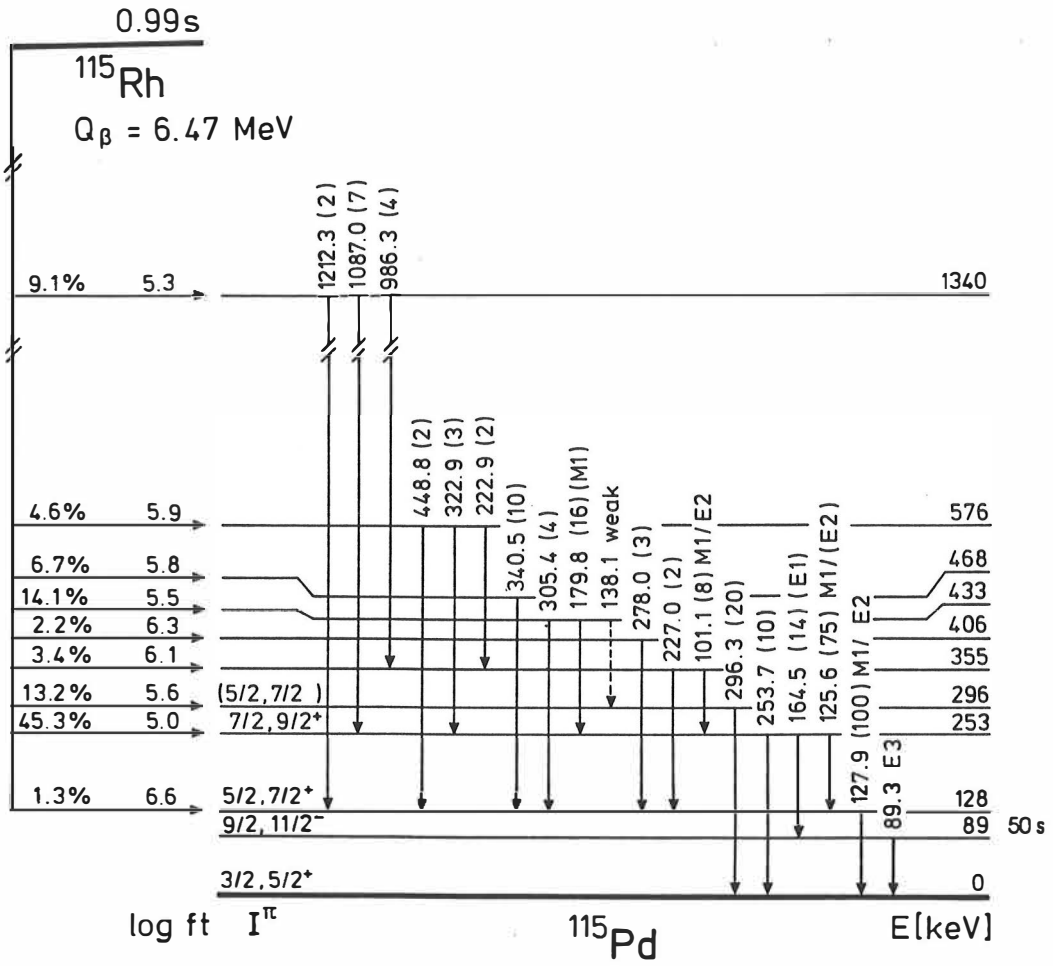

Figure 4.20. The level scheme of ^{115}Pd. The zero ground state branching is based on the measurement; for details, see the text and (Äys88a).

The ground state branching in the ^{115}Rh β-decay was determined experimentally. A β-telescope consisting of a ΔEβ and a 6 cm thick plastic scintillator was used as β-counter. The total intensity of the ^{115}Rh β-decay was deduced from the 1.0 s component in the decay of the mass separated A = 115 source. There were other short-lived β-activities in the source due to A = 99 contaminations. The nuclei with A = 99 were mass separated as monoxide molecules, as explained in chapter 3. Their contribution was taken into account by subtracting a

background time spectrum experimentally measured at A = 99 and then normalized with the gamma transition intensities observed in a simultaneously measured (γ)(β) spectrum. The β-feeding to the excited states of ^{115}Pd was deduced from the gamma transition intensity in the (γ)(β) spectrum. The total β-intensity and β-feeding to the excited states appeared to be equal with 15 % uncertainty. Thus, a zero ground state branching was deduced for the ^{115}Rh β-decay (Äys88a).

Spin and parity assignments.

The ground state. The ground state of ^{115}Pd is assigned to be $5/2^+$ or $3/2^+$. The isomeric state at 89.4 keV is assigned to be $11/2^-$ or $9/2^-$, respectively (Fog88). In the present measurement the ground state branching in the ^{115}Rh decay was determined experimentally to be zero, as explained above. Spin and parity $7/2^+$ can be assumed for the ground state of ^{115}Rh on the basis of the levels systematics of lighter odd-A Rh nuclei, while the observed zero ground state branching supports a $3/2^+$ assignment. The β-decay properties of the isotone, ^{113}Ru, also support a spin lower than 5/2 for the ground state of this nucleus. A change of the ground state I^π from $5/2^+$ to $3/2^+$ would then be connected with the increasing of neutron number.

The 89.4 keV level. The isomerism in odd-A Pd nuclei arises from the low-lying $h_{11/2}$ single particle neutron state. The lowest levels in odd-A Pd nuclei correspond to single particle states. The E3 assignment of the 89.4 keV transition results in an $11/2^-$ or $9/2^-$ assignment for the isomeric state, depending on the spin and parity $5/2^+$ or $3/2^+$ of the ground state.

The 127.9 keV and 253.7 keV levels. The 125.6 keV and 127.9 keV transitions have similar α_K coefficients and they have either M1 or E2 multipolarity. Thus, there is no parity change between the ground state and the 127.9 keV and 253.7 keV levels. The 164.5 keV transition does involve a parity change. This is consistent with an E1 assignment made above. The E1 assignment means a change of one spin unit between the 253.7 keV level and the isomeric 11/2 $(9/2)^-$ level. On the other hand, because the 253.6 keV gamma cross-over transition is observed but the corresponding conversion electron transition is not, the change in spin between the ground state and the 253.7 keV level cannot be higher than 2 units. Thus, the spin and parity of the 253.7 keV level are fixed to 9/2 $(7/2)^+$. The relatively low log *ft* value in the β-decay of ^{115}Rh to this level supports the $9/2^+$ assignment. The spin and parity of the 127.9 keV level depend on the multipolarity of the 125.6 keV and the 129.7 keV transitions. If they both include an M1 component, the only possibility for the spin and parity of the 129.7 keV level is 7/2 $(5/2)^+$. If any of them is purely E2, spin and parity values of 5/2 (3/2) and 9/2 $(7/2)^+$ also become possible.

The 296.3 keV level. The β-decay properties support spins from 5/2 to 9/2, if the ground state of ^{115}Rh is 7/2$^+$. Because the conversion electron measurement results in an L = 1 (E1 or M1) assignment for the 296.3 keV transition to the ground state, it seems that the spin 9/2 is excluded.

Other levels. No additional spin and parity assignments were made. A noteworthy thing in the presented level scheme is that the 1/2$^+$ single-quasiparticle state, corresponding to the $s_{1/2}$ neutron single-particle orbital, which appears at low energies in the lighter Pd isotopes and is expected on the basis of shell-model calculations, is not found. On the basis of systematics the 1/2$^+$ state could be expected to be the ground state of ^{115}Pd. Spin and parity 1/2$^+$ for the ground state seems to be ruled out, but here are 12 transitions given in table 4.16 that are not placed in the present level scheme, which reflects the fact the level scheme of ^{115}Pd is at least as complicated as the level scheme of ^{113}Pd. Further experiments are needed to complete the level scheme of ^{115}Pd. The location of the 1/2$^+$ single-quasiparticle state is one interesting question. Another interesting question is the origin of the possible 3/2$^+$ ground state, since such a state has not been seen at low excitation energy in the lighter odd-A Pd isotopes.

The level scheme of ^{117}Pd

The 34.5 keV, 97.1 keV, 131.7 keV, 168.6 keV and 481.6 keV gamma transitions were observed in coincidence with characteristic K X-rays of Pd, as explained in chapters 4.1. and 4.2. The first four of these transitions, in addition with a 71.5 keV transition, are mostly produced in the decay of a 19 ms isomeric state in ^{117}Pd. The first three transitions and the 481.6 keV transition are also following the β-decay of ^{117}Rh. The production rate of ^{117m}Pd in the present measurements was about one order of magnitude higher than the production rate of ^{117}Rh.

The 34.6 keV transition was observed in coincidence with the 168.8 keV and the 97.1 keV γ-transitions. Since the sum of the 34.6 keV and the 97.1 keV transitions is 131.7 keV, the 34.5 keV and 131.7 keV levels and the corresponding transitions were placed in the level scheme as shown in figure 4.21. The 203.1 keV level results from the placement of the 168.6 keV transition in the level scheme. The energy difference of the 131.7 keV and the 203.1 keV levels is 71.4 keV. A converted transition corresponding to a 71.5 keV γ-transition in Pd was observed in coincidence with the characteristic K X-rays of Pd. A 71.5 keV gamma transition was also observed in the singles gamma spectrum. Unfortunately, there was also a 71.1 keV transition following the decay of ^{117}In present in the low energy gamma spectrum. The energy resolution of 800 eV at FWHM of the 1.4 cm^3 Ge-detector did not allow a unique

solution of this doublet; therefore, the intensity of the 71.1 keV gamma transition was deduced from the intensity of the 89.7 keV gamma rays belonging to the same decay (Led79). The intensity of the 71.5 keV gamma transition was deduced by subtracting the calculated intensity of the 71.1 keV gamma transition. The placement of the 71.5 keV transition in the level scheme is obvious, even though it was not confirmed via any coincidences. Furthermore, the 71.5 keV transition explains why the 131.7 keV transition can be seen in coincidence with the characteristic X-rays of Pd. The multipolarities of the observed transitions were determined by conversion electron measurements. The results are given in table 4.18.

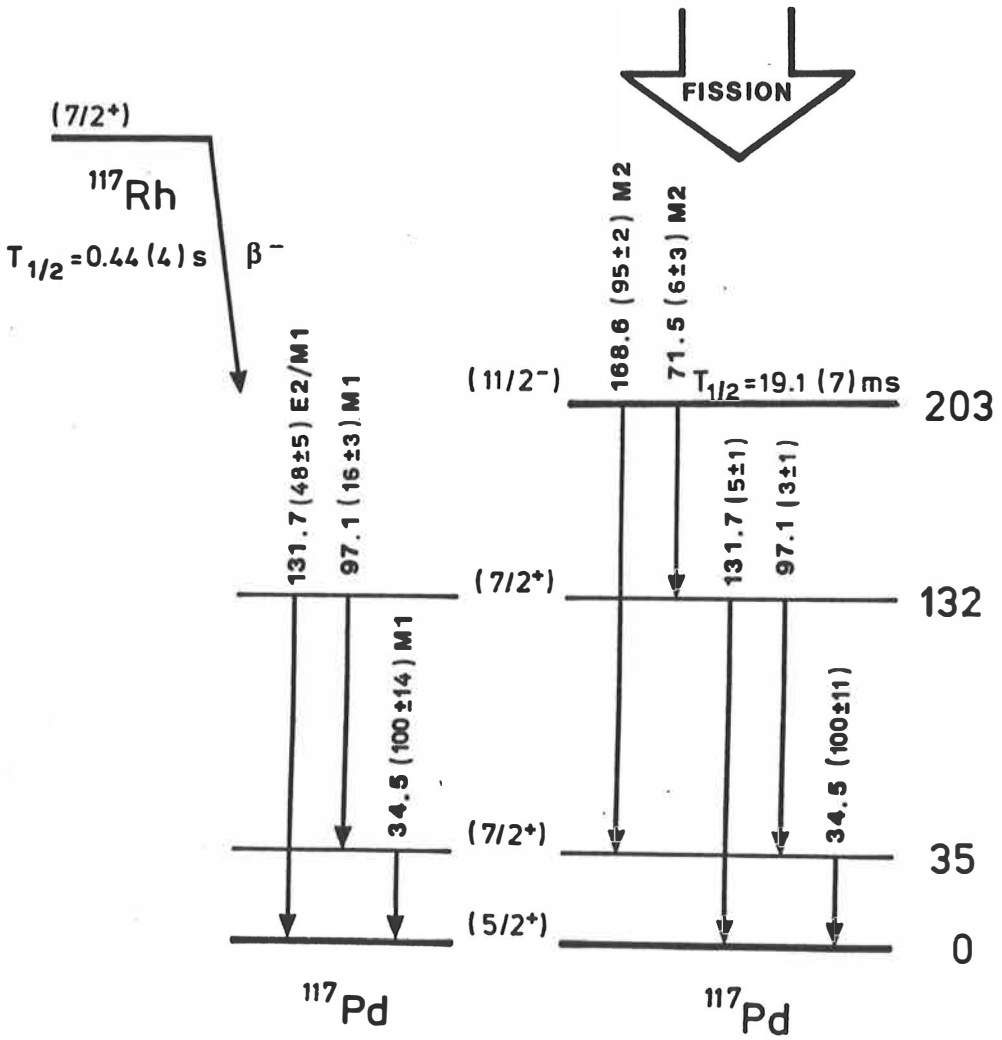

Figure 4.21. The level scheme of ^{117}Pd. The 131.7 keV transition is assumed to have a 85 % E2 contribution on the basis of the observed α_K. The right part of the figure shows the levels in ^{117}Pd known from the decay of the isomeric state which is fed directly in fission.

Table 4.18. The internal conversion coefficients of transitions in ^{117}Pd.
D: simultaneous measurement of conversion electrons and gamma rays;
FX: calculation based on the fluorescence yield of the characteristic X-rays of Pd.

Transition / keV	α_K (exp)	Method	α_K (theor)	Multipolarity
34.5	7.1 (9)	FX	M1 7.34	M1
	α_L = 0.62 (18)	D	α_L(M1) = 0.83	
71.5	7^{+15}_{-4}	D [1]	E2 3.15	M2
			M2 11.3	
97.1	0.42 (16)	D	M1 0.369	M1
131.7	0.38 (9)	D	M1 0.158	E2/M1
			E2 0.412	
168.6	0.55 (7)	D	M2 0.518	M2

[1]) γ–transition intensity is deduced by subtracting the calculated intensity of the 71.1 keV gamma rays from the total intensity of the 71.5keV/71.1keV doublet.

The energy levels of ^{117}Pd were thus established as well as the multipolarities of the transitions. This is, however, not enough for the spin and parity assignments. The spin and parity assignments are important to clarify the nature of the observed 19 ms isomeric state in ^{117}Pd. In the other odd-A Pd isotopes the isomerism results from the presence of the $h_{11/2}$ neutron orbital. The spin and parity assignments of the observed levels in ^{117}Pd and especially the spin and parity of the isomeric state were the main goals in the experiment performed to search for ^{117}Rh as described above. The β-decay properties of ^{117}Rh and ^{117}Pd were used for the final spin and parity assignments of the levels of ^{117}Pd.

Spin and parity assignments.

The β-decay scheme of ^{117}Rh is shown in figure 4.21 together with the earlier established decay scheme of ^{117m}Pd. The 481.6 keV transition could not be placed in the decay scheme. To determine the spin and the parity of the ^{117}Pd levels from the β-decay of ^{117}Rh a $7/2^+$ ground state for ^{117}Rh was assumed. This assumption is derived from the level systematics of the lighter odd-A Rh nuclei, where the ground state has been uniquely assigned with $7/2^+$ and the first excited state has been observed to be $9/2^+$ with an excitation energy of about 200 keV. These levels follow a very smooth systematic behavior starting from A = 107. The strongest observed β-decay feeding goes to the 34.5 keV level in ^{117}Pd. Positive parity ($5/2^+ - 9/2^+$) is thus concluded for this level. A similar assignment can also be made for the 131.7 keV level.

Since the ground state and the 34.5 keV state must have the same parity as can be seen in table 4.18, the β-branching to the ground state may be large. A recent systematic study of the

cumulative fission yields of neutron-rich nuclei indicate substantial ground state feeding (Lei91). An average drop of a factor of five between neighboring isotopes with increasing neutron number was observed for the neutron rich rhodium isotopes. On the basis of the β-gated gamma ray intensity the fission yield seems to drop a factor of 20 in comparison with ^{116}Rh. This suggests that about 70 % of the β-decays could go to the ground state of ^{117}Pd, implying a spin in the range of $5/2^+$ to $9/2^+$ for the ground state of ^{117}Pd.

The above information, the observed branching ratios and the decay of the isomeric state via the cascade of the 168.6 keV M2 and the 34.6 keV M1 transitions result finally in the $11/2^-$, $7/2^+$ and $5/2^+$ assignments for the isomeric 203.1 keV, 34.5 keV and the ground states, respectively. The M2 assignment for the 71.5 keV transition fixes the spin of $7/2^+$ for the 131.7 keV level.

It is easy to notify that the β-decay of ^{117}Pd could immediately highlight the validity of these assignments. The β-decay of ^{117}Pd to the levels of ^{117}Ag is discussed below, but the key information to deduce the properties of the ground state of ^{117}Pd, the branching to the $7/2^+$ state in ^{117}Ag, is missing. This is due to experimental difficulties because of the low energy of the E3 transition between the $7/2^+$ state and the $1/2^-$ ground state. If the $5/2^+$ assignment for the ground state of ^{117}Pd holds, and if the $5/2^+$ state has the same structure as the $5/2^+$ ground states in the lighter odd-A Pd isotopes, fast β-decay to the $7/2^+$ state is expected. The β-decay properties observed in the present work are discussed in more details below.

The level scheme of ^{117}Ag

Altogether 25 gamma transitions were assigned to the β-decay of ^{117}Pd, and 21 of them were placed in the level scheme given in figure 4.23. on the basis of the (γ)(γ) coincidences given in table 4.19. To show the quality of the (γ)(γ) coincidence data, a gamma spectrum gated by the 247.3 keV gamma transition is shown in figure 4.22.

The multipolarity was determined only for two transitions. This was because the yield of ^{117}Ag nuclei was too low, and also because the internal conversion of most of the transitions was low due to their relatively high energy. The deduced α_K values are given in table 4.20.

Spin and parity assignments.

From the systematics of the odd-mass neutron-rich Ag nuclei the negative parity levels $1/2^-$, $3/2^-$ and $5/2^-$ as well as the positive parity levels $7/2^+$ and $9/2^+$ are known to appear at low energy. The energies of these levels, which have been explained as three quasiparticle clusters

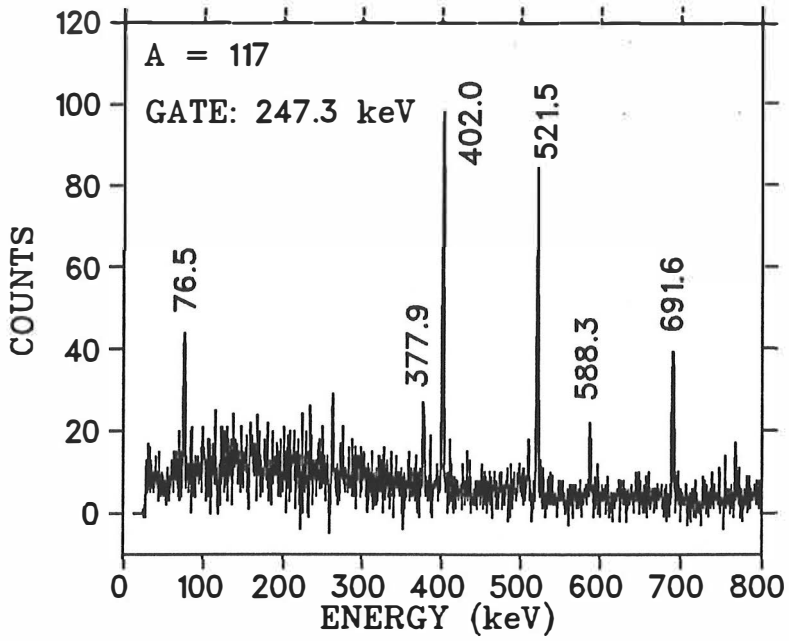

Figure 4.22. The γ–spectrum gated by the 247.3 keV γ–transition. Transitions labeled with energy are placed in the level scheme. The peaks at about 260 keV are due to backscattering of the 511 keV annihilation photons.

coupled to the collective vibrations (Paa73), behave very smoothly as a function of the increasing neutron number in the mass range A = 105 – 115 as expected from the behavior of the low-lying collective levels in the neutron-rich even-even Pd isotopes.

The ground state and the 28.6 keV level. ^{117}Ag was known to have two β-decaying states (Fog76) with $I^{\pi} = 1/2^-$ and $I^{\pi} = 7/2^+$. The order and position of these levels in figure 4.23 was adopted from (Fog88), (Fog91).In the present measurement the L- and M-conversion electrons from the 28.6 keV transition were not observed, which was most probably because of the noise level of the electron detector in the experiment at mass number A = 117.

The 175.7 keV and 657.8 keV levels. A 147.1 keV gamma transition was assigned to the decay of ^{117}Pd on the basis of its half-life and the fact that it was not observed in the decay of ^{117}Ag (Fog76). This transition has been assigned to this decay also in (Rog90b) on the basis of its half-life. The 147.1 keV transition is in coincidence with a 482.2 keV γ-transition.The 482 keV gamma rays appeared to be a triplet consisting of a 481.6 keV transition belonging to the decay of ^{117}Rh, a 482.2 keV transition following the β-decay of ^{117}Pd and a 482.4 keV transition belonging to the β-decay of ^{117}Ag. The sum of 147.1 keV and 482.2 keV is

629.3 keV, which coincides with a 629.3 keV transition, observed in the (γ)(β) spectrum and having a half-life of 4.5 s. In (Rog90b) a 630±1 keV transition was also assigned to the decay of ^{117}Pd on the basis of its half-life. The placement of these three transitions above the isomeric $7/2^+$ state instead of a feeding to the $1/2^-$ ground state is based on one hand on the experimental level systematics, since the placement of the $9/2^+$ state at 175.7 keV follows the smooth change of the excitation energy of the $9/2^+$ states observed in the lighter odd-A Ag nuclei, and on the other on the observation of a 657.8 keV gamma transition, which could be the cross-over transition to the ground state. The intensity of the 657.8 keV transition was unfortunately so low that its β-delayed half-life could not be measured and thus its belonging to the level scheme is uncertain. If the placement is correct, $9/2^+$ and $5/2^+$ can be suggested for the 175.6 keV and 657.8 keV levels on the basis of systematics.

Table 4.19. The γ-transitions following the β-decay of ^{117}Pd. The intensities are determined from the (γ)(β) spectrum and normalized to the 247.3 keV γ-transition intensity.

Energy / keV	Relative intensity	Coincident gamma rays / keV
76.5 (2)	2.8 (3)	247, 302, 1935
147.1 (3)	6.9 (5)	482.2
247.3 (2)	100.0 (13)	76, 378, 402, 510, 521, 588, 691, 767 [1], 858 [1], 918 [1], 1935, 2105
301.7 (3)	2.9 (3)	
323.8 (3)	35.8 (12)	301, 326, 510, 670 [1], 1935
325.8 (3)	2.5 (3)	
377.9 (4) [2]	2.6 (5)	247
402.0 (3)	10.2 (8)	247, 1702
482.2 (4) [2]	5.4 (6)	147, 338 [3]
510.3 (4) [2]	1.2 (4)	
521.5 (3) [2]	11.5 (9)	
588.3 (3)	1.8 (4)	
625.5 (4)	20.3 (8)	
629.4 (4)	18.7 (8)	
649.4 (4)	33.6 (9)	
657.8 (4)	3.9 (5)	
691.6 (4)	8.9 (4)	247
769.2 (4)	12.4 (7)	
834.5 (5)	2.5 (4)	
1701.9 (6)	13.0 (9)	
1934.8 (7)	9.5 (9)	
2104.5 (7)	14.0 (11)	

[1]) Not placed in the level scheme.
[2]) Energy and intensity are determined from gamma gated spectrum.
[3]) ^{117}Ag decay.

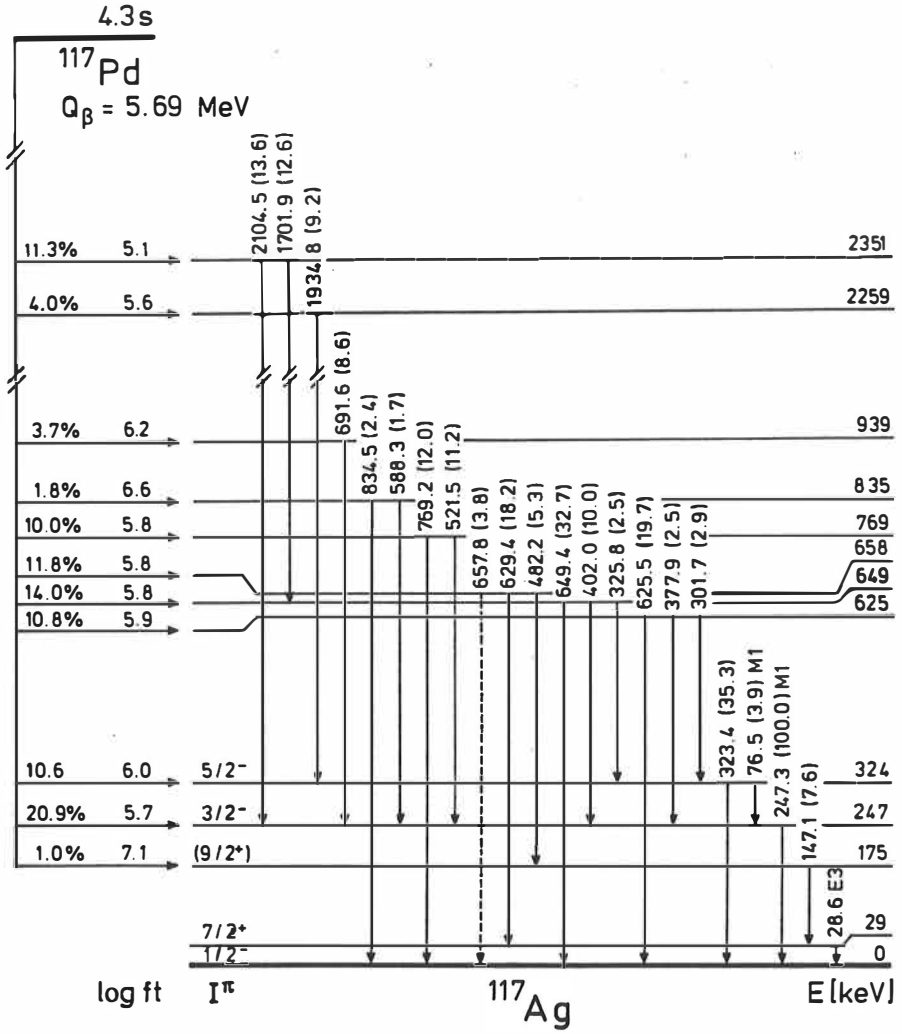

Figure 4.23. The level scheme of ^{117}Ag.

Table 4.20. The internal conversion coefficients for transitions in ^{117}Ag.
D: simultaneous measurement of conversion electrons and gamma rays.

Transition/keV	α_K (exp)	Method	α_K (theor)	Multipolarity
76.5	0.57 (10)	D	E1 0.285	M1
			M1 0.725	
			E2 2.547	
247.3	0.042 (7)	D	E1 0.0102	M1/E2
			M1 0.0292	
			E2 0.0476	

The 247.3 keV and 323.8 keV levels are assigned as $3/2^-$ and $5/2^-$, respectively, belonging to the $1/2^-$, $3/2^-$, $5/2^-$ triplet expected in odd-A Ag nuclei. The observed multipolarities of the transitions support this assignment. On the other hand, there is more β-feeding to the assumed $3/2^-$ state from the $(5/2^+)$ ground state of ^{117}Pd than to the $5/2^-$ state. There are two possible explanations for this. Firstly, there are transitions like 767 keV, 858 keV and 918 keV that are not placed in the level scheme. They are most probably populating the 247.3 keV level. There can also be some additional, high-energy transitions to the 247.3 keV level: the Q_β window is large and allows β-decays to levels at high excitation energies. A feeding to the $3/2^-$ state would lower the β-branching. This is, however, speculation with no experimental support at the moment. Secondly, the $(5/2^+)$ assignment for the ^{117}Pd ground state can be wrong; it was partly based on the systematics of odd-A Rh nuclei, which supports a $7/2^+$ assignment for the ground state. If the ground state of ^{117}Pd is $3/2^+$, the isomeric state in ^{117}Pd would become $9/2^-$. This would not be against the systematics, since the isomeric state in ^{113}Pd is assigned as $9/2^-$ and the β-decay properties of ^{115}Rh support $3/2^+$ ground state assignment also for ^{115}Pd. The third possibility is to give up the $3/2^-$, $5/2^-$ assignment, which is very strongly supported by the level systematics of the lighter Pd isotopes.

Other levels. The 2351 keV level has a low log *ft* value; its spin and parity could then be $3/2^+$, $5/2^+$ or $7/2^+$ corresponding the allowed β-decay.

There are several states appearing at 600 – 1000 keV excitation energy. States belonging to the deformed, rotational-like coexisting band known in the lighter odd-A Ag isotopes (Fog88), (Rog90c), are expected to lie in this energy region. However, no clear candidates for the members of a coexisting band can be pointed out on the basis of the present data. As can be seen in figure 4.23, the possible interband transitions are missing, as well as multipolarity assignments of the transitions. Neither were the lifetime experiments performed. The present data shows that there are good possibilities to study the intruder band structure of ^{117}Ag, if the experiment is devoted especially to this purpose and not to the studies of β-decay of ^{117}Rh and the 19.1 ms isomeric decay of ^{117m}Pd.

The level scheme of ^{119}Ag

Five gamma transitions were assigned to the decay of ^{119}Pd. Only two coincidence relations were observed: these were coincidences between the 69.9 keV and the 256.6 keV gamma transitions and coincidences between the 129.9 keV and 507.2 keV gamma transitions. The 326.1 keV cross-over transition was found in the β-gated spectrum. The constructed level scheme is shown in figure 4.24.

The conversion coefficient of $\alpha_K = 1.0$ (4) for the 69.9 keV transition, corresponding to M1 multipolarity, was deduced on the basis of the fluorescence yield of the characteristic K X-rays of Ag observed in coincidence with the 256.6 keV transition. No other multipolarity assignments were made, mainly because of the low statistics due to low production rate of the very neutron rich precursor ^{119}Pd.

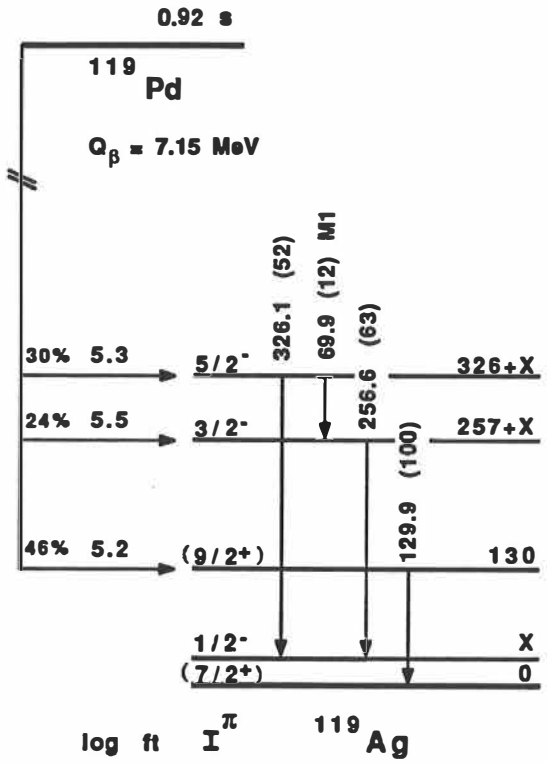

Figure 4.24. Level scheme of ^{119}Ag

The experimental level systematics of the 1/2⁻, 3/2⁻ and 5/2⁻ as well as the 7/2⁺ and 9/2⁺ levels at low energies in the odd-mass neutron rich Ag nuclei can be extendet to ^{119}Ag. In the decay study of ^{119}Ag (Kaw75) only one β-decaying isomer with $I^\pi = 7/2^+$ was observed. The 7/2⁺ state is thus expected to become ground state of the more neutron rich Ag nuclei, while the 1/2⁻ state is expected to rise to higher excitation energy in analogy to odd-A Rh nuclei.

The 1/2⁻, 3/2⁻ and 5/2⁻ states in the level scheme in figure 4.24. are based on the observed three transitions and experimental systematics. The 129.9 keV γ-transition was also placed in the level scheme given in figure 4.24. as a $9/2^+ \rightarrow 7/2^+$ transition on the basis of experimental

systematics. However, the 129.9 keV transition was assigned to the β-decay of ^{119}Ag on basis of the half-life. The only proof for the $9/2^+ \rightarrow 7/2^+$ assignment is the expected existence of the $9/2^+$ level slightly below 200 keV.

The E3 transition between the $1/2^-$ and $7/2^+$ levels is of special interest, and this transition was intensively searched for in a conversion electron measurement. No sign of the isomeric state was found in a run as long as 28 hours. This might in the first place be due to the low yield of the extremely neutron rich ^{119}Pd precursor. Secondly, the energy of the isomeric transition may be so low that it could not be observed in the present study. In the search for this transition the possibility to perform experiments utilizing also the L X-ray coincidences might have been of great importance.

5. Discussion

5.1. The level systematics

5.1.1 The odd proton level systematics:

Intruder states. A significant property of the odd-A Rh as well as the odd-A Ag nuclei is the shape coexistence (Hey83), (Fog88), (Kaf88), (Rog88), (Rog90a), (Rog90c). In these nuclei, deformed rotational-like intruder bands, suggested to originate from the $d_{5/2}$ and $g_{7/2}$ orbitals from the $\mathcal{N} = 4$ proton shell intruding across the Z = 50 shell closure, coexist with spherical shell model states and their core-coupled configurations.

In the odd-A Ag nuclei the intruder state systematics was known up to ^{115}Ag. In the present studies, the experiment performed at Louvain-la-Neuve, besides identification of the β-decay of ^{117}Rh, resulted in a level scheme of ^{117}Ag. In this level scheme, shown in figure 4.19, some levels appear at such an excitation energy that they could be candidates for intruder states. However, very little can be concluded with certainty from the present data. Since the production rate of the very neutron rich ^{119}Pd was quite low only few levels could be placed in the level scheme of ^{119}Ag and no levels at an excitation energy expected for the intruding band members could be identified.

The intruder states in ^{111}Rh have been studied in (Rog90a) and in the lighter odd-A Rh isotopes in (Rog88). In ^{111}Rh the lowest member of the intruding band lies at 395 keV. It was identified by its half-life (Rog90a) of 87 ns. This half-life was confirmed in the present study. For ^{113}Rh, the energy of the lowest member of the coexisting band is expected to lie at higher energies. In the present study the best candidate for the intruder band member at a reasonable excitation energy is the $(3/2^+)$ state at 601 keV. With the present data, no further conclusions can be made. The low yield of the very exotic isotope ^{113}Ru prevented a more detailed study, especially level lifetime measurements.

The experimental systematics of intruder states in odd-A Ag and Rh nuclei are shown in figures 5.1 and 5.2. Even though this systematics was not remarkably improved, the present study shows that the possibilities to search for the intruder bands in ^{117}Pd and in ^{113}Rh are reasonable. The yield of the radioactive species with the IGISOL is relatively low if compared with the rapid chemical separation (Ska80) or the mass separation with a plasma ion source

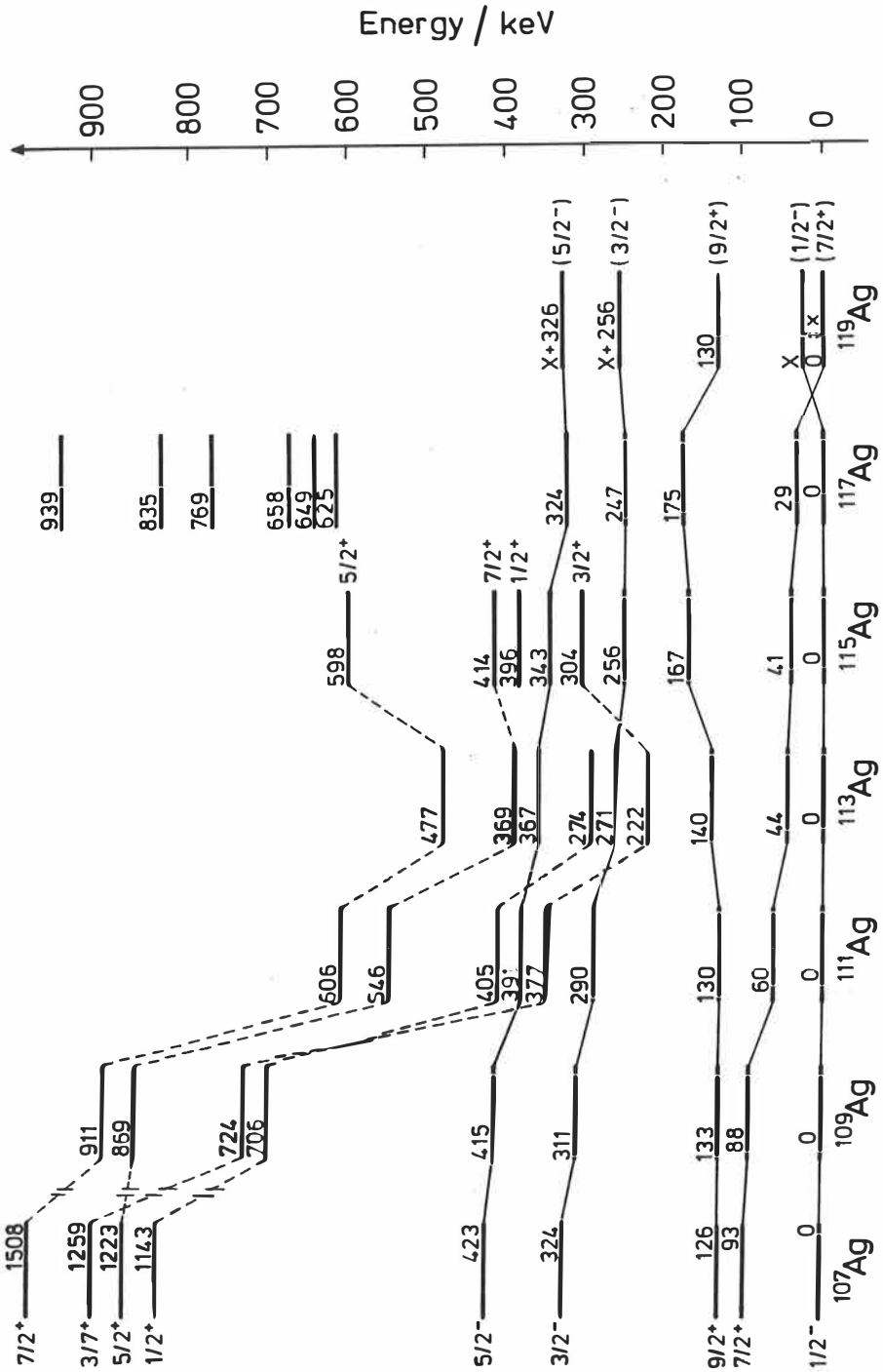

Figure 5.1. The experimental level systematics of selected levels in odd-A Ag isotopes. The data for ^{105} - ^{115}Ag is taken from the references (Hey83), (Bla84), (Fog88), (Rog90c) and (Bla90). Intruder band members are indicated by thick lines. The levels of ^{117,119}Ag are from the present work.

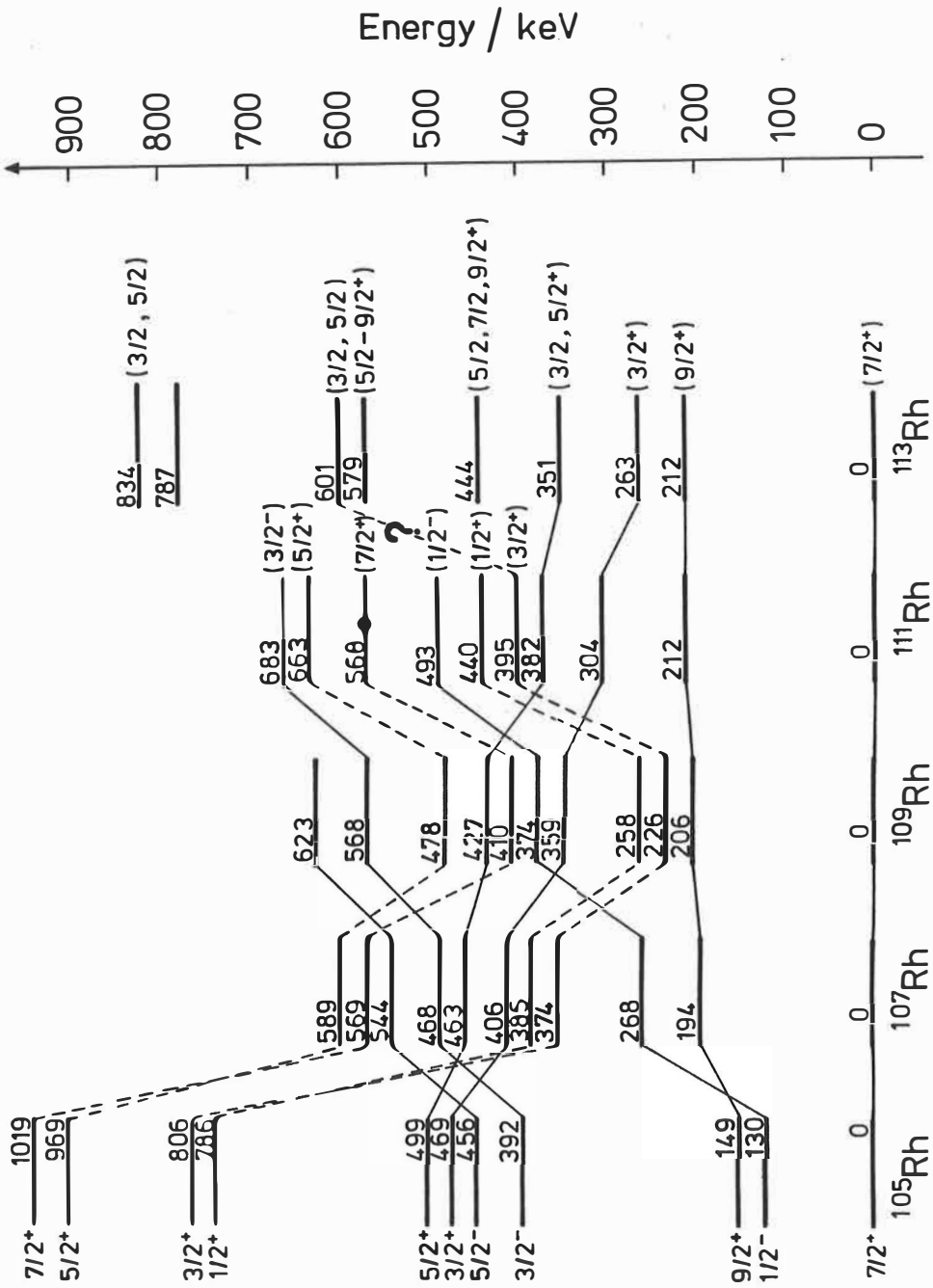

Figure 5.2. The experimental level systematics of the selected levels in odd-A Rh isotopes. The data for $^{105-109}$Rh is taken from references (Rog88) and (Rog90a). Levels of ^{111}Rh are based on the present work and ref. (Rog90a). Levels taken from this reference are indicated by dots. Levels of ^{113}Rh are based on the present work.

(Jac87), but only as long as the decay losses due to the short half-life of the isotopes do not become critical. The limit where the decay losses hinder further studies with the mentioned techniques seems to lie at the separation of 0.80 s ^{113}Ru and 0.92 s ^{119}Pd in the present region of interest. The improved efficiency of the ion guide set-up in the new K-130 cyclotron laboratory at Jyväskylä will make the IGISOL to the most powerful device in the studies of the intruder bands in ^{113}Rh, ^{117}Pd and beyond already in the near future.

Normal states. The normal low-lying states in odd-A Ag and also in odd-A Rh nuclei have been studied by the Mainz and Studsvik groups. Their results concerning the structure of these states will be published (see (Fog90) and (Rog90c)). The results of the present study are compared with a systematics deduced in their previous papers below.

The systematics of selected low-lying states in Ag nuclei is shown in figure 5.1. Prior to the present study, the level systematics was known up to ^{115}Ag (Fog88), (Rog90c), and the location and relative order of the $1/2^-$, $7/2^+$ states was known in ^{117}Ag (Fog88), (Fog90). A $(7/2^+)$ state in ^{119}Ag with β-decay to the levels of ^{119}Cd was also known (Kaw75). The systematic was extended to the levels of ^{117,119}Ag in the present study. The assignment of these levels was discussed in chapter 4.4.

Experimental level systematics has proved to be an important tool in the construction of the level schemes. Such structures as the known negative parity $1/2^-$, $3/2^-$, $5/2^-$ triplet have been introduced on this basis. In the case of ^{119}Ag this causes a puzzling situation, since the β-decaying state in ^{119}Ag was assigned with $(7/2^+)$ in (Kaw75). The observed triplet in the β-decay of ^{119}Pd, however, is similar to the $1/2^-$, $3/2^-$, $5/2^-$ triplet known in the lighter silver isotopes. No transition connecting the opposite parity states was observed. The β-decay of a $1/2^-$ state was not observed either. In the decay of all heavier odd-Ag isotopes the ground state has been assigned a spin and parity of $7/2^+$ and no sign of the $1/2^-$ state has been reported. It clearly seems that more experimental data is needed to solve this puzzle.

The experimental systematics of selected low-lying states from ^{103}Rh up to ^{113}Rh is shown in figure 5.2. Prior to the present study, this systematics was known up to ^{109}Rh; in the course of the present studies, the results of (Rog90a) on the levels in ^{111}Rh became available. These results are in general in good agreement with the present ones. The levels of ^{113}Rh have not been published elsewhere.

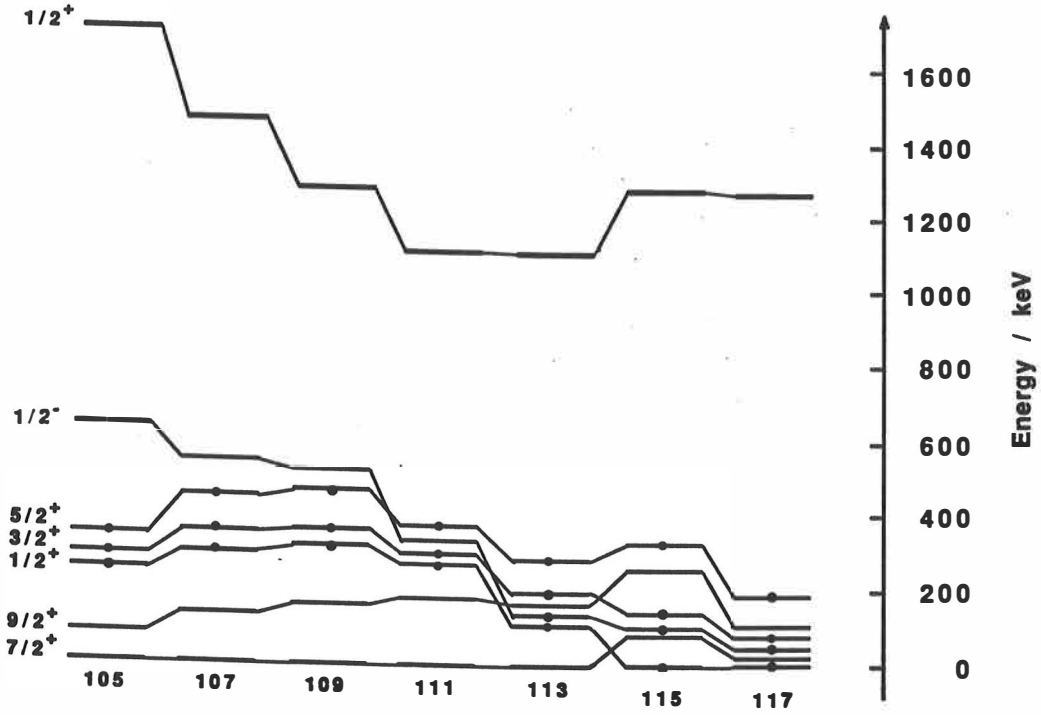

Figure 5.3. The calculated states for odd-A Ag nuclei. A dot in the middle of a line corresponding to a level indicates total energy minimum at oblate deformation for the state in question.

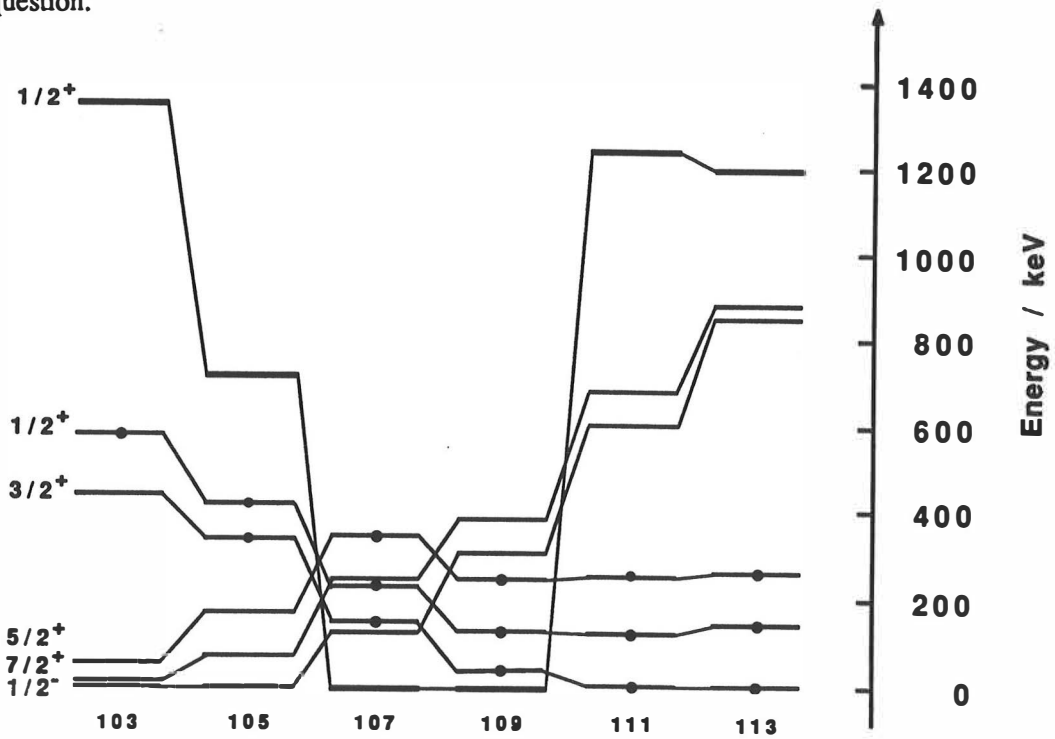

Figure 5.4. The calculated states for odd-A Rh nuclei. The dots have same meaning as in the case of odd-A Ag nuclei.

Results of the macroscopic-microscopic model. The levels calculated with the microscopic-macroscopic model as explained in chapter 2 are shown in figures 5.3. and 5.4. for odd-A Rh and Ag nuclei, respectively. At the first sight, the agreement between the observed and the calculated levels appears poor. However, as one recalls that no collectivity is included in the model, it reproduces quite satisfactorily many of the qualitative features of the experimental spectra.

The low-lying $7/2^+$ and $9/2^+$ states in the odd-A Ag nuclei are reproduced with the present model. However, as pointed out in (Paa73), many of the properties of these states cannot be explained without including collectivity in the model and the observed agreement may rather be coincidental. The calculated location of the $7/2^+$ and $9/2^+$ states in odd-A Rh nuclei which are much softer against deformation is very different from the experimentally observed ones. This supports the collective origin for the experimentally observed $7/2^+$ and $9/2^+$ states.

The close location characteristic of the $7/2^+$ and $1/2^-$ states can be reproduced for Rh and Ag nuclei with both oblate and prolate deformations. This is obvious from figure 2.3, where the $7/2^+(1)$ and $1/2^-(6)$ single-particle orbits come near to each other at $\beta_2 \approx \pm 0.25$. When the pairing energy and the macroscopic energy are included, the lowest energy of both states corresponds to prolate deformation. However, the order of the $7/2^+$ and $1/2^-$ states is reversed; while in the odd-A Ag nuclei the experimentally lowest state is $1/2^-$, the calculation gives $7/2^+$ as the lowest state. In the odd-A Rh nuclei the calculation results in a $1/2^-$ state below $7/2^+$, while the experimentally observed order is just the opposite. Furthermore, in Rh nuclei the $1/2^-$ state is experimentally observed to rise in energy when going to heavier isotopes, while the $7/2^+$ state remains as the ground state and the separation between these states increases. From this point of view it seems that the $7/2^+$ state is best described as a three proton-hole cluster coupled to the 2^+ vibration of the even-even core (Hey86), (Paa73). Since the collective properties of the state brings it at low energy, it is clear that a pure single-particle model cannot describe the state.

Perhaps the most interesting property of the calculated spectra is the strongly intruding $1/2^+$ state in odd-A Rh nuclei. Its origin lies in the $1/2^+(6)$ state intruding across the Z = 50 shell closure at large prolate deformation as is seen in figure 2.3. In (Rog88), (Rog90a) the intruding band observed in odd-A Rh nuclei was suggested to result from a rotational band build on the $1/2^+[400]$ Nilsson orbital. In the present formalism the $1/2^+(6)$ state corresponds best to the $1/2^+[400]$ Nilsson orbital, with an amplitude of 0.7488 at $\beta_2 = 0.25$, $\beta_4 = 0.0$. An interesting feature in the present result is that there is no additional neutron-proton interaction beyond the common shape of the potential for protons and neutrons. The lowering in energy

of the $1/2^+$ state is simply due to shell structure that favours larger deformations. The intruding state becomes too low, but it is within the expected accuracy of a few hundreds of keV of the calculation. The intruder state becomes at its lowest position in ^{109}Rh, as observed experimentally. In the odd-A Ag nuclei the $1/2^+(6)$ state has its lowest position in the middle of the neutron shell, but it remains at high excitation energy and does not so clearly show the experimentally observed intruding character. Lower pairing interaction strength usually favors larger deformation, but in the Ag nuclei the location of the $1/2^+(6)$ state is quite insensitive to the change of pairing energy within realistic limits. However, the lowest energy of this state is reached at ^{113}Ag, where also the experimentally observed intruding band has its lowest energy.

The calculation produces $1/2^+$, $3/2^+$ and $5/2^+$ states with oblate deformation at low energy both in Ag and Rh. Their origin is in the splitting of the $g_{9/2}$ spherical shell model orbital. Oblate deformation is favoured within the model with increasing neutron number. In lighter isotopes the prolate deformation of these states is sometimes favoured, as seen in figures 5.3. and 5.4. In the experimental spectra, however, such states cannot be found.

Furthermore, since the collective vibrations and rotations are not included in the present model, the low-lying $5/2^-$ and $3/2^-$ states are not reproduced. They can be reproduced within the IBFM (interacting boson fermion model) by the $p_{1/2}$ hole state coupled to the 2^+ vibration of the core. Also, the $7/2^+$ state situated below the $9/2^+$ state can be reproduced as a $g_{9/2}$ neutron coupling to the 2^+ vibration with the same set of coupling strength parameters as the negative parity states. The low-lying states were quite satisfactory reproduced also in the Coriolis coupling model (Bre89). No comparison of the energy of the lowest positive and negative parity states was, however, given in those calculations.

The second lowest $5/2^-$ and $3/2^-$ states have also rather smooth behavior as a function of the mass number A. If this systematics is compared with even-even Ru systematics (Äys90) it is tempting to explain the $5/2^-$ and $3/2^-$ states as the $p_{1/2}$ proton coupling to the 2^+ excitation of the even-even Ru core. The low energy of the second 2^+ state in the even-even Ru nuclei implies triaxial deformation. Breaking of axial symmetry in these nuclei resulted also from the calculations of ref. (Fra87). In (Cha91) triaxial deformations of the ground state were predicted for the nuclei in the middle of both the $\mathcal{N}=4$ neutron main shell and the $g_{9/2}$ proton subshell.

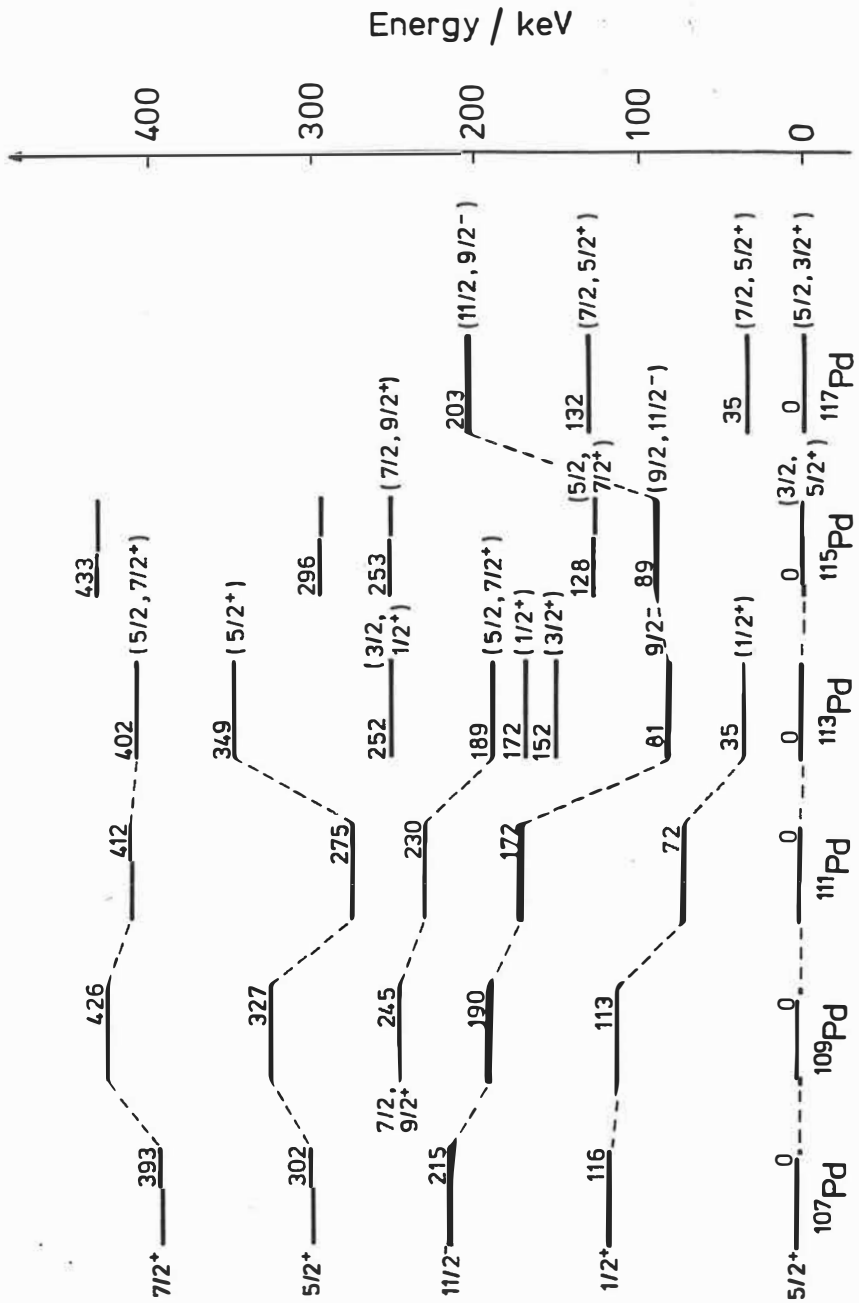

Figure 5.5. The experimental level systematics of selected levels in odd-A Pd nuclei. The isomeric states are indicated by thick lines. Data for ^{105} - ^{111}Pd is taken from references (DeF86) for ^{105}Pd , (Bla91) for ^{107}Pd, (Kan78) and (Bar77) for ^{109}Pd, and (Kaf84) for ^{111}Pd. States in ^{113,115,117}Pd are based on the present studies.

5.1.2. The odd neutron level systematics

The level systematics of the odd neutron rich Pd nuclei was extended remarkably in the present study. Prior to the present studies, only the 50 (3) s ($11/2^-$, $9/2^-$) isomeric state at 81.4 keV in ^{115}Pd (Fog88) was known about the excited levels of ^{113,115,117}Pd. The experimental systematics of selected states from ^{105}Pd up to ^{117}Pd is shown in figure 5.5. The spin and parity assignments of these states in ^{113,115,117}Pd were discussed and more complete decay schemes were shown in chapter 4.4.

The negative parity isomeric states. The experimental level systematics of low-lying negative parity isomeric states in odd-A Pd nuclei from A = 105 up to A = 117 is shown in figure 5.5. These isomeric states decay via very hindered E3 or M2 transitions. The origin of these states is the $h_{11/2}$ single particle neutron orbital, whose energy decreases towards the middle of the $\mathcal{N} = 4$ neutron shell. In odd-A Sn nuclei $11/2^-$ becomes the ground state at the neutron number N = 66.

The spin and parity of these isomeric states were deduced to be $11/2^-$ up to ^{111}Pd. In the present study the isomeric state in ^{113}Pd was deduced to have a spin and parity of $9/2^-$. In the case of ^{115}Pd the ground state branching in the β-decay of ^{115}Rh supports a $3/2^+$ assignment for the ground state of ^{115}Pd and thus spin and parity of $9/2^-$ for the isomeric state (Äys88a). This result is not in disagreement with (Fog88), where the ground state of ^{115}Pd was assigned to have spin and parity $5/2^+$ or $3/2^+$ on the basis of the properties of its β-decay. The $5/2^+$ assignment for the ground state was favoured on the basis of the experimental level systematics and the $11/2^-$ assignment for the isomeric level was expected according to lighter Pd nuclei. Since the isomeric state in ^{113}Pd has been deduced to be $9/2^-$, this argument does not hold any more.

The breaking of the systematics of the $11/2^-$ states is probably due to the onset of deformation in the middle of the neutron shell. If the structure of the odd 4-proton-hole Pd nuclei is compared to the odd 4-proton-particle Xe nuclei, a similar change in the spin of the lowest negative parity state is observed when moving towards the mid-shell. The $^{129-135}$Xe nuclei near the magic neutron number N = 82 have $11/2^-$ isomeric states, whereas the ^{125,127}Xe nuclei have $9/2^-$. Lighter odd-A Xe isotopes tend to be well deformed and have a $7/2^-$ state as the lowest negative parity state. The comparison of the even-even Xe and Pd isotones shows a striking similarity of their structure (Äys88b).

The structure of the negative parity states in odd-A Xe isotopes has been explained in the framework of the particle-core model by coupling of the $h_{11/2}$ neutron to a triaxial core

(Hel81). However, the hindrance in the decay of the negative parity isomeric states in odd-A Pd nuclei is much larger than that in the odd-A Xe nuclei, reflecting the importance of the large neutron excess. The hindrance of the 172.2 keV E3 transition in ^{111}Pd is the largest known for E3 transitions in this mass region (End81). The hindrances for the isomeric transitions are given in table 5.1 and they are all among the largest known hindrances for E3 and M2 transitions in this mass region.

This isomerism has been suggested to be the consequence of pairing, which causes the cancellation of the transition rate between the states above and below the Fermi level (Fog90). However, the pairing hindrance effects only on Eλ transitions. Thus, the hindrance factor of about 10^4 for an M2 transition cannot be due to pairing effects, but may reflect very different nuclear shapes of the negative parity states compared to the positive parity states.

Table 5.1. The hindrance of E3/M2 transitions in odd-A Pd nuclei compared to the Weisskopf estimates. The experimental data is from [1] (Led78) [2] (Fog88) [3] (Fog90).

Isotope	Ref. #	Transition (keV)	Branch %	Mλ	Weisskopf $T_{1/2}$ (s)	Observed $T_{1/2}$ (s)	Partial γ $T_{1/2}$ (s)	Hindrance
^{105}Pd	1)	182.8	100	M2	$6.935\ 10^{-6}$	$36.1\ 10^{-6}$	$52.5\ 10^{-6}$	7.6
^{107}Pd	1)	214.9	100	E3	$81.72\ 10^{-3}$	21.3	31	379
^{109}Pd	1)	190.0	100	E3	0.1865	281	495	2 654
^{111}Pd	1)	172.2	73	E3	0.358	$19.8\ 10^{6}$	$59.1\ 10^{6}$	165 200
		β decay	27					
^{113}Pd		81.3	100	M2	$0.380\ 10^{-3}$	0.4	3.84	10 120
^{115}Pd	2,3)	89.3	8	E3	33.07	50	$16.4\ 10^{3}$	497
		β decay	92					
^{117}Pd		71.0	5	M2	$0.730\ 10^{-3}$	$19.1\ 10^{-3}$	4.95	6780
		168.6	95	M2	$9.668\ 10^{-6}$		$32.9\ 10^{-3}$	3400

The ground state. The $5/2^+$ ground state is observed for the lighter odd-A nuclei. Its origin for the light odd-A Pd nuclei clearly lies in the spherical shell model $d_{5/2}$ neutron orbital. However, it is difficult to understand how the $d_{5/2}$ neutron orbital could be responsible for the ground state spin of heavier Pd nuclei.

Even though the relative location of single particle orbits changes remarkably from N = 50 to N = 82, so that the $g_{7/2}$ orbital is well below the $d_{5/2}$ orbital near ^{132}Sn, the $g_{7/2}$ is still above the $d_{5/2}$ orbital in $^{107}Pd_{61}$, in which neutrons should already fill the $g_{7/2}$ orbital. In fact, it is known that the $5/2^+$ ground state of odd-A Pd nuclei has a mixture of both the $d_{5/2}$ and the $g_{7/2}$ spherical shell model orbitals (Hey86). In terms of the present calculations, the $5/2^+$ state is mainly the $5/2^+(3)$ state in light odd-A nuclei and changes to the $5/2^+(4)$ state in heavier isotopes. The decomposition of the $5/2^+(4)$ state in asymptotic Nilsson base was shown in table 2.2. The remarkable mixing of the $g_{7/2}$ spherical shell model state in the ground state wave function results in fast β-decay to the $7/2^+$ state in the odd-A Ag nuclei (Hey86).

The experimental data for ^{115}Pd strongly suggest that the ground state of this nucleus is $3/2^+$. The β-decay properties of ^{117}Pd do not rule out a $3/2^+$ for the ground state of ^{117}Pd either, even though $5/2^+$ seems to be slightly more probable. The origin of the $3/2^+$ ground state, on the other hand, is not clear. The $1/2^+$ state which is observed at low energies in nuclei lighter than ^{115}Pd has a strong single-particle character, and would be expected to become the ground state on the basis of the experimental systematics. Spherical shell model calculations would suggest a $3/2^+$ state originating from the $d_{3/2}$ orbital to become the ground state already in ^{111}Pd or ^{113}Pd. No states corresponding to the $3/2^+$ shell model state are experimentally observed in lighter odd-A Pd nuclei.

The collective $5/2^+$ states. A characteristic feature of the β-decay of the odd-A Rh nuclei up to ^{113}Rh is the strong population of a $5/2^+$ state at about 300 keV excitation energy. Its energy corresponds to the energy of the first 2^+ state in even-even Pd nuclei, and its origin may be the 2^+ state of the even-even core coupled to the neutron in the $5/2^+(4)$ orbital. The fast β-decay from the $7/2^+$ ground state of odd-A Rh isotopes to these $5/2^+$ states implies large $g_{7/2}$ componenet in the wave function. Because of the fast β-decay, these states are also suggested to be three-quasiparticle congficurations (Kan78). Such a state would be strongly populated in the β-decay but it is not found in ^{115}Pd. The ground state of ^{115}Pd is probably not $5/2^+$ either. From the scarce information on ^{117}Pd no conclusions can yet be drawn.

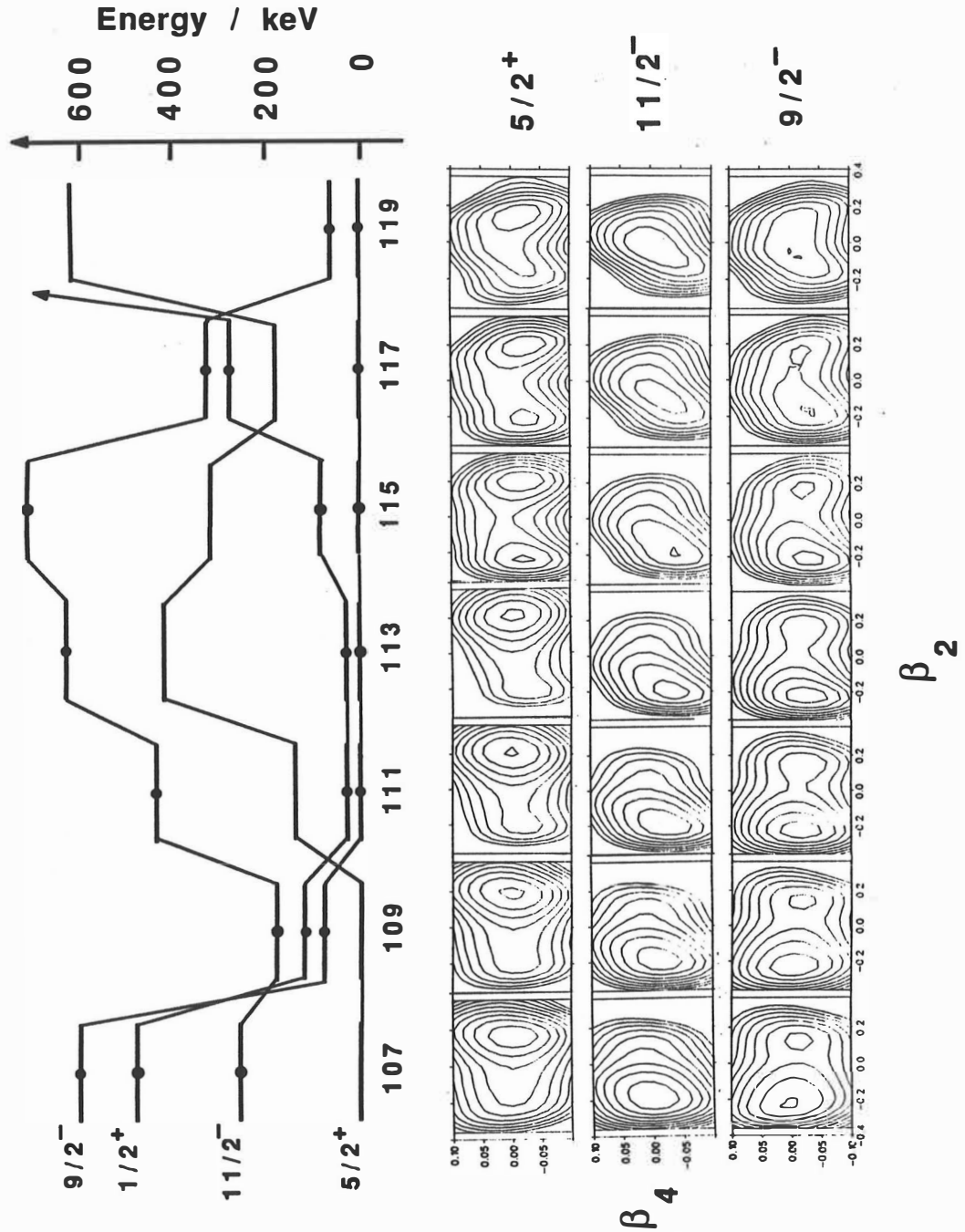

Figure 5.6. The calculated systematics of selected states in odd-A Pd nuclei. The states shown are the ones most probably responsible for the occurence of isomerism in these nuclei. The total energy surfaces in the (β_2,β_4) plane are given for the $5/2^+$, $11/2^-$ and $9/2^-$ states in order to show the evolution of nuclear shape as a function of neutron number. The energy of states in the upper part of the figure corresponds to the deepest minimum of the state in the (β_2,β_4) plane. The separation of the contours in the lower part of the figure is 0.5 MeV.

Macrosopic-microsopic calculations. A calculated systematics of selected states is odd-A Pd nuclei is shown in figure 5.6. It is worth noting that the $5/2^+$ state was not the calculated ground state for any of the odd-A Pd nuclei. However, $5/2^+$ was always the lowest state with prolate deformation.

As is seen in figure 5.6., the $11/2^-$ state becomes low in energy only with oblate deformation. The low energy of the $11/2^-$ state has previously been suggested to reflect oblate deformation (Sch69). The $5/2^+$ state, instead, has both oblate and prolate minima. Their energy difference is of the order of the reliability of the present calculations, but the prolate deformation is slightly favoured.

The experimentally observed strong hindrance of the transitions connecting the $11/2^-$ and $5/2^+$ states seems now to be the key. As mentioned above, the hindrance of E3 transitions in the odd-A Ag and Rh nuclei has been explained as pairing hindrance (Fog90), (Boh75). In the case of odd-A Pd nuclei this type of hindrance is also possible for E3 transitions, but the hindered M2 transitions cannot be explained in this way, because pairing hindrance does not effect Mλ transitions between single-quasiparticle states (Boh75). Furthermore, if the wave functions of the $11/2^-$, $9/2^-$ and $5/2^+$ states are decomposed in the Nilsson base, the main components of the $11/2^-$ and $9/2^-$ states are always the $11/2^-[505]$ and $9/2^-[514]$ asymptotic Nilsson states, respectively. The main components of the $5/2^+$ state at oblate deformation are the $5/2^+[413]$ and $5/2^+[422]$ Nilsson states, and at prolate deformation the $5/2^+[402]$ and $5/2^+[413]$ Nilsson states. The selection rules for either E3 or M2 transitions do not hinder the transitions. Thus, since the other possibilities are ruled out, the hindrance of the E3 and M2 transitions has to originate from the different shapes of the nucleus connected with the $11/2^-$ ($9/2^-$) and $5/2^+$ states. The whole experimentally observed systematics become consistently explained, if the isomeric negative parity states are connected to oblate and the $5/2^+$ ground states to prolate deformation.

The fact that the N=71 nucleus ^{117}Pd has an $11/2^-$ state as an excited state, suggests that the pairing strength for the $h_{11/2}$ neutrons is considerably larger than that for the nearby s and d orbital neutrons. This effect obviously becomes very important in the structures of the neutron-rich nuclei in this region as was already pointed out in connection with the observation of the onset of the γ-soft deformation in neutron-rich Ru nuclei (Äys90).

The unplaced partial level schemes. The model calculations result in several oblate deformed states with low spin at low energy. These states have not been observed experimentally, except if the unplaced partial level schemes of ^{111}Pd and ^{113}Pd are traces of such states. They

are difficult to study, because they are very weakly populated in the β-decay of most probably prolate or triaxially deformed Rh nuclei. In the case of ^{113}Pd this speculation is supported by the fact that the whole level structure finally decays via the 84.9 keV E1 transition. Another possibility is that these structures are build on a high-spin isomer at high excitation energy, which then decays via high-energy transitions which are not observed in the present study. More experiments are needed to explain these unplaced partial level schemes and to clarify their importance for our understanding of nuclear structure.

5.2. Half-life systematics

The present work has remarkably extended the half-life systematics for the neutron rich nuclei in the $Z \leq 50$ region. Ten new or improved (^{109}Tc, ^{111}Ru and ^{117}Pd) half-lives are reviewed in chapter 4.2. In addition, another ten new half-lives in this region have been deduced in the course of the present studies with the IGISOL. References to these were given in chapter 4.2.

New half-lives can be directly used to test various β-decay half-life calculations, since these results were not available when the models were developed. The reliability of the models is important for astrophysical calculations of nucleosynthesis of heavy elements. The rapid nucleosynthesis via neutron capture and β-decay in supernova explosions, the r-process, is analogous to the formation of heavy elements in slow neutron capture and β-decay, the s-process, but its path is expected to lie far beyond the most neutron rich isotopes experimentally known at the moment. Since no experimental data on the nuclear properties of these nuclei is available, the calculations have to be based on extrapolations of the present nuclear models (Thi92). Testing of these models with new experimental data is thus essential in the process to improve their reliability.

A classical model predicting the β-decay half-lives far from stability is the gross theory (Tak73), whose importance as a valuable pioneering work is generally accepted. The gross theory, however, do not take the shell structure of nuclei into account, and as it is seen in figure 5.7, the gross theory overestimates the half-lives in this region almost by an order of magnitude.

The highest total log *ft* value of the β-decays studied in the present work, calculated using the decay energy from the mass formula of Möller and Nix (Möl88) and the experimental β-decay half-lives, is 5.5 for ^{111}Pd. The nuclei further from stability have lower total log *ft* values. However, a total log *ft* value of 4.5 seems to be a kind of saturation value in this region. This value is typical for the allowed spin flip transitions (Jok91). In this region these transitions has

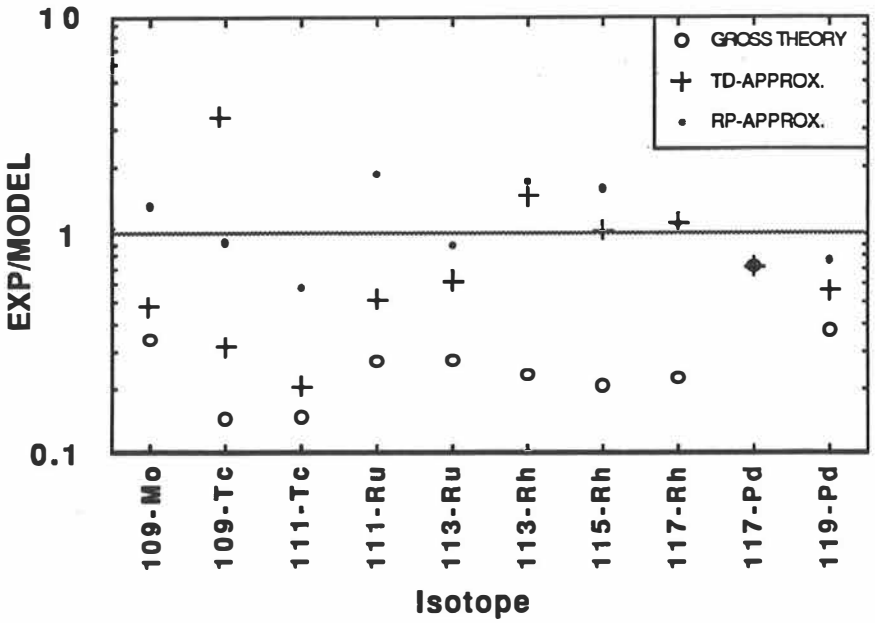

Figure 5.7. A comparison between the experimental β-decay half-lives and various models. The experimental half-lives were given in table 4.2 and discussed in chapter 4.2. The calculated values are taken from (Tak73), (Kla84) and (Sta90).

to be mediated via the $\nu g_{7/2} \rightarrow \pi g_{9/2}$ transformation. Above N > 64 this necessarily involves the decay of the "core" neutrons, and consequently the states with complex core-coupled wave functions are required to give adequate description of the process.

In figure 5.7 a comparison of present new half-lives to the calculations performed using Tamm-Dancoff -approximation (Kla84) is also shown. In this approach, the structure of nuclei is taken into account in a more quantitative way, and much better agreement with the experimental values is achieved.

Comparison with even more advanced β-decay half-life predictions using neutron-proton quasiparticle random phase approximation (Sta90) is also shown in figure 5.7. The major drawback of these calculations, as compared both with gross theory and TDA-calculations, is that the β-decay energies are not calculated within the model but are introduced as parameter. Thus, the half-life predictions of unknown nuclei depend on the mass formula used to calculate the β-decay energy. Some other features in the calculations in (Sta90), as for example the treatment of Gamow-Teller strength parameter, have also been criticized. A more detailed discussion of the subject, as well as an extended comparison of npQRPA calculations to the new experimental half-lives, including all the new results from the IGISOL facility, can be found in (Äys92).

6. Summary

As a result of this study the half-life and level systematics of neutron rich odd-A nuclei with A = 109 – 119 were extended. New or improved beta decay half-lives were measured for ten isotopes and seven new isotopes were discovered. In odd-proton nuclei the coexistence of the spherical shell model states with states with large prolate deformation was known prior to this work. The experimental systematics of these states was not remarkably improved in this study. The most important result of the present studies is the experimental systematics of negative parity isomeric states in odd-A Pd nuclei. The large hindrance of their decay seems to support coexistence of oblate and prolate shapes, which is also reproduced in deformed shell model calculations.

Otherwise the calculations with a macroscopic-microscopic model using an axially deformed Wood-Saxon potential, the Möller-Nix mass formula and the BCS-treatment of pairing only partially reproduces the experimentally observed properties of the studied nuclei. Even within the expected accurary of a few hundred keV, it seems clear that the properties of these nuclei cannot be reproduced without including collective degrees of freedom in the model.

The new JYFL K-130 cyclotron will provide interesting possibilities for the installation of the ion guide isotope separator. In addition to the application of the ion guide technique for heavy ion reactions, the use of the light ion reactions, especially fission, will most probably be very fruitful in the near future. The improved efficiency of the ion guide, with more intense light ion beams available, will most probably result in extension of both beta half-life and level systematics. The expected more intense sources will allow lifetime studies of the excited levels of the very exotic neutron rich nuclei. This is especially important for identification of the intruder states.

Since nuclear spectroscopy does not provide possibility to directly determine the sign of deformation, a very useful combination could be laser spectroscopy of the mass separated ion beams. The ion guide is able to produce the most interesting isotopes at primary beams for laser spectroscy. The improved coincidence measurement techniques have made laser spectroscopy capable to deal also with relatively low intensity ($\leq$ 100 ions/s) ion beams typical for the ion guide separators. Especially the laser spectroscopy for the odd-A Pd isomers to probe the existence of oblate deformation will be worthy of large experimental efforts.

References

Alt90 T.Altzitzoglou, J.Rogowski, M. Skålberg, J. Alstad, G. Herrmann, N. Kaffrell, G. Skarnemark, W. Talbert and N. Trautmann, FAST CHEMICAL SEPARATION OF TECHNETIUM FROM FISSION PRODUCTS AND DECAY STUDIES OF ^{109}Tc AND ^{110}Tc, Radiochim. Acta **51**, 145 (1990).

Ärj81a J. Ärje and K. Valli, HELIUM-JET ION GUIDE FOR AN ON-LINE ISOTOPE SEPARATOR, Nucl. Instr. and Meth. **179**, 533 (1981).

Ärj81b J .Ärje, J. Äystö, J.Honkanen, K.Valli and A. Hautojärvi, A STUDY OF HELIUM-JET ION GUIDE FOR AN ON-LINE ISOTOPE SEPARATOR Nucl. Instr. and Meth. **186**, 149 (1981).

Ärj85 J. Ärje, J. Äystö, H. Hyvönen, P. Taskinen, V. Koponen, J. Honkanen, A. Hautojärvi and K. Vierinen, SUBMILLISECOND ON-LINE MASS SEP ARATION OF NONVOLATILE RADIOACTIVE ELEMENTS: AN APPLICATION OF CHARGE EXCHANGE AND THERMALIZATION PROCESSES OF PRIMARY RECOIL IONS IN HELILUM, Phys. Rev. Lett. **54**, 99 (1985).

Ärj86 J. Ärje, ION GUIDE METHOD FOR ISOTOPE SEPARATOR, Ph.D. thesis, 1986, Res. Rep. no. 3/86 Dept. Physics, University of Jyväskylä, Finland.

Ärj87 J. Ärje, J. Äystö, P. Taskinen, J. Honkanen and K. Valli, ION GUIDE METHOD FOR ON-LINE ISOTOPE SEPARATION, Nucl. Instr. and Meth. **B26**, 384 (1987).

Ast91 A. Astier, R. Beraud, A. Bouldjedri, R. Duffait, A. Emsallem, M. Meyer, S. Morier, P. Pangaud, N. Redon, D. Barneoud, J. Blachot, J. Genevey, A. Gizon, R. Guglielmini, J. Inchaouh, G. Margotton, J. L. Vieux-Rochaz, J. Ärje, J. Äystö, P. P. Jauho, A. Jokinen, H. Penttilä, K. Eskola, M. E. Leino and J. B. Marquette, STATUS REPORT OF THE SARA IGISOL USED IN ^{238}U(α 40 MeV, f) REACTION, to be published in Nuclear Instr. and Meth., (1991).

Aub68 R.L. Auble, J. B. Ball and C. B. Fulmer, THE (d,^{3}He) REACTION ON ^{126}Te, ^{128}Te AND ^{130}Te NUCLEI, Nucl. Phys. **A116**, 14 (1968).

Aub79 R.L. Auble, NUCLEAR DATA SHEETS FOR A = 119, Nuclear Data Sheets **26**, 207 (1979).

Äys84 J. Äystö, J. Ärje, V. Koponen, P. Taskinen, H. Hyvönen, A. Hautojärvi and K.Vierinen, BETA DECAY OF $T_z = -1/2$ NUCLIDES ^{51}Fe AND ^{55}Ni: A NEW APPROACH TO ON-LINE ISOTOPE SEPARATION, Phys. Lett. **138B**, 369 (1984).

Äys87 J. Äystö, P. Taskinen, M. Yoshii, J. Honkanen P. Jauho, J. Ärje and K. Valli, SEPARATION OF FISSION PRODUCTS BY THE ION GUIDE FED ISOTOPE SEPARATOR, IGISOL, Nucl. Instr. and Meth. **B26**, 394 (1987).

Äys88a J.Äystö, P.Taskinen, M.Yoshii, J.Honkanen, P.Jauho, H.Penttilä, C.N.Davids, IDENTIFICATION AND DECAY OF NEW NEUTRON-RICH ISOTOPES ^{115}Rh AND ^{116}Rh, Phys. Lett. **201B**, 211 (1988).

Äys88b J. Äystö, C.N.Davids, J.Hattula, J.Honkanen, K.Honkanen, P.Jauho, R.Julin, S.Juutinen, J.Kumpulainen, T.Lönnroth, A.Pakkanen, A.Passoja, H.Penttilä, P.Taskinen, E.Verho, A.Virtanen, M.Yoshii, LEVELS IN ^{110}Pd, ^{112}Pd, ^{114}Pd AND ^{116}Pd FROM THE BETA DECAYS OF THE ON-LINE MASS SEPARATED Rh ISOTOPES, Nucl. Phys. **A480**, 104 (1988).

Äys88c J. Äystö, P. Taskinen, J. Ärje, M. Huyse, P. Dendooven, J. Wouters, G. Reusen, and P. vanDuppen, Progress Report 1986/87 Instituut voor Kern- en Stralingfysika, Katholieke Universiteit Leuven, Belgium.

Äys90 J. Äystö, P.P. Jauho, Z. Janas, A.Jokinen, J.M.Parmonen, H.Penttilä, P.Taskinen, R. Béraud, R. Duffait, A. Emsallem, J. Meyer, M. Meyer, N. Redon, M. E. Leino, K. Eskola and P.Dendooven, COLLECTIVE STRUCTURE OF THE NEUTRON-RICH NUCLEI, ^{110}Ru AND ^{112}Ru, Nucl. Phys. **A515**, 365 (1990).

Äys92 J. Äystö, A. Astier, T. Enqvist, K. Eskola, Z. Janas, A. Jokinen, K.-L. Kratz, M.E.Leino, H. Penttilä, B. Pfeiffer and J. Zylicz, DISCOVERY AF RARE NEUTRON-RICH Zr, Nb, Mo, Tc AND Ru ISOTOPES IN FISSION: TEST OF β-HALF-LIFE PREDICTIONS VERY FAR FROM STABILITY, Submitted to Phys. Rev. Letters.

Bar77 H. Bartsch, K. Huber, U. Kneissl and H. Krieger, INVESTIGATION OF THE NEUTRON RICH NUCLEI ^{108}Rh AND ^{109}Pd, Z. Phys. A **283**, 199 (1978).

Bla84 J. Blachot, NUCLEAR DATA SHEETS FOR A = 109, Nuclear Data Sheets **41**, 139 (1984), updated in Nuclear Data Sheets **64**, 913 (1991).

Bla87 J. Blachot and G. Marguier, NUCLEAR DATA SHEETS FOR A = 117, Nuclear Data Sheets **50**, 63 (1987).

Bla90 J. Blachot, NUCLEAR DATA SHEETS FOR A = 111, Nuclear Data Sheets **60**, 889 (1990), and references given therein.

Bla91 J. Blachot, NUCLEAR DATA SHEETS FOR A = 107, Nuclear Data Sheets **62**, 709 (1991), and references given therein.

Blo76 H.P. Blok, L. Hulstman, E.J. Kaptein and J. Blok, INVESTIGATION OF ^{91}Zr BY HIGH RESOLUTION (d,p), (p,p') AND (p,d) REACTIONS, Nucl. Phys. **A273**, 142 (1976).

Boh52 A. Bohr, THE COUPLING OF NUCLEAR SURFACE OSCILLATIONS TO THE MOTION OF INDIVIDUAL NUCLEONS, Kgl. Dan. Vid. Selsk. Mat-Fys. Medd. **26**, no.14 (1952).

Boh75 A. Bohr and B. R. Mottelson, NUCLEAR STRUCTURE, vol II, Nuclear Deformations, pp. 244 - 246. W.A.Benjamin, Reading, Massachusetts, USA (1975).

Bor87 J. W. Borgs, H. -P. Kohl, G. Lhersonneau, H. Ohm, U. Paffrath, K. Sistemich, D. Weiler, and R. A. Meyer, IMPROVEMENTS AT JOSEF AND NEW SETUP FOR FISSION-PRODUCT SPECTROSCOPY, Nucl. Instr. and Meth. B**26**, 304 (1987).

Bre89 Å. Bredbacka, M. Brenner and F. B. Malik: LEVEL SPECTRA, μ, Q, B(M1), B(E2) AND SPECTROSCOPIC FACTORS FOR ODD-Rh ISOTOPES IN THE CORIOLIS COUPLING MODEL, Nucl. Phys. **A504**, 49 (1989).

Brü75 W. Brüchle, UNTERSUCHUNG VON KURTZLEBIGEN NEUTRONEN-REICHEN PALLADIUM- UND SILBERISOTOPEN NACH SCHNELLER CHEMISCHER TRENNUG AUS SPALTPRODUCTEN, Ph.D. thesis, pp. 102 - 103. Johannes Gütenberg Universität, Mainz, 1975.

Cha91 R. R. Chassman, NUCLEAR EQUILIBRIUM SHAPES NEAR A = 100, Z. Phys. **A 339**, 111 (1991).

Che79 Cheifez ym, EVEN-EVEN NEUTRON RICH ISOTOPES, pp. 193 - 207, in Till von Egidy (ed.): Nuclear specroscopy of fission products, Inst. Phys. Conf. Ser. No **51**, Bristol, Great Britain, 1980.

Coh55 B. L. Cohen, B. L. Ferrel-Bryan, D. J. Coombe and M. K. Hullings, ANGULAR DISTRIBUTION OF FISSION FRAGMENTS FROM 22-MeV PROTON-INDUCED FISSION OF ^{238}U, ^{235}U, ^{232}Th, AND ^{230}Th, Phys. Rev. **98**, 685 (1955).

Ćwi87 S. Ćwiok, J. Dudek, W. Nazarewicz, J. Skalski and T. Werner, SINGLE PARTICLE ENERGIES, WAVE FUNCTIONS, QUADRUPOLE MOMENTS AND g-FACTORS IN AN AXIALLY DEFORMED WOODS-SAXON POTENTIAL WITH APPLICATIONS TO THE TWO-CENTRE-TYPE NUCLEAR PROBLEMS, Computer Phys. Comm. **46**, 379 (1987).

DeF86 D. De Frenne, E. Jacobs, M. Verboven, and P. De Gelder, NUCLEAR DATA SHEETS FOR A = 105, Nuclear Data Sheets **47**, 261 (1986).

Dud78 J. Dudek and T. Werner, NEW PARAMETERS OF THE DEFORMED WOODS-SAXON POTENTIAL FOR A = 110 – 210 NUCLEI, J. Phys. **G4**, 1543 (1978).

Dud79 J. Dudek, A. Majhofer, J. Skalski, T. Werner, S. Ćwiok and W. Nazarewicz, PARAMETERS OF THE DEFORMED WOODS-SAXON POTENTIAL OUTSIDE A = 110 – 210 NUCLEI, J. Phys. **G5**, 1359 (1979).

Dud80 J. Dudek, W. Nazarewicz and T. Werner, DISCUSSION OF THE IMPROVED PARAMETRISATION OF THE WOODS-SAXON POTENTIAL FOR DEFORMED NUCLEI, Nucl. Phys. **A341**, 253 (1980).

Dud81 J. Dudek, Z. Szymánski and T. Werner, WOOD-SAXON POTENTIAL PARAMETERS OPTIMIZED TO THE HIGH SPIN SPECTRA IN THE LEAD REGION, Phys. Rev. C **23**, 920 (1981).

Dud82 J. Dudek, Z. Szymánski, T. Werner, A. Faessler and C. Lima, DESCRIPTION OF THE HIGH SPIN STATES IN ^{146}Gd USING THE OPTIMIZED WOODS-SAXON POTENTIAL, Phys. Rev. C **26**, 1712 (1982).

Eks86 B. Ekström, B. Fogelberg, P. Hoff, E. Lund and A. Sangariyavanish, DECAY PROPERTIES OF $^{75\text{-}80}$Zn AND Qβ-VALUES OF NEUTRON-RICH Zn AND Ga ISOTOPES, Physica Scripta **34**, 614 (1986).

End81 P.M. Endt, STRENGTHS OF GAMMA-RAY TRANSITIONS IN A = 91 – 150 NUCLEI, At. Data and Nucl. Data Tables **26**, 47 (1981).

Eng85 H.A.Enge, ELECTROMAGNETIC SEPARATORS FOR RECOILING REACTION PRODUCTS, in Treatise on Heavy Ion Science, vol. 8, ed. D. A. Bromley, Plenum Press, New York (1989).

Fet75 P. Fettweis and P. del Marmol, STUDY OF SHORT-LIVED Ru-ISOTOPES PRODUCED IN THERMAL NEUTRON FISSION OF ^{235}U, Z. Phys. A **275**, 359 (1975).

Fog76 B. Fogelberg, Y. Kawase, J. McDonald and A. Bäcklin, LEVELS IN ^{117}Cd STUDIED IN THE DECAYS OF ^{117}Ag AND ^{117m}Ag, Nucl. Phys. **A267**, 317 (1976).

Fog88 B.Fogelberg, E.Lund, Y.Zongyuan, and B.Ekström, TRANSITION PROBABILITIES BETWEEN INTRUDER STATES IN HEAVY Ag ISOTOPES, pp. 296–304 in Proceedings of the 5th International Conference on Nuclei far from stability, Rosseau Lake, 1987, AIP Conf. Proc. No. 164, ed. by Ian S. Towner, AIP, New York (1988).

Fog90 B. Fogelberg, Y. Zongyuan, B. Ekström, E. Lund, K. Aleklett and L. Sihver, ISOMERISM, TOTAL DECAY ENERGIES, AND ABSOLUTE γ-RAY INTENSITIES OF THE HEAVY Pd AND Ag ISOTOPES, Z. Phys. A **337**, 251 (1990).

Fra78 G. Franz and G. Herrmann, IDENTIFICATION OF SHORT-LIVED RUTHENIUM AND RHODIUM ISOTOPES IN FISSION BY RAPID CHEMICAL SEPARATIONS, J. Inorg. Nucl. Chem. **40**, 945 (1978).

Fra87 A. Frank, P. Van Isacker and D. D. Warner, SUPERSYMMETRY IN TRANSITIONAL NUCLEI AND ITS APPLICATION TO THE Ru AND Rh ISOTOPES, Phys. Lett. **197B**, 474 (1987).

Gov71 N. B. Gove and M. J. Martin, LOG-f TABLES FOR BETA DECAY, At. Data and Nucl. Data Tables **10**, 205 (1971).

Gra89 M. Graefenstedt, P. Jürgens, U. Keyser, F. Münnich, F. Schreiber, K. Balog, T. Winkelmann and H. R. Faust, EXPERIMENTAL BETA-DECAY ENERGIES OF VERY NEUTRON-RICH FISSION PRODUCTS WITH $107 \leq A \leq 109$, Z. Phys. A **224**, 239 (1989).

Ham89 J. Hamilton, STRUCTURES OF NUCLEI FAR FROM STABILITY, pp. 1–98 in Treatise on Heavy-Ion Science, vol. 8, ed. D. A. Bromley, Plenum Press, New York (1989).

Has82 A. Hashizume, Y. Tendow, K. Kitao, M. Kanbe and T. Tamura, NUCLEAR DATA SHEETS FOR A = 127, Nuclear Data Sheets **35**, 181 (1982).

Hel81 H. Helppi, J. Hattula, A. Luukko, M. Jääskeläinen and F. Dönau, IN-BEAM STUDY OF $^{127,129}Xe$ AND COLLECTIVE DESCRIPTION OF THE LEVEL STRUCTURES IN ODD-A Xe NUCLEI, Nucl. Phys. **A357**, 333 (1981).

Hey83 K. Heyde, P. VanIsacker, M. Waroquier, J.L. Wood, R.A. Meyer, COEXISTENCE IN ODD-MASS NUCLEI, Phys. Rep. **102**, 291 (1983).

Hey86 K. Heyde and V. Paar, ON THE NATURE OF LOW-LYING $7/2^+$ STATES IN ODD-A Tc, Rh AND Ag NUCLEI, Phys. Lett. **179B**, 1 (1986).

Hop72 F. F. Hopkins, J. R. White, G. W. Phillips, C. F. Moore, P. Richard, FURTHTER MEASUREMENTS OF GAMMA TRANSITIONS IN SPONTANEOUS FISSION FRAGMENTS OF ^{252}Cf, Phys. Rev. C **5**, 1015 (1972).

Hop73 F. F. Hopkins, J. R. White, C. F. Moore, P. Richard, GAMMA CASCADES IN ^{252}Cf SPONTANEOUS FISSION FRAGMENTS, Phys. Rev. C **8**, 380 (1973).

Hon87 J. Honkanen, V. Koponen, H. Hyvönen, P. Taskinen, J. Äystö and K. Ogawa, EXPERIMENTAL AND SHELL-MODEL STUDY OF THE BETA DECAY OF ^{43}Ti, Nucl. Phys. **A471**, 489 (1987).

Hon89 J. Honkanen, V. Koponen, P. Taskinen, J. Äystö, K. Eskola, S. Messelt, K.Ogawa, BETA STRENGTH TO EXCITED STATES IN THE DECAYS OF $f_{7/2}$ MIRROR NUCLIDES, Nucl. Phys. **A496**, 462 (1989).

Hot91 M.A.C. Hotchkins, J.L. Durrell, J.B. Fitzgerald, A.S. Mowbray, W.R. Phillips, I. Ahmad, M.P. Carpenter, R.V.F. Janssens, T.L. Khoo, E.F. Moore, L.R. Morss, Ph. Benet, and D.Ye, ROTATIONAL BANDS IN THE MASS 100 REGION, Nucl. Phys. **A530**, 111 (19

Huy88 M. Huyse, P. Dendooven, and K. Deneffe, PRODUCTION AND MASS SEPARATION OF SHORT-LIVING NEUTRON-DEFICIENT ACTINIDES, Nucl. Instr. and Meth. **B31**, 483 (1988).

Jac87 L.Jacobsson, B.Fogelberg, B. Ekström and G. Rudstam, AN UNCONVENTIONAL BI-MODE ION SOURCE (ANUBIS) FOR THE OSIRIS FACILITY, Nucl. Instr. and Meth. **B26**, 223 (1987).

Jau92 P.P.Jauho, J. Äystö, K. Eskola, A. Jokinen. M. E. Leino, J.M.Parmonen and H. Penttilä, FISSION PRODUCT YIELDS WITH 15 – 20 MeV PROTONS, to be published in Phys. Rev. C.

Jen84 A. S. Jensen, P. G. Hansen, B. Jonson NEW MASS RELATIONS AND TWO- AND FOUR-NUCLEON CORRELATIONS, Nucl. Phys. **A431**, 393 (1984).

Joh70 W.John, F.W.Guy and J.J.Wesolowski, FOUR-PARAMETER MEASUREMENTS OF ISOMERIC TRANSITIONS IN ^{252}Cf FISSION FRAGMENTS, Phys. Rev. C **2**, 1451 (1970).

Jok91 A. Jokinen, J. Äystö, P. Dendooven, K. Eskola, Z. Janas, P.P. Jauho, M.E. Leino, J.M. Parmonen, H. Penttilä, K. Rykaczewski and P. Taskinen, SPIN-FLIP BETA DECAY OF EVEN-EVEN DEFORMED NUCLEI ^{110}Ru AND ^{112}Ru, Z. Phys **A 340**, 21 (1991).

Kaf84 N. Kaffrell, H. Tetzlaff, N. Trautmann, P. Hill, S. Hoglund, G. Skarnemark, J. Alstad, P. de Gelder, E. Jacobs, K. Wolfsberg and H. Seyfarth, LEVELS IN ^{111}Pd, Inst. für Kernchemie, Univ. Mainz, Jahtesbericht 1983, 63 (1984).

Kaf87 N. Kaffrell, P. Hill, J. Rogowski, H. Tetzlaff, N. Trautmann, E. Jacobs, P. de Gelder, D. de Frenne, K. Heyde, S. Börjesson, G. Skarnemark, J. Alstad, N. Blasi, M. N. Harakeh, W. A. Sterrenburg and K. Wolfsberg, LEVELS IN ^{109}Rh, Nucl. Phys. **A470**, 141 (1987).

Kaf88 N. Kaffrell, J. Rogowski, H. Tetzlaff, N. Trautmann, D. DeFrenne, K. Heyde, E.Jacobs, G. Skarnemark, J. Alstad, M.N. Harakeh, J.M. Schippers, S.Y. van der Werf, W. R. Daniels and K. Wolfsberg, EVIDENCE FOR SHAPE COEXISTENCE IN NEUTRON-RICH Rh AND Ag ISOTOPES, pp. 286–294 in Proceedings of the 5th International Conference on Nuclei far from stability, Rosseau Lake, 1987, AIP Conf. Proc. No. 164, ed. by Ian S. Towner, AIP, New York (1988).

Kan78 M. Kanazawa, S.Ohya, T.Tamura, Z. Matumoto and N. Mutsuro, DECAY OF ^{109}Rh, Phys. Soc. Jpn **44**, 25 (1978).

Kan89 J. Kantele, A SIMPLIFIED METHOD FOR COMPUTING K INTERNAL-CONVERSION COEFFICIENTS FOR E1, E2, E3, M1, M2, AND M3 TRANSITIONS FROM TABULATED VALUES, Nucl. Instr. and Meth. **A275**, 149 (1989).

Kaw75 Y. Kawase, B. Fogelberg, J. McDonald and A. Bäcklin, STATES IN ^{119}Cd STUDIED IN THE DECAY OF ^{119}Ag, Nucl. Phys. **A241**, 237 (1975).

Kla84 H. V. Klapdor, J. Metzinger, and T. Oda, BETA DECAY HALF-LIVES OF NEUTRON-RIC NUCLEI, At. Data and Nucl. Data Tables **31**, 81 (1984).
^{109}Tc, ^{111}Ru, ^{113}Ru, ^{113}Rh half-lives from private communication.

Kra86 K.-L. Kratz, H. Gabelmann, W. Hillebrandt, B. Pfeiffer, BETA DECAY $T_{1/2}$ OF ^{130}Cd AND ITS IMPORTANCE FOR ASTROPHYSICAL r-PROCESS SCENARIOS, Z. Phys. **A 325**, 483 (1986).

Led78 C. M. Lederer and V. S. Shirley (ed.), Table of isotopes, 7th edition, Wiley, New York (1978).

Lei91 M. E. Leino, P.P. Jauho, J. Äystö, P. Decrock, P. Dendooven, K. Eskola, M. Huyse, A. Jokinen, J. M. Parmonen, H. Penttilä, G. Reusen, P. Taskinen, P. Van Duppen and J. Wauters, INDEPENDENT AND CUMULATIVE YIELDS OF VERY NEUTRON-RICH NUCLEI IN 20 MeV p- AND 18 – 41 MeV d-INDUCED FISSION OF ^{238}U, Phys. Rev. C **44**, 336 (1991).

Lhe86 G. Lhersonneau, D. Weiler, P. Kohl, H. Ohm, K. Sistemich and R. A. Meyer, A NEW HIGH-SPIN ISOMER IN ^{97}Y, Z. Phys. **A 323**, 59 (1986).

Lön84 T. Lönnroth, J. Äystö, J.Ärje, J.Honkanen, V.Koponen, P.Taskinen and H.Hyvönen, HALF-LIFE AND CONFIGURATION OF THE $1/2^+$ INTRUDER STATE IN ^{203}Bi, Z. Phys **A 319** (1984) 149.

Mad88 D. G. Madland and J. R. Nix, NEW MODEL OF THE AVERAGE NEUTRON AND PROTON PAIRING GAPS, Nucl. Phys. **A476**, 1 (1988).

Mat76 V. Matschoß and K. Bächmann, SEPARATION IN THE GAS PHASE OF SHORT-LIVED NUCLIDES OF Ru, in Proceedings of the Third international conference on Nuclei Far From Stability, Cargése, Corsica (France), pp.59 - 62. CERN, Genéve 1976.

Mol75 E. Moll, H. Schrader, G. Siegert, M. Asghar, J. P. Bocquet, G. Bailleul, J. P. Gautheron, H. Ewald, H. Wollnik, P. Armbruster, G. Fiebig, H. Lawin and K. Sistemich, ANALYSIS OF ^{236}U-FISSION PRODUCTS BY THE RECOIL SEPARATOR "LOHENGRIN", Nucl. Instr. and Meth. **123**, 615 (1975).

Mül80 H. W. Müller, NUCLEAR DATA SHEETS FOR A = 91, Nuclear Data Sheets **31**, 181 (1980).

Mül86 H.-W. Müller and D. Chmielewska, NUCLEAR DATA SHEETS FOR A = 99, Nuclear Data Sheets **48**, 663 (1986).

Möl88 P. Möller and J. R. Nix, NUCLEAR MASSES FROM A UNIFIED MACROSCOPIC-MICROSCOPIC MODEL, At. Data Nucl. Data Tables **39**, 213 (1988).

Möl90 P. Möller and J. Randrup, NEW DEVELOPMENTS IN THE CALCULATION OF β-STRENGTH FUNCTIONS, Nucl. Phys. **A514**, 1 (1991):
references [15,16]) therein.

Nil55 S. G. Nilsson, BINDING STATES OF INDIVIDUAL NUCLEONS IN STRONGLY DEFORMED NUCLEI, Kgl. Dan. Vid. Selsk. Mat-Fys. Medd. **29**, n:o 16 (1955).

Nom88 T. Nomura, J. Tanaka, M. Oyaidzu, Y. Iwata, N. Ikeda, K. Valli, K. Morita, Y. Nagai, T. Toriyama, Y. Murakoimi, Y. Torii and S. Harada, AN ION-GUIDE TECHNIQUE FOR ON-LINE ISOTOPE SEPARATION COUPLED WITH A RECOIL-TYPE BEAM SEPARATOR, Nucl. Instr. and Meth. **A269**, 23 (1988).

Paa73 V. Paar, COUPLING OF A THREE-PARTICLE (HOLE) VALENCE-SHELL CLUSTER TO QUADRUPOLE VIBRATIONS (ALAGA MODEL), Nucl. Phys. **A211**, 29 (1973).

Par91 J.-M. Parmonen, Z. Janas, W. H. Trzaska, J. Äystö, J. Kantele, P. P. Jauho, A. Jokinen and H. Penttilä, ELECTRON-TRANSPORTER SPECTROMETER FOR ON-LINE ISOTOPE SEPARATOR, Nucl. Instr. and Meth. **A306**, 504 (1991).

Pau73 H. C. Pauli ON THE SHELL-MODEL AND ITS APPLICATIONS TO THE DEFORMATION ENERGY OF HEAVY NUCLEI, Phys. Rep. **7**, 35 (1973).

Pen88 H. Penttilä, P. Taskinen, P. P. Jauho, V. Koponen, C. N. Davids and J. Äystö, HALF-LIFE MEASUREMENTS FOR NEUTRON-RICH Tc, Ru, Rh AND Pd ISOTOPES. IDENTIFICATION OF THE NEW ISOTOPES ^{111}Tc, ^{113}Rh AND ^{113}Rh, Phys. Rev. C **38**, 931 (1988).

Pen90 H. Penttilä, J. Äystö, P. P. Jauho, A. Jokinen, J.-M. Parmonen, P. Taskinen, K. Eskola, M. E. Leino, P. Dendooven and C. N. Davids, NEW NEUTRON-RICH NUCLEI AND ISOMERS PRODUCED IN SYMMETRIC FISSION, Physica Scripta **T32**, 38 (1990).

Pen91a H. Penttilä, J. Äystö, K. Eskola, Z. Janas, P. P. Jauho, A. Jokinen, M. E. Leino, J. M. Parmonen and P. Taskinen, FIRST OBSERVATION OF THE BETA DECAY OF ^{117}Pd AND THE DISCOVERY OF A NEW ISOTOPE ^{119}Pd, Z. Phys. A **338**, 291 (1991).

Pen91b H. Penttilä, P. P. Jauho, J. Äystö, P. Decrock, P. Dendooven, M. Huyse, G. Reusen, P. Van Duppen and J. Wauters, IDENTIFICATION OF THE RARE NEUTRON-RICH ISOTOPE ^{117}Rh, Phys. Rev. C **44**, 935 (1991).

Rag89 P. Raghavan, TABLE OF NUCLEAR MOMENTS, At. Data and Nucl. Data Tables **42**, 189 (1989).

Rai50 J. Rainwater, NUCLEAR ENERGY LEVEL ARGUMENT FOR A SPHEROIDAL NUCLEAR MODEL, Phys. Rev. **79**, 432 (1950).

Rav89 H.L.Ravn and B.W.Allardyce, ON-LINE MASS SEPARATORS, p. 363 in Treatise on Heavy Ion Science, vol. 8, ed. D. A. Bromley, Plenum Press, New York (1989).

Rei71 W. Reisdorf, J. P. Unik, H. C. Griffin, and L. E. Glendenin, FISSION FRAGMENT K X-RAY EMISSION AND NUCLEAR CHARGE DISTRIBUTION FOR THERMAL NEUTRON FISSION OF ^{233}U, ^{235}U, ^{239}Pu AND SPONTANEOUS FISSION OF ^{252}Cf, Nucl. Phys. **A177**, 337 (1971).

Rek76 J. Rekstad and G. Løvhøiden, AN INVESTIGATION OF THE NILSSON MODEL POTENTIAL IN THE SPHERICAL LIMIT, Nucl. Phys. **A267**, 40 (1976).

Rog90a J. Rogowski, J. Alstad, M. M. Fowler, D. DeFrenne, K. Heyde, E. Jacobs, N. Kaffrell, G. Skarnemark and N. Trautmann, EVIDENCE FOR INTRUDER STATES IN ^{111}Rh, Z. Phys **A 337**, 233 (1990).

Rog90b J.Rogowski, J.Alstad, N. Kaffrell, G.Skarnemark, M.Skålberg, W. Talbert, N. Trautmann, HALBWERTSZEITBESTIMMUNG VON ^{117}Pd, IK Mainz Jahresbericht 1989, p. 14, Mainz 1990.

Rog90c J. Rogowski, J. Alstad, S. Brant, W. R. Daniels, M. M. Fowler, D. DeFrenne, K. Heyde, E. Jacobs, N. Kaffrell, V. Paar, G. Skarnemark and N. Trautmann, INTRUDER STATES IN ODD-MASS Ag ISOTOPES, Phys. Rev. C **42**, 2733 (1990).

Ros68 E. Rost, PROTON SHELL-MODEL POTENTIALS FOR LEAD AND THE STABILITY OF SUPERHEAVY NUCLEI, Phys. Lett. **26B**, 184 (1968).

Rud76 G. Rudstam, THE ON-LINE MASS SEPARATOR OSIRIS AND THE STUDY OF SHORT-LIVED FISSION PRODUCTS, Nucl. Instr. and Meth. **139**, 239 (1976).

Ryk89 K.Rykaczewski, K.-L.Gippert, N.Kaffrell, P.Kirchner, O.Klepper,V.T.Koslowsky, W.Kurcewicz, W.Nazarewicz, E.Roeckl, E. Runte, D.Schardt,W.-D.Schmidt-Ott and P. Tidemand-Petersson, INVESTIGATION OF NEUTRON-RICH RARE-EARTH NUCLEI INCLUDING THE NEW ISOTOPES ^{177}Tm AND ^{184}Lu, Nucl. Phys. **A499**, 529 (1989).

Rös78 F. Rösel, H. M. Fries, K. Alder and H. C. Pauli, INTERNAL CONVERSION COEFFICIENTS FOR ALL ATOMIC SHELLS, At. Data and Nucl. Data Tables **21**, 91 (1978).

Sch69 W. C. Schick Jr and W. L. Talbert, Jr: GAMMA RAY DECAY SCHEMES OF ^{109g}Pd, ^{111g}Pd AND ^{111m}Pd, Nucl. Phys. **A128**, 353 (1969).

Sie89 H. Sievers, NUCLEAR DATA SHEETS FOR A = 89, Nuclear Data Sheets **58**, 351 (1989).

Sin90 B.Singh and J.A.Szucz, NUCLEAR DATA SHEETS FOR A = 100, Nuclear Data Sheets **60**, 1 (1990).

Ska80 G. Skarnemark, P. O. Aronsson, K. Brodén, J. Rydberg, T. Björnstad, N. Kaffrell, E. Stender, and N. Trautmann, AN IMPROVED SYSTEM FOR FAST, CONTINUOUS CHEMICAL SEPARATIONS ("SISAK 2") IN NUCLEAR SPECTROSOPIC STUDIES, Nucl. Instr. and Meth. **171**, 323 (1980).

Sta90 A. Staudt, E. Bender, K. Muto and H. V. Klapdor-Kleingrothaus, SECOND-GENERATION MICROSCOPIC PREDICTIONS OF BETA-DECAY HALF-LIVES OF NEUTRON-RICH NUCLEI, At. Data Nucl. Data Tables **44**, 79 (1990).

Ste70 P. C. Stevenson, J. T. Larsen and J. J. Leary, THE LIVERMORE FISSION FRAGMENT ANALYZER, Proc. Int. Conf. on the Properties of Nuclei Far From the Region of Beta-Stability, CERN 70-30, 143 (1970).

Str67 V. M. Strutinsky, SHELL EFFECTS IN NUCLEAR MASSES AND DEFORMATION ENERGY, Nucl. Phys. **A95**, 420 (1967).

Tak73 K. Takahashi, M. Yamada, and T. Kondoh, BETA DECAY HALF-LIVES CALCULATED ON THE GROSS THEORY, At. Data and Nucl. Data Tables **12**, 101 (1973)

Tam79 T. Tamura, Z. Matumoto, A. Hashiuzume, Y. Tendow, K. Miyano, S. Ohya, K. Kitao and M. Kanabe, NUCLEAR DATA SHEETS FOR A = 121, Nuclear Data Sheets **26**, 385 (1979).

Tam80 T. Tamura, Z. Matumoto, K. Miyano and S. Ohya, NUCLEAR DATA SHEETS FOR A = 123, Nuclear Data Sheets **29**, 453 (1980).

Tam81 T. Tamura, Z. Matumoto, and M. Ohshima, NUCLEAR DATA SHEETS FOR A = 125, Nuclear Data Sheets **32**, 497 (1981).

Tas89 P. Taskinen, H. Penttilä, J. Äystö, P. Dendooven, P.Jauho, A. Jokinen and M. Yoshii, EFFICIENCY AND DELAY OF THE FISSION ION GUIDE FOR ON-LINE MASS SEPARATION, Nucl. Instr. and Meth. **A281**, 539 (1989).

Thi92 F.-K. Thielemann, J.-P. Bitouzet, K.-L. Kratz, P. Möller, J. J. Cowan and J. W. Truran, OPERATION OF THE r-PROCESS AND COSMOCHRONOLOGY, to be published in Phys. Rep.

Tra76 N. Trautmann, N. Kaffrell, H. Ahrens, P. F. Dittner, IDENTIFICATION OF ^{109}Tc AND ^{110}Tc IN FISSION OF ^{249}Cf, Phys. Rev. C **13**, 872 (1976).

Trz89 W. H. Trzaska, 0^+ STATES IN EVEN-EVEN LEAD ISOTOPES, Ph.D. thesis, 1989, Res. Rep. no. 2/89 Dept. Physics, University of Jyväskylä, Finland.

Wei68 H. V. Weiss, J. L. Elzie, J. M. Fresco, IDENTIFICATION AND YIELD OF 5.0-sec ^{117}Pd IN THE THERMAL-NEUTRON FISSION OF ^{235}U, Phys. Rev. **172**, 1269 (1968).

Wil69 J. B. Wilhelmy, HIGH-RESOLUTION GAMMA AND X-RAY SPECTROSCOPY ON UNSEPARATED FISSION PRODUCTS, Ph.D.Thesis, UCRL-18978, 1969, University of California, USA 1969.

Vir89 A. Virtanen, COMPLEX ALIGNMENT MECHANISM AND LIFETIMES OF HIGH SPIN STATES IN ^{172}Os AND ^{173}Os, Ph.D. thesis, 1989, Res. Rep. no. 3/89 Dept. Physics, University of Jyväskylä, Finland.

Appendix:
Determination of the ground state branchings.

The ground state branching in the β–decay of the parent nucleus can be deduced from the growth-in component in the decay of its daugther during the beam-off period. In this work this method was applied for ^{111,113}Rh (Chapter 4.4).

There are both Ru and Rh atoms present in the source at the moment in which the separator beam is turned off (t = 0). Let the numbers of Ru and Rh nuclei be N_{Ru} and N_{Rh}. The number of Tc nuclei is assumed to be neglible; this assumption is justified by the low yield of Tc nuclei compared to Ru and Rh in mass numbers A = 111 and A = 113 (Lei91).

The number of Ru and Rh nuclei during the decay period is

$$N_{Ru} = N_0^{Ru} \times e^{-\lambda_{Ru} t} \tag{A1}$$

$$N_{Rh} = N_0^{Rh} \times e^{-\lambda_{Rh} t} + N_0^{Ru} \frac{\lambda_{Ru}}{\lambda_{Rh} - \lambda_{Ru}} \times (e^{-\lambda_{Ru} t} - e^{-\lambda_{Rh} t}) \tag{A2}$$

where N_0^{Ru} and N_0^{Rh} are the numbers of Ru and Rh atoms at t = 0 and λ_{Ru} and λ_{Ru} are the decay constants of Ru and Rh nuclei. The latter equation also reads

$$N_{Rh} = \left[\frac{\lambda_{Ru}}{\lambda_{Rh}-\lambda_{Ru}} \times N_0^{Ru}\right] e^{-\lambda_{Ru} t} + \left[N_0^{Rh} - \frac{\lambda_{Ru}}{\lambda_{Rh}-\lambda_{Ru}} \times N_0^{Ru}\right] e^{-\lambda_{Rh} t}$$

$$= C_1 e^{-\lambda_{Ru} t} + C_2 e^{-\lambda_{Rh} t} \tag{A3}$$

Equation (2) can be written for the activity of Rh decays by multiplying both sides by λ_{Rh}, the decay constant of Rh. The constant C_1 is then given by

$$C_1 = \frac{\lambda_{Ru}\lambda_{Rh}}{\lambda_{Rh} - \lambda_{Ru}} \times N_0^{Ru} \tag{A4}$$

The constants C_1 and C_2 can be determined from the decay curve of the daughter nucleus by fitting two exponential curves. Examples of the fit can be seen in figures 4.5 and 4.14. The constant C_1 has still to be normalized with the detector efficiencies before N_0^{Ru} is calculated.

This value gives the total number of the parent nucleus nuclei in the beginning of the beam off–period (at t = 0). If the decay period is long enough practically all the parent nuclei decay, and the γ-transition intensities during the beam off -period can be directly used to calculate the number of the parent nuclei that β-decayed to the excited states of ^{111}Rh. The difference between the deduced two numbers gives the ground state branching in the β–decay of the parent nucleus.

Use of this method involves good knowledge of the levels and the transitions in the daughter nucleus. If there is an unknown transition to the ground state, the branching of depopulated level is included in the ground state branching. The deduced ground state branchings are thus upper limits.